量子ビームでさぐるソフトマターの物性

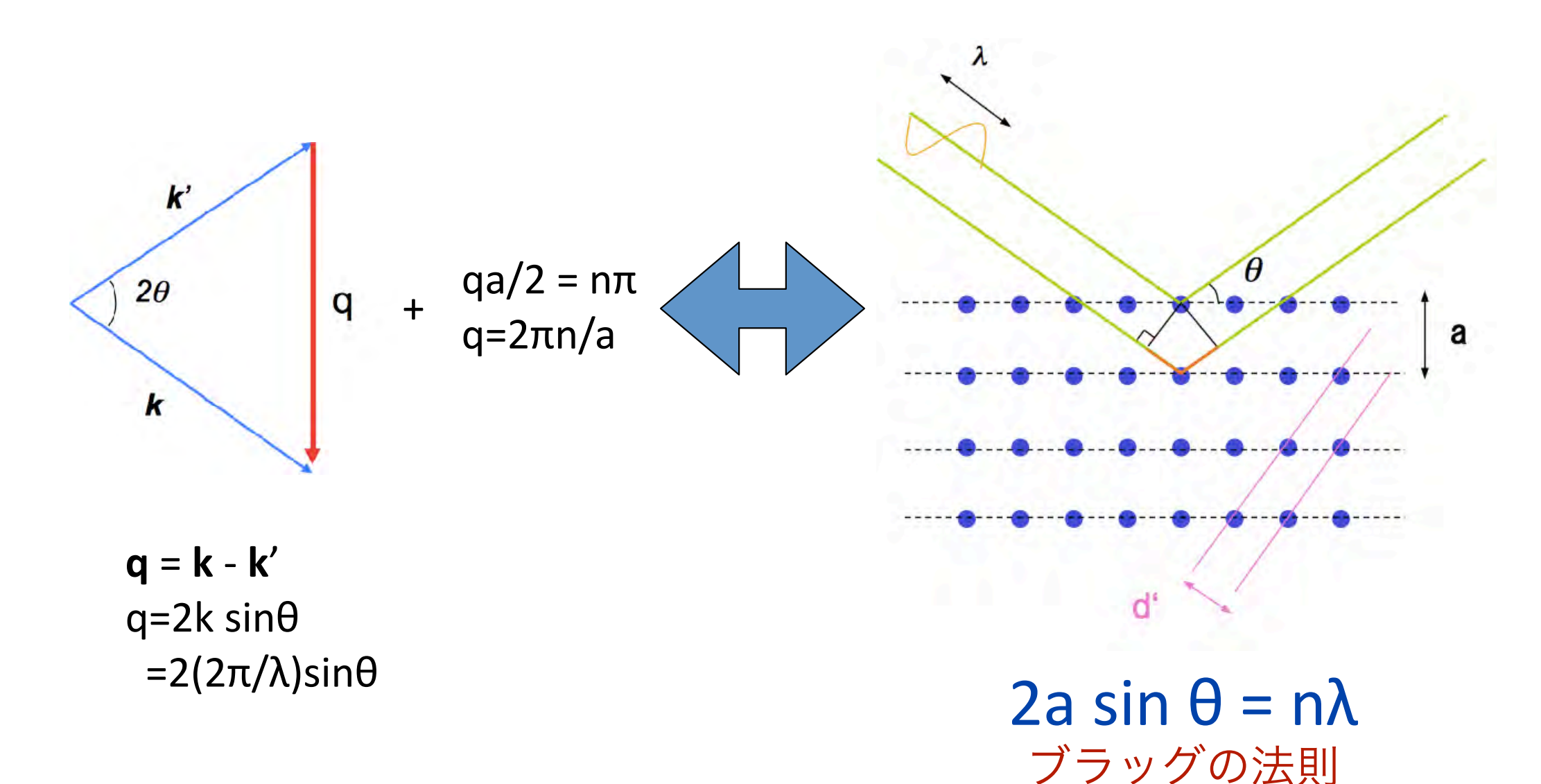
X線·中性子小角散乱

瀬戸秀紀

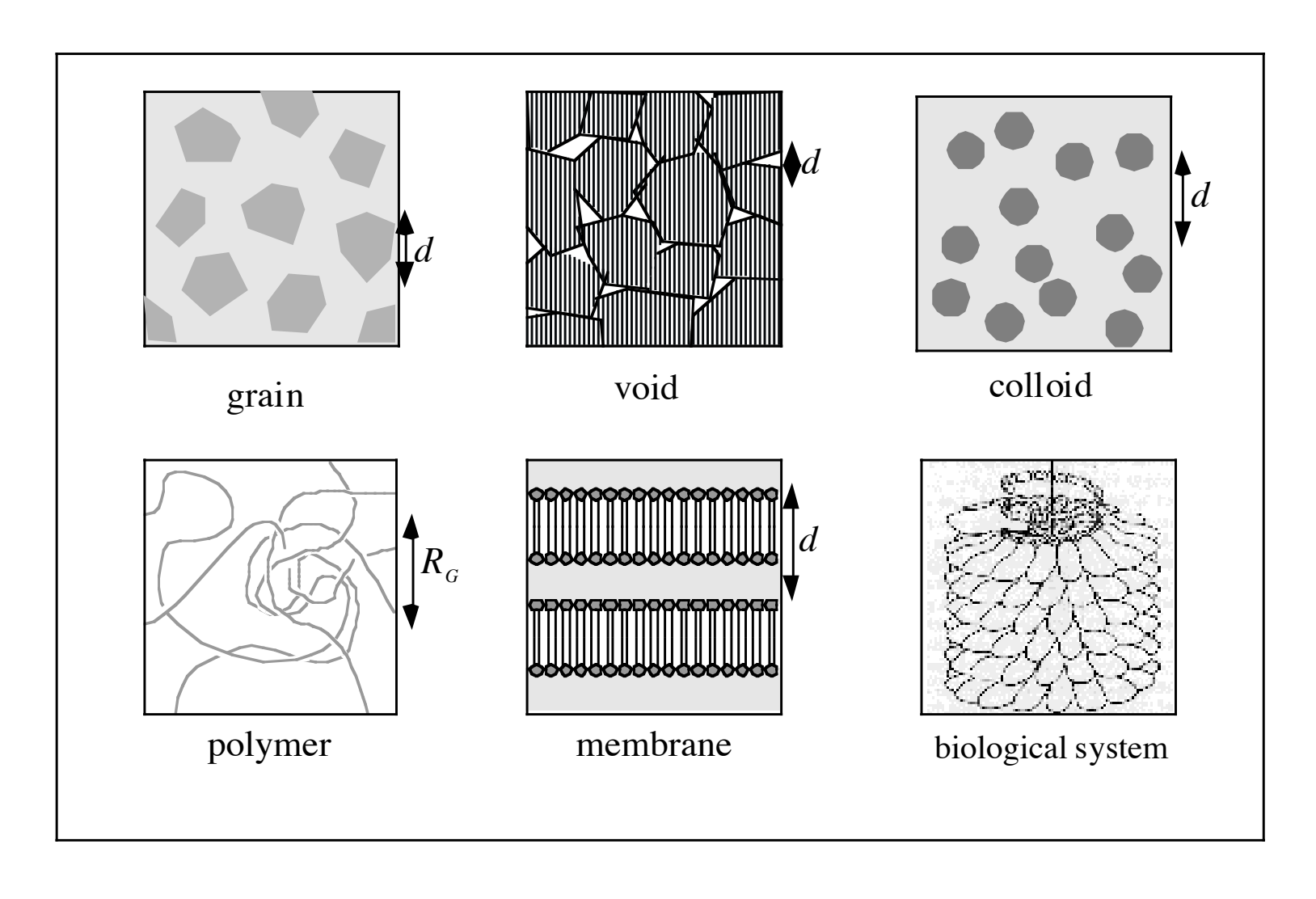
CROSS

High Energy Accelerator Research Organization

中性子散乱:結晶構造が分かる



結晶ではない物質



1. 中性子小角散乱概論

~ 小角散乱の研究例 ~

大きさ: 1 ナノメートル~ 1 マイクロメートル程度

得られる情報: 形・大きさ・並び ⇒ いわゆる「構造」に関する情報.

良く測定されている系: 高分子 (繊維, プラスティック, ゲル) ・液晶 ・コロイド (食品, 洗剤, 化粧品, ナノ粒子) ・結晶のモザイクの大きさ

中性子小角散乱は、結晶の格子間隔よりも大きいナノ〜サブ μ mの構造を調べる実験手法である。Braggの法則によれば、波長 λ の中性子が格子間隔dを持つ物質に散乱されると入射中性子に対して散乱角 θ の2倍の角度に回折線が現れる。

$$2d\sin\theta = \lambda \tag{1}$$

ここで

$$q = \frac{2\pi}{d} = \frac{4\pi \sin\theta}{\lambda}$$
 (2)

は運動量遷移(または波数)である。散乱実験に用いられる X 線や中性子線の波長は数 \mathring{A} 程度なのに対して、ナノスケールの構造の特徴的な長さd はその 106 ~ 100 倍程度である。従って式(1) より散乱角 θ は数度以下になる。それが「小角散乱」と言う名前の由来である。

小角散乱によってそれぞれの運動量遷移qにおける散乱強度I(q)が次のように得られる。

$$I(q) = I_0 SDT_s \frac{d\Sigma}{d\Omega}(q)\Delta\Omega$$
 (3)

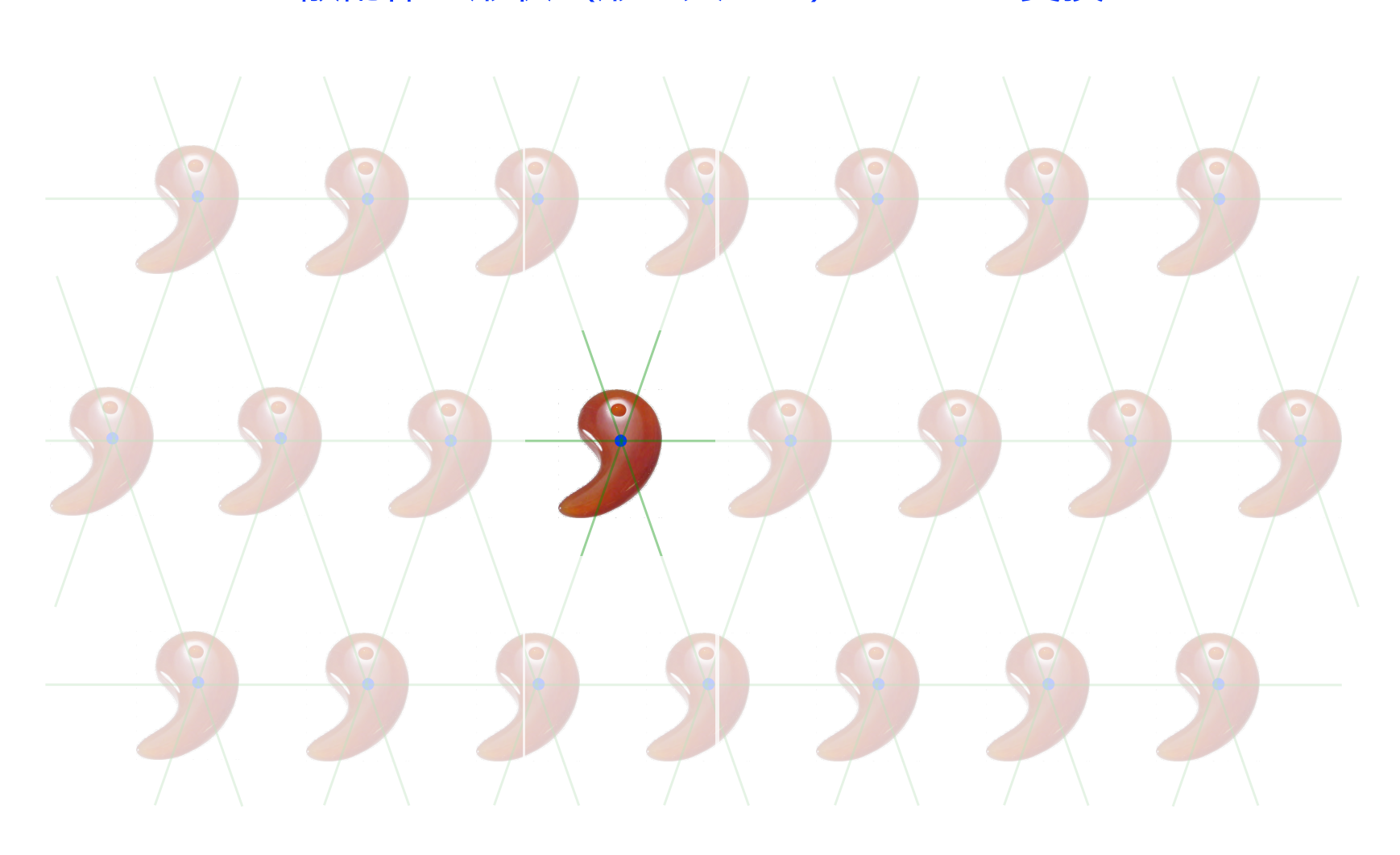
ここでloは入射強度、SとDは試料の断面積と厚み、Tsは試料の透過率、ΔΩは検出器の素子が見ている立体角である。この中で微分散乱断面積は

$$\frac{\partial \Sigma}{\partial \Omega}(q) = \Delta \rho^2 n V^2 P(q) S(q)$$
 (4)

 $(\Delta \rho$ は散乱のコントラスト、nとVは散乱体の数密度と体積)で与えられるが、実験結果を散乱体形状のフーリエ変換である形状因子P(q)と、散乱体同士の空間相関のフーリエ変換である構造因子S(q)に分けて解析することによって、物質の構造の詳細が分かる。

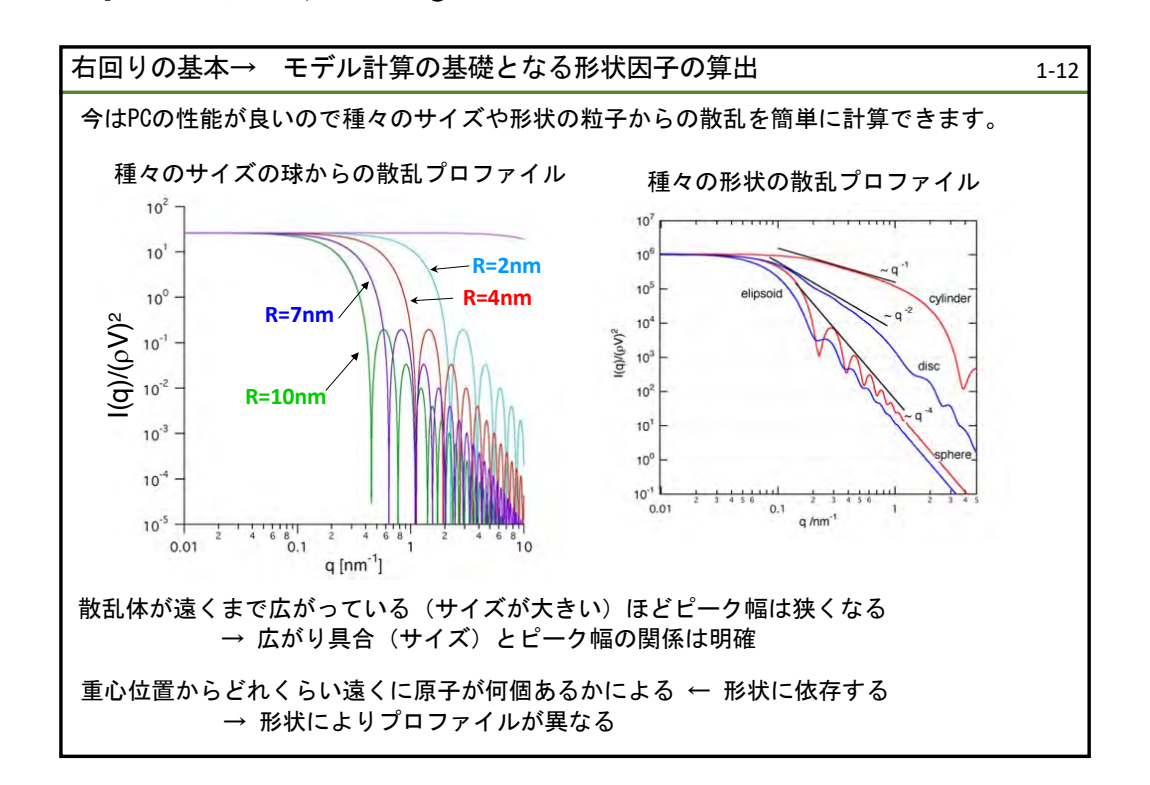
形状因子

散乱体の形状(形と大きさ)のFourier変換



形状因子を実験的に求める方法

- 希薄系(濃度数%程度)ならばS(Q)~1と仮定できるので、構造因子を考えなくて良い。
- 得られた小角散乱プロファイルを既知のモデルと比較してフィッティングする。



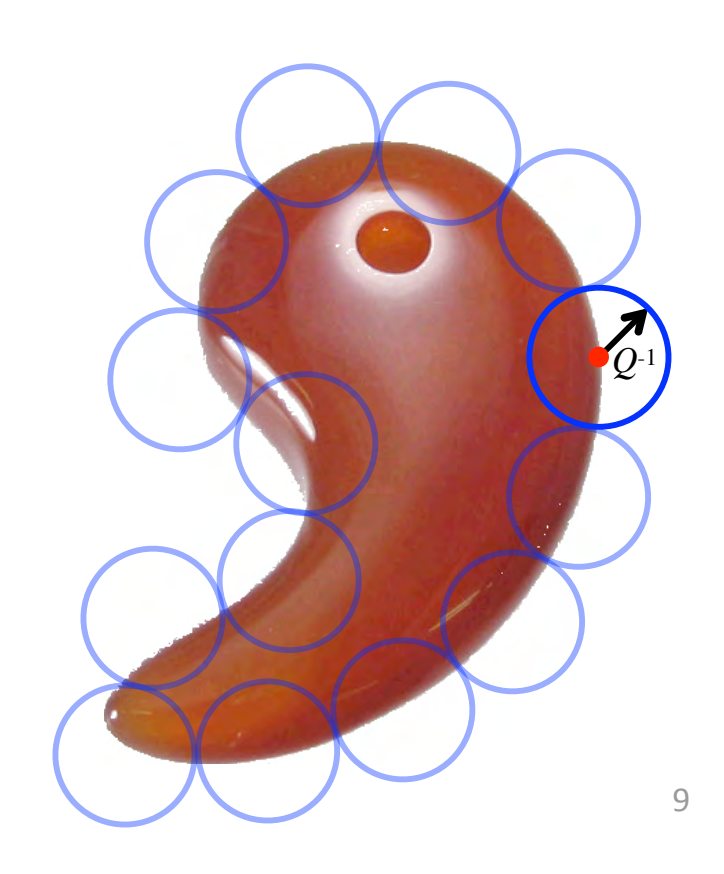
濃厚系や多分散系等の場合

まずは簡単な近似からスタート

Guinier近似

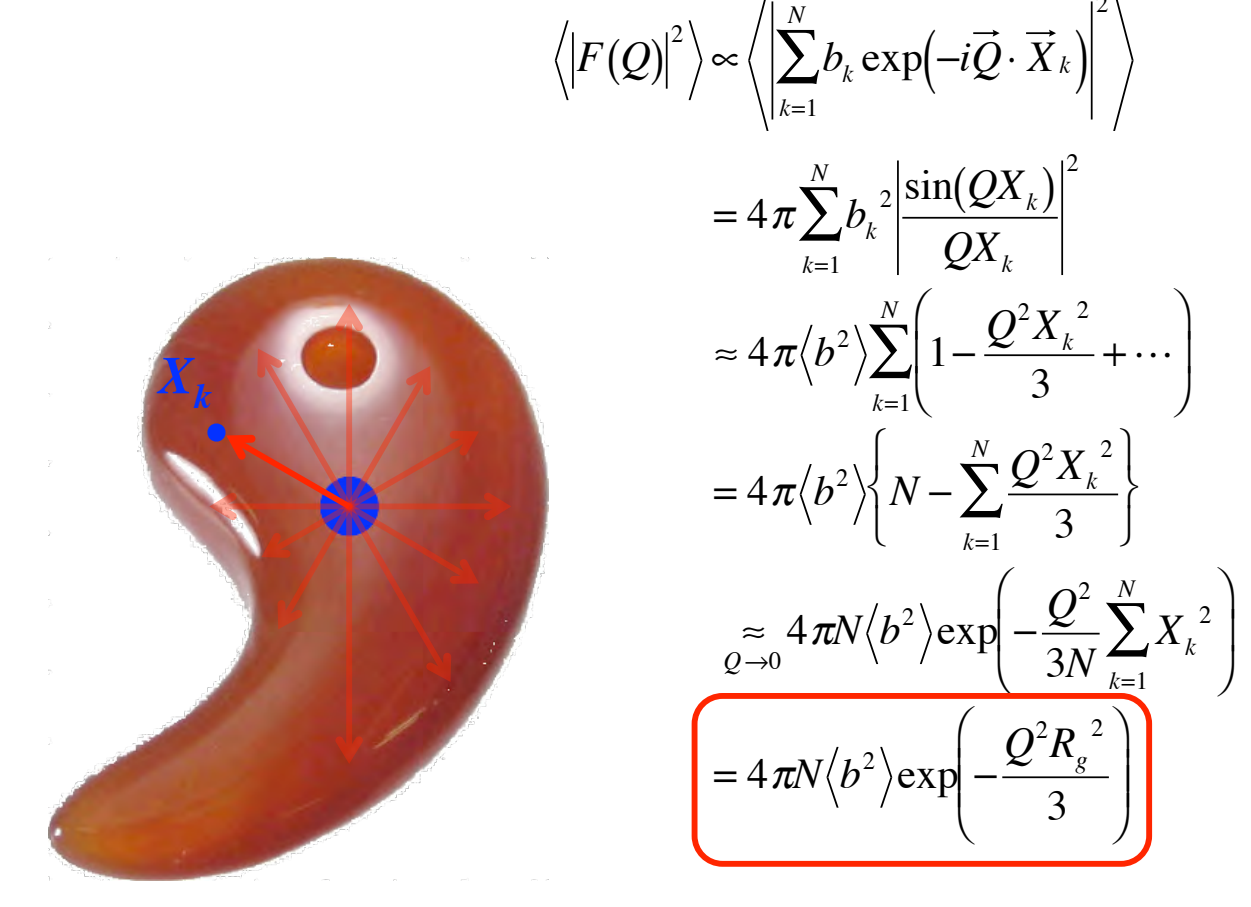


Porod則



Guiner近似

形状因子F(Q)をマクローリン展開し、2次の項まで考慮した近似。





André Guinier(1911-2000: フランス人)

回転二乗半径R_g2の定義

$$R_g^2 = \frac{1}{N} \sum_{k=1}^{N} X_k^2$$

 X_k : 重心からの距離

Q→0の極限で、散乱強度は回転半径の関数として記述出来る。
(光散乱でも有用な法則)

回転半径

例1:「半径Rの球」の回転二乗半径

$$R_g^2 = \frac{1}{N} \sum_{k=1}^{N} X_k^2 = \frac{\int_0^R X^4 dX}{\int_0^R X^2 dX} = \frac{3}{5} R^2$$



$$R_g^2 = \frac{1}{N} \sum_{k=1}^{N} X_k^2 = \frac{\int_{-L/2}^{L/2} X^2 dX}{\int_{-L/2}^{L/2} dX} = \frac{L^2}{12}$$

二次のモーメント の計算

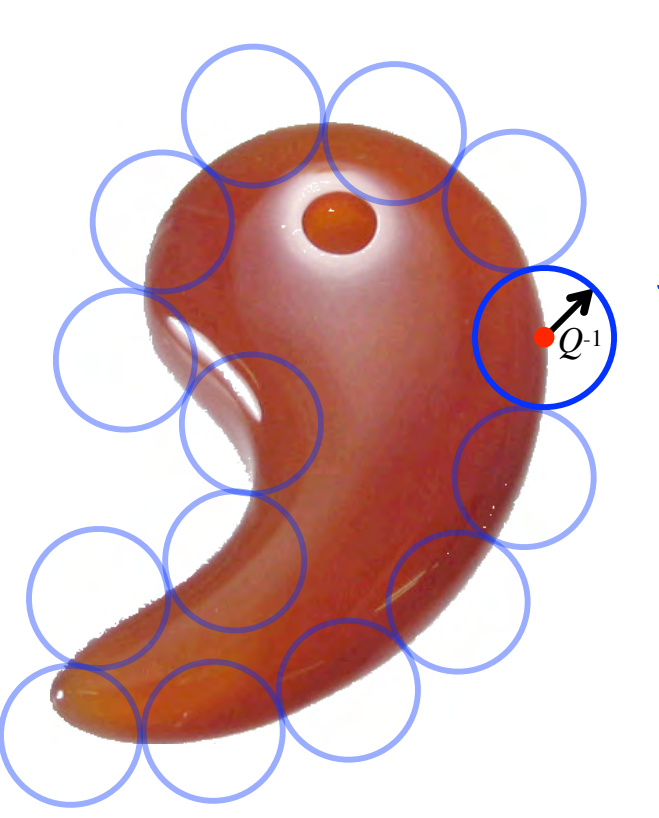


$$R_g^2 = \frac{1}{N} \sum_{k=1}^{N} X_k^2 = \frac{\int_0^r X^3 dX}{\int_0^r X dX} = \frac{r^2}{2}$$



Porod則

連続体近似では、Qが大きい領域($Q>> 1/R_g$)では界面からの散乱が支配的になる.



$$I(Q) = 2\pi\Delta\rho^2 \frac{S}{V} Q^{-4}$$



Günther Porod (1919 - 1984: Graz 大学・オーストリア人)

比界面積:単位体積あたりの界面積

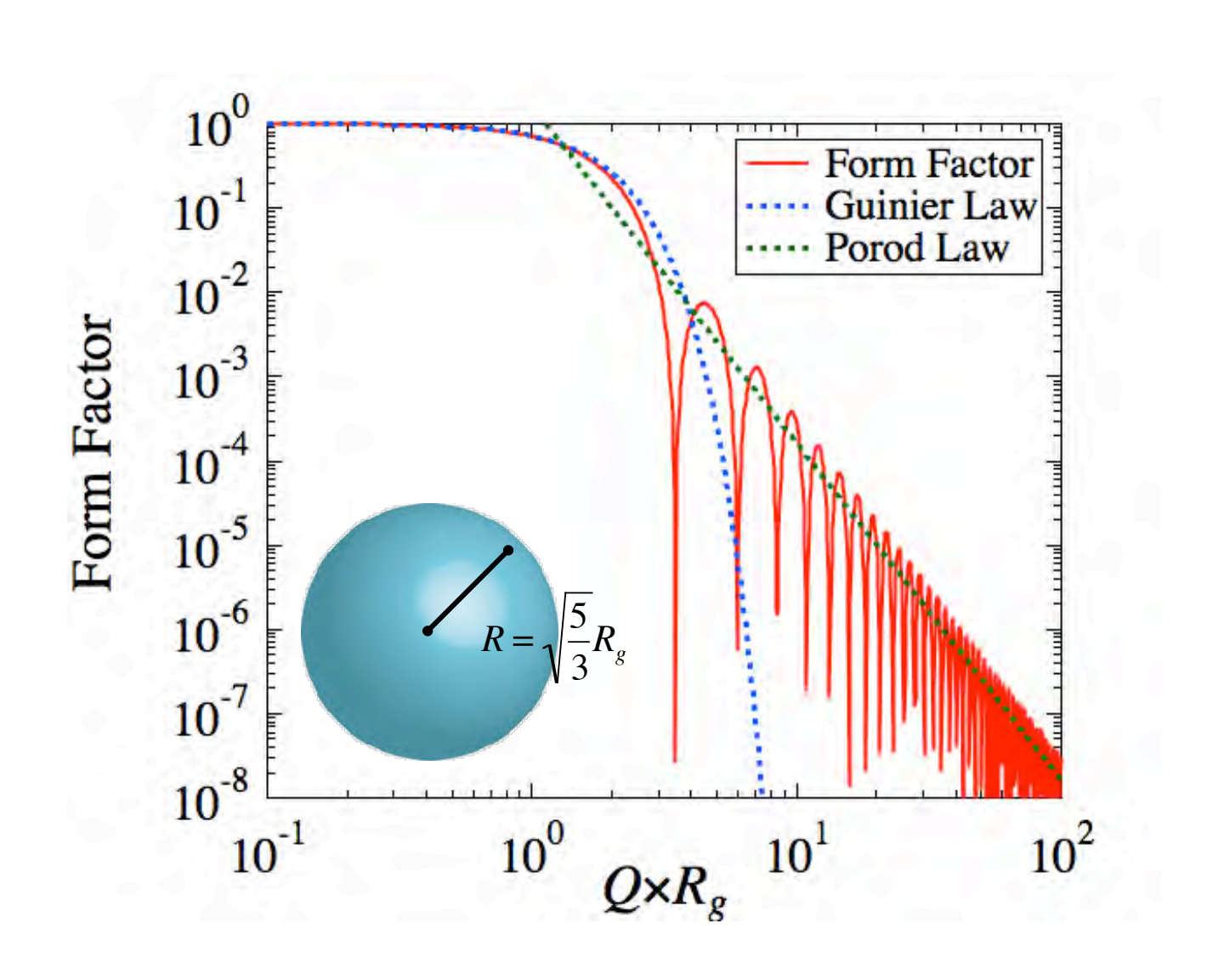
球(半径R)の場合: $S/V = 4\pi R^2 \times n$

円柱(半径R, 高さh)の場合: $S/V = (2\pi R^2 + 2\pi Rd) \times n$

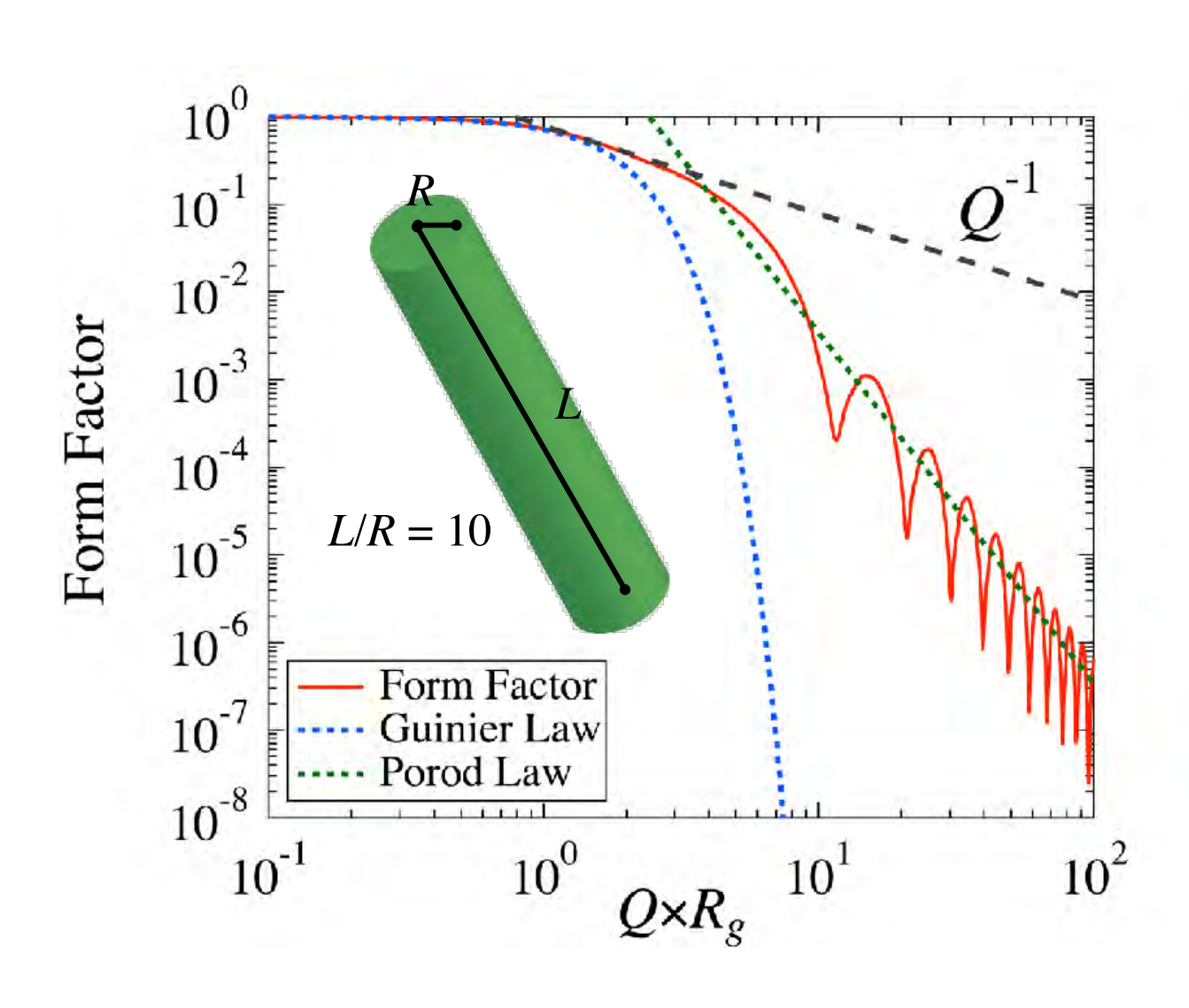
n: 散乱体の数密度

絶対強度が分かれば、 $Q>> 1/R_g$ で界面積が定量的に評価出来る. (界面積が大きいと散乱強度は増す。)

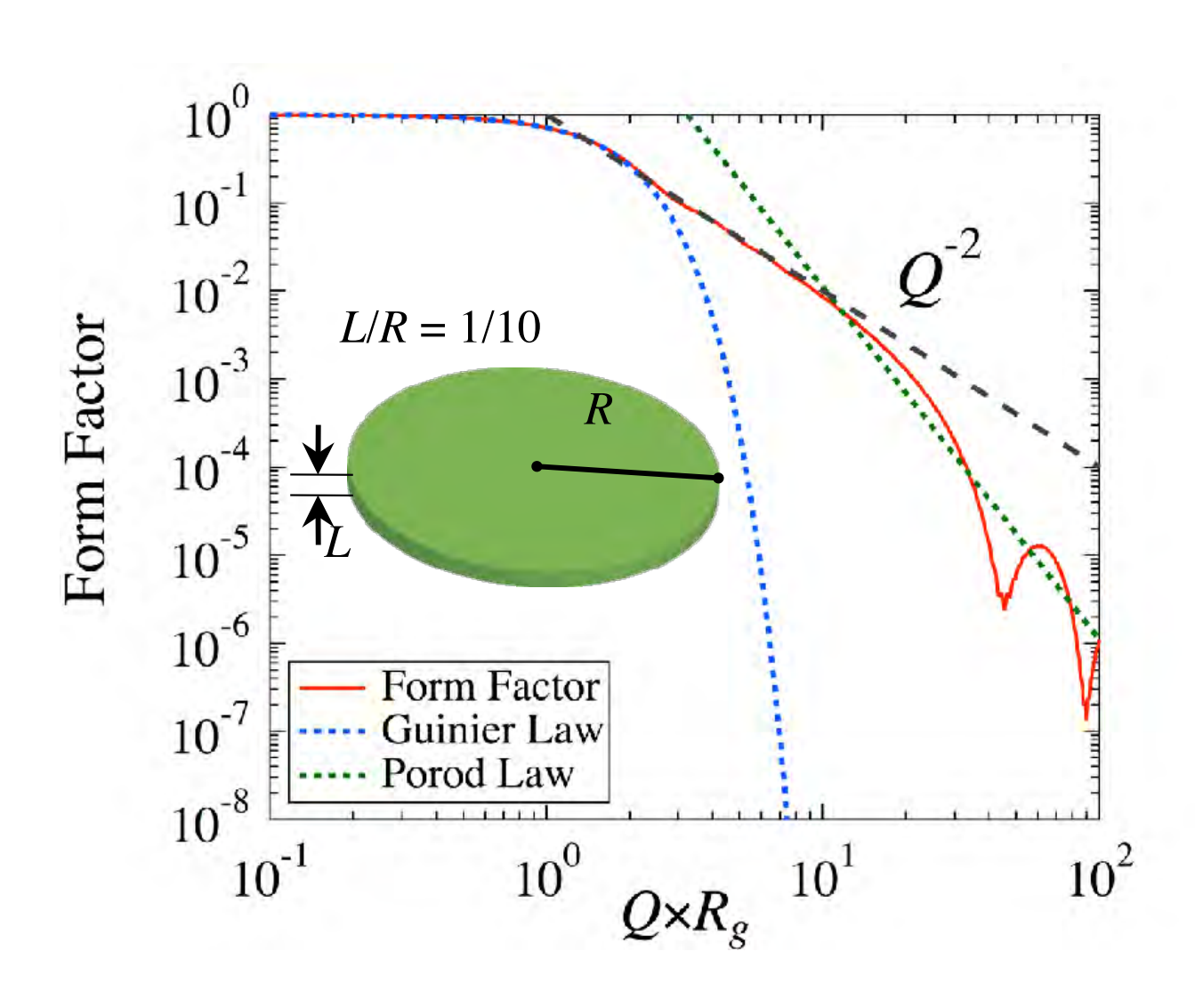
球の形状因子



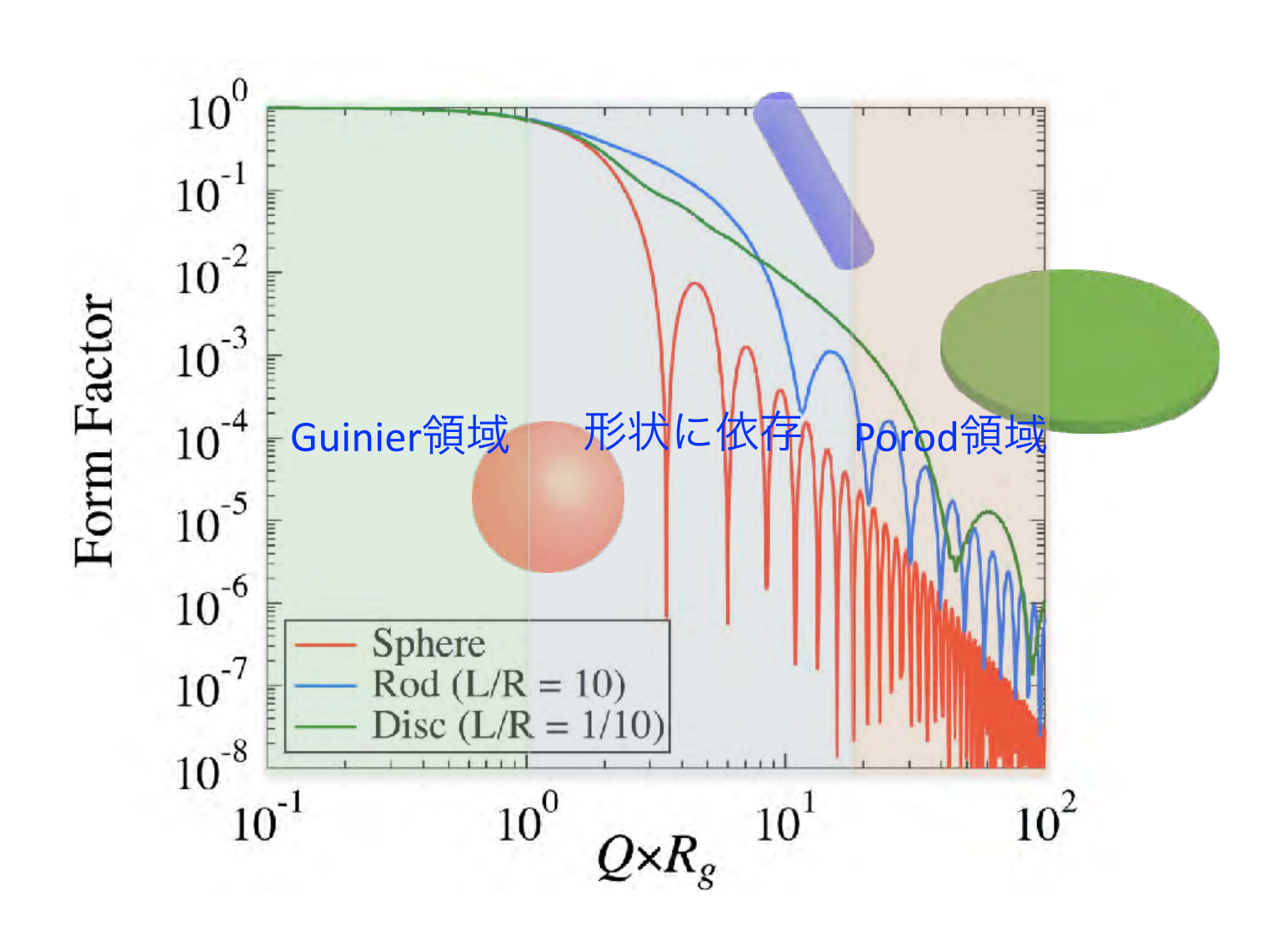
円柱の形状因子



円盤の形状因子

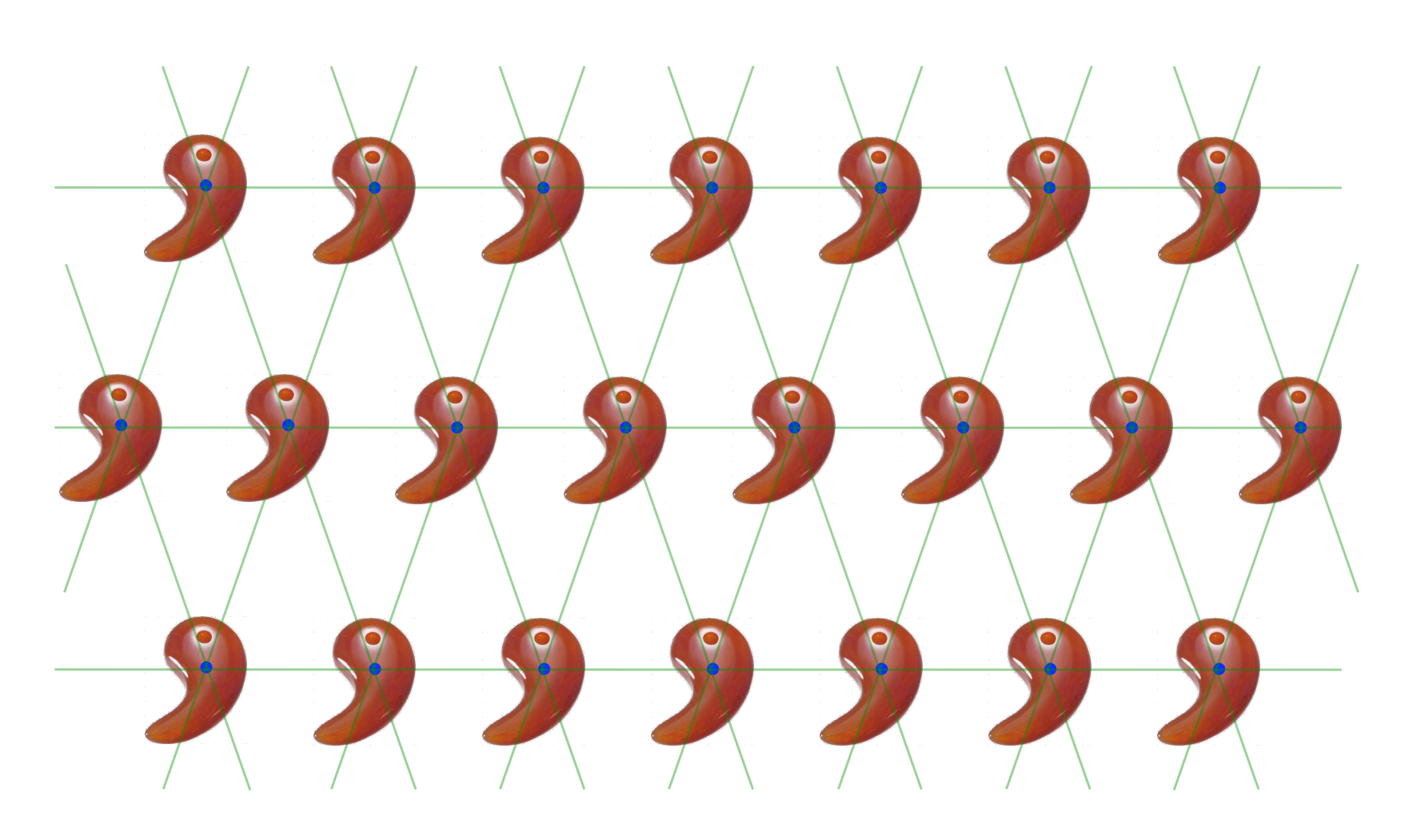


形状因子の比較



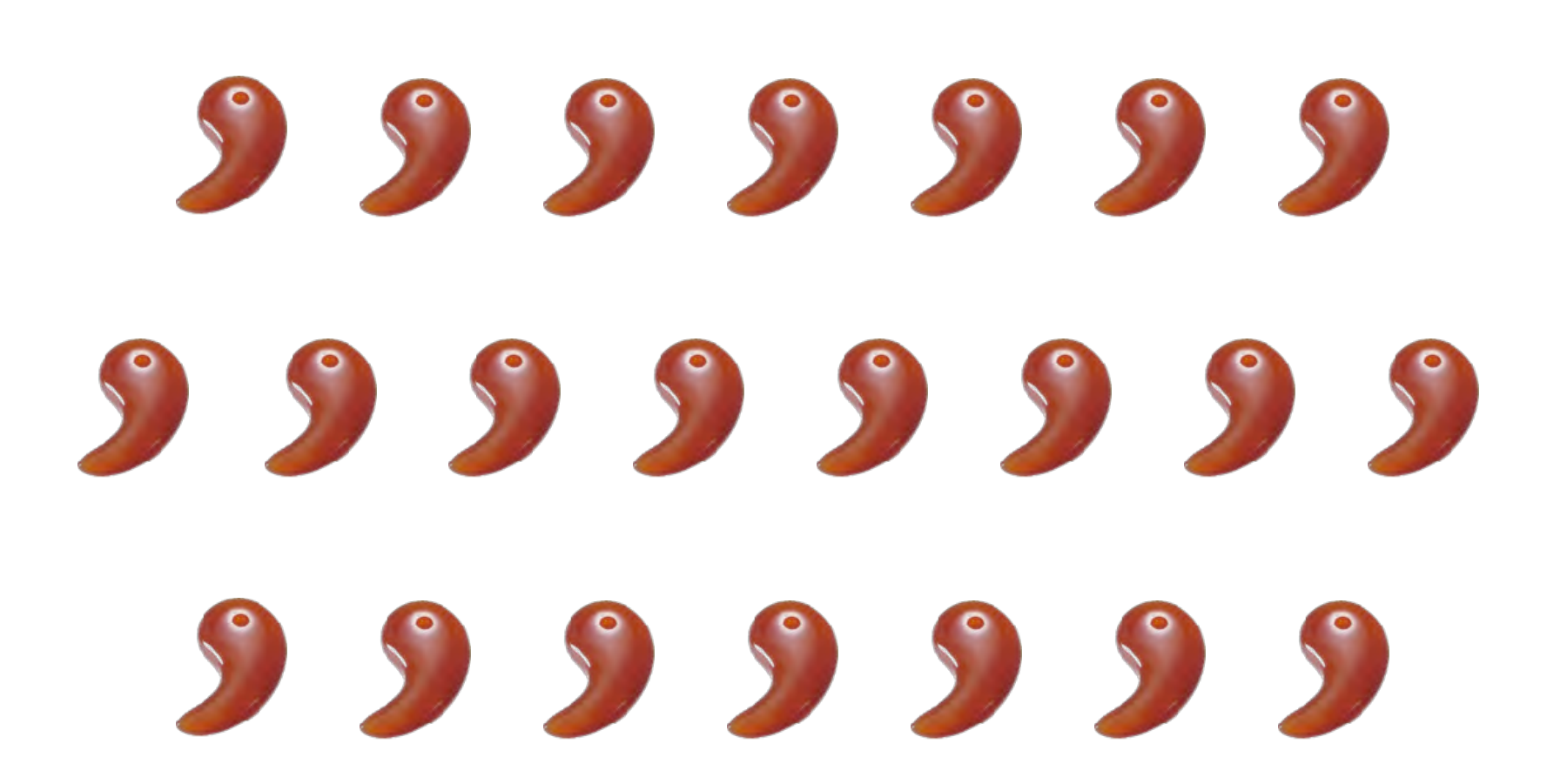
構造因子

各粒子の重心の位置の相関を表す



構造因子は粒子間の相互作用によって決まる:適切なモデルを使わなければ解けない

小角散乱強度=形状因子×構造因子



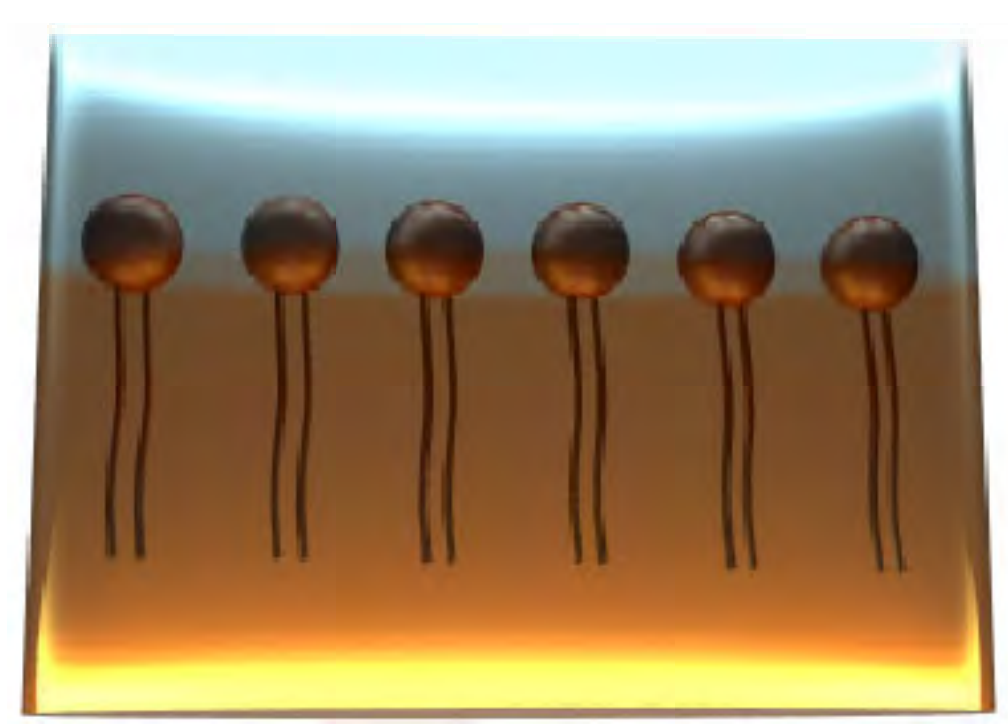
研究例-1

Microemulsion

マイクロエマルションの臨界現象

H. Seto, et al. J. Chem. Phys. 99, 5512 (1993)

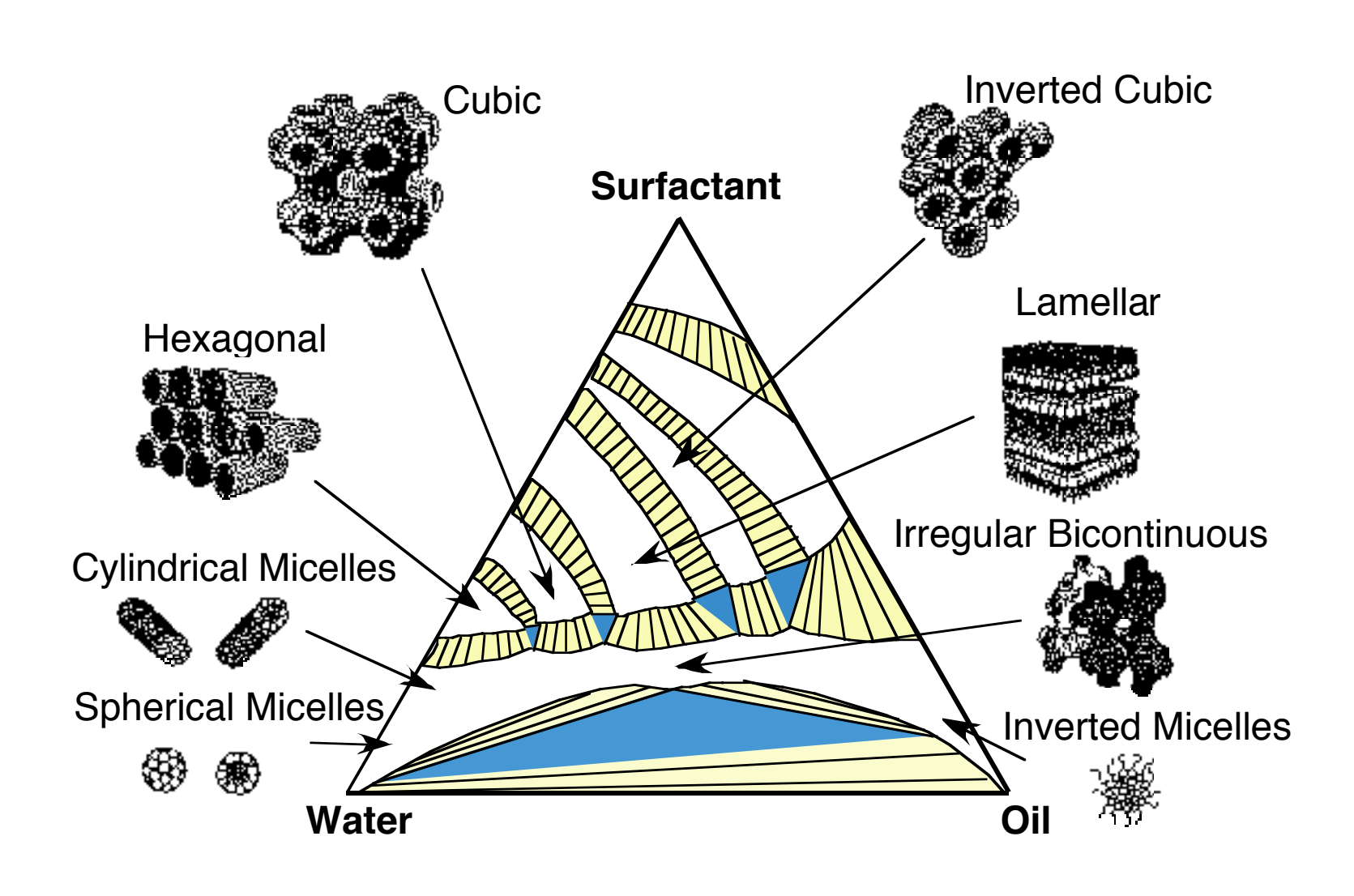
hydrophilic hydrophobic



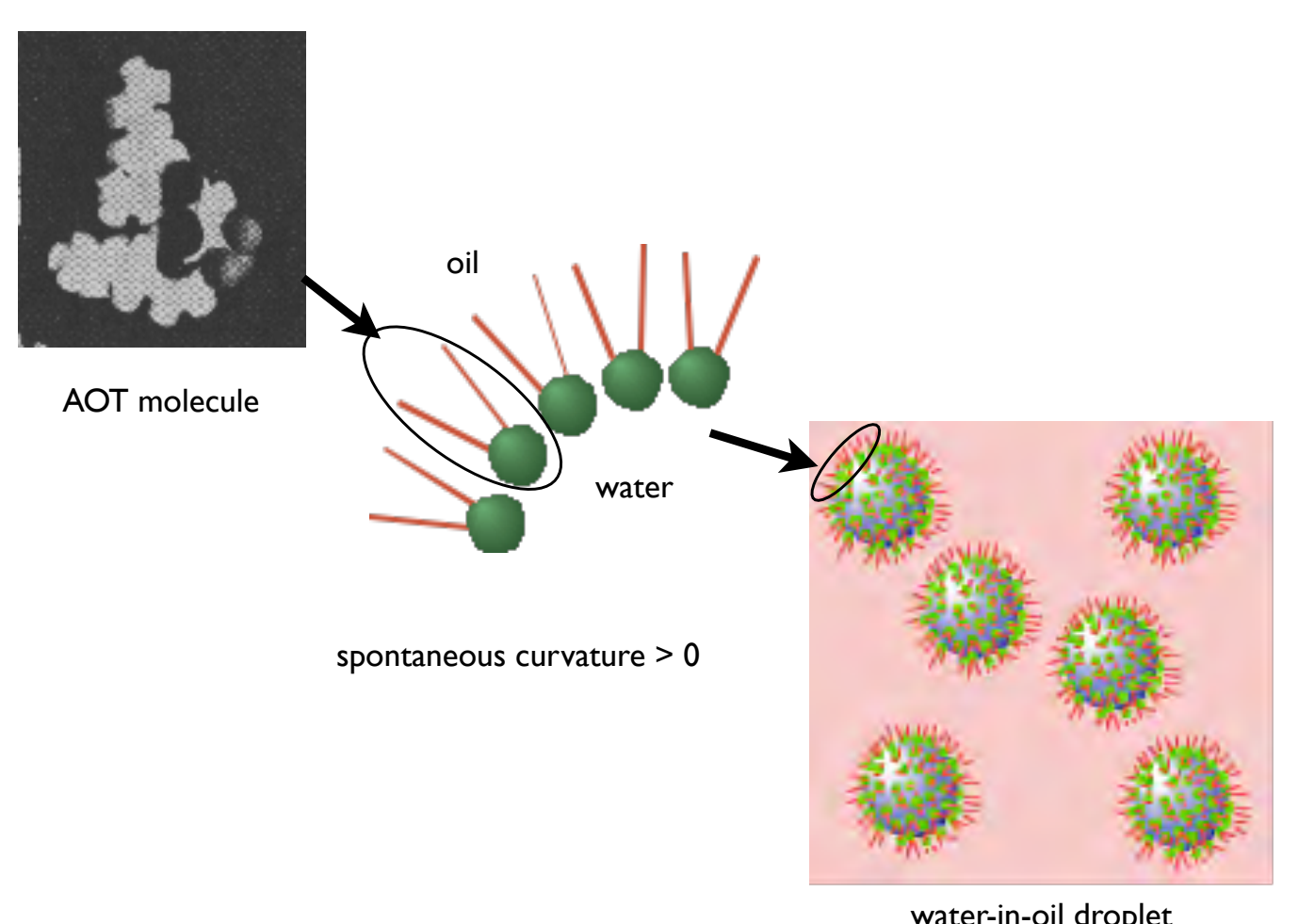
water

oil

マイクロエマルションの構造

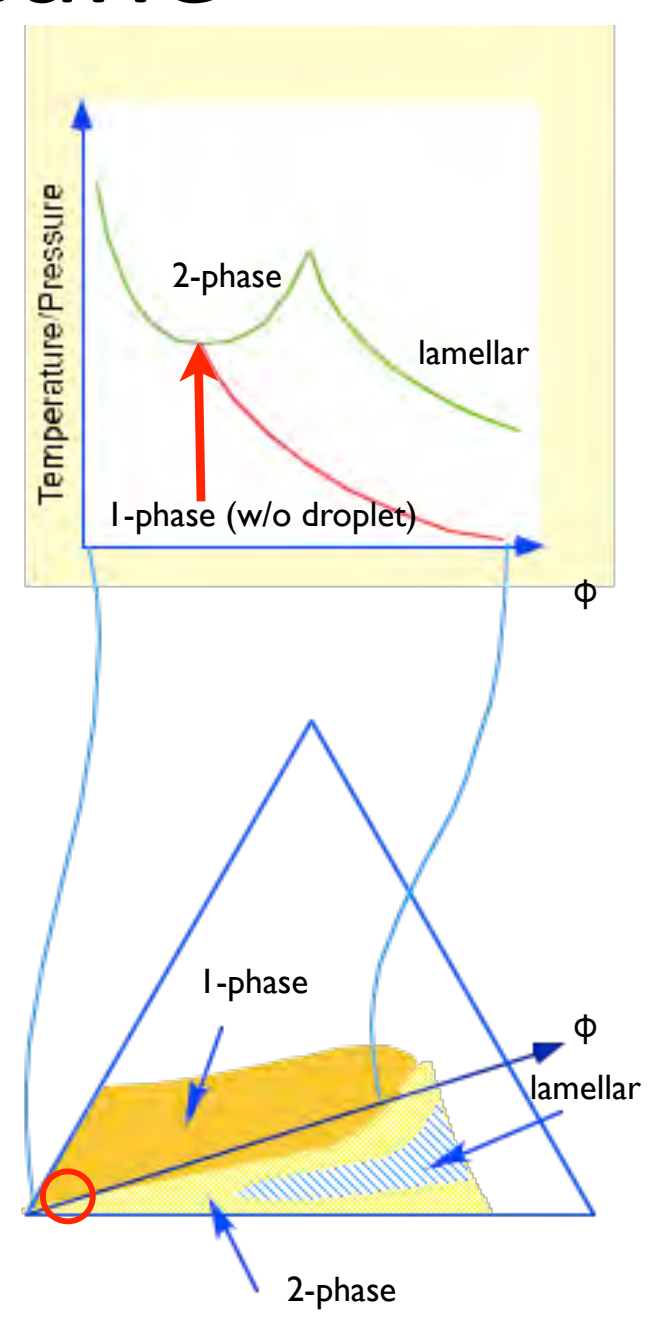


$AOT + D_2O + n$ -decane



water-in-oil droplet

dropletの相分離に伴う臨界現象を調べる H. Seto, et al. J. Chem. Phys., 1993



dropletの形状因子

$$I(Q) = \frac{I^{\text{obs}}(Q)}{\int Q^2 I^{\text{obs}}(Q) dQ} = F(Q)S(Q) (\mathring{A}^3)$$

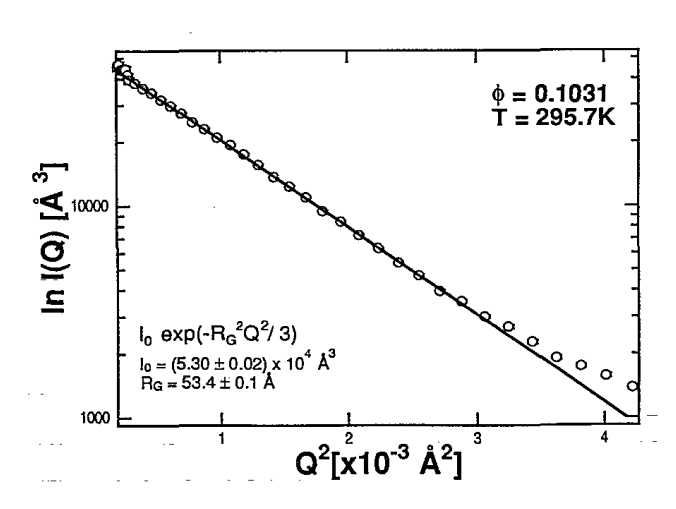


FIG. 2. The scattering profile for ϕ =0.1031 at T=295.72 K in the Guinier plot is presented. The straight line indicates the fitted Guinier approximation.

$$\begin{split} F(Q) = & \frac{I_0^G \exp(-R_G^2 Q^2/3)}{\int Q^2 I^{\text{obs}}(Q) dQ} \\ = & \frac{\phi_w \Delta \rho^2 \Omega \exp(-R_G^2 Q^2/3)}{2\pi^2 \phi_w (1 - \phi_w) \Delta \rho^2} \\ = & \frac{\Omega \exp(-R_G^2 Q^2/3)}{2\pi^2 (1 - \phi_w)}, \end{split}$$

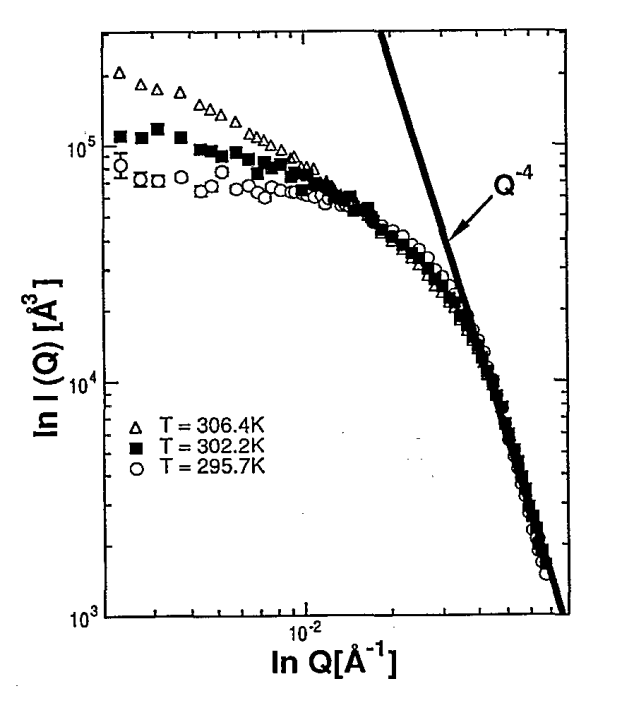


FIG. 4. Temperature change of the observed scattering profiles for $\phi=0.1031$ in double logarithmic plot are presented. The straight line indicates the Q^{-4} line suitable for the observed profiles of high-Q region.

$$F(O) = P'O^{-4}$$

with

$$P' = \frac{2\pi(\phi_w/\Omega)S\Delta\rho_{dw}^2}{\int Q^2 I^{\text{obs}}(Q)dQ} = \frac{3}{\pi(1-\phi_w)R}$$

形状因子と構造因子

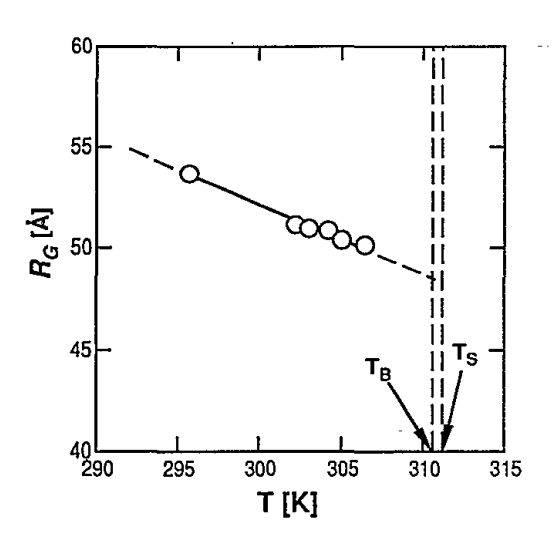


FIG. 3. Temperature variations of the observed Guinier radius for $\phi=0.1031$ is given. The open circles are the observed points, and the solid and dashed line is the fitted straight line. Error bars are less than the size of the plot characters. In order to determine the form factor for all the scattering curves, this fitted values were used.

$$\begin{split} F(Q) = & \frac{I_0^G \exp(-R_G^2 Q^2/3)}{\int Q^2 I^{\text{obs}}(Q) dQ} \\ = & \frac{\phi_w \Delta \rho^2 \Omega \exp(-R_G^2 Q^2/3)}{2\pi^2 \phi_w (1 - \phi_w) \Delta \rho^2} \\ = & \frac{\Omega \exp(-R_G^2 Q^2/3)}{2\pi^2 (1 - \phi_w)}, \\ S(Q) = & I(Q) / F(Q) \end{split}$$

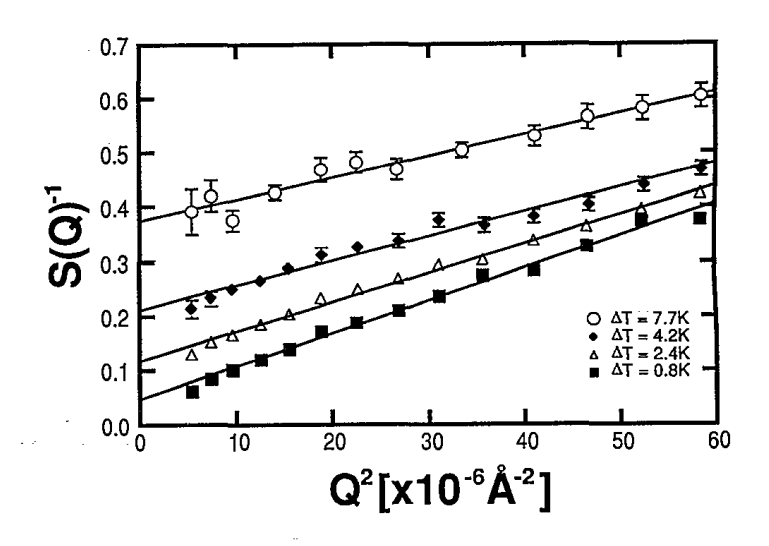


FIG. 5. The scattering profile in Zimm representation at different temperatures; horizontal axis denotes the square of wave number Q and the vertical axis the inverse of structure factor S(Q), for $\phi=0.1031$ composition. The open circles are the data taken at $\Delta T=7.69$ K, difference from the spinodal point T_s , the full rhombus at $\Delta T=4.18$ K, the open triangles at $\Delta T=2.44$ K, and the full squares at $\Delta T=0.81$ K. Straight lines indicate the fitted Ornstein–Zernike formula.

Ornstein-Zernike

$$S(Q) = S(0)/(1 + \xi^2 Q^2)$$

浸透圧縮率: x

相関距離: ξ

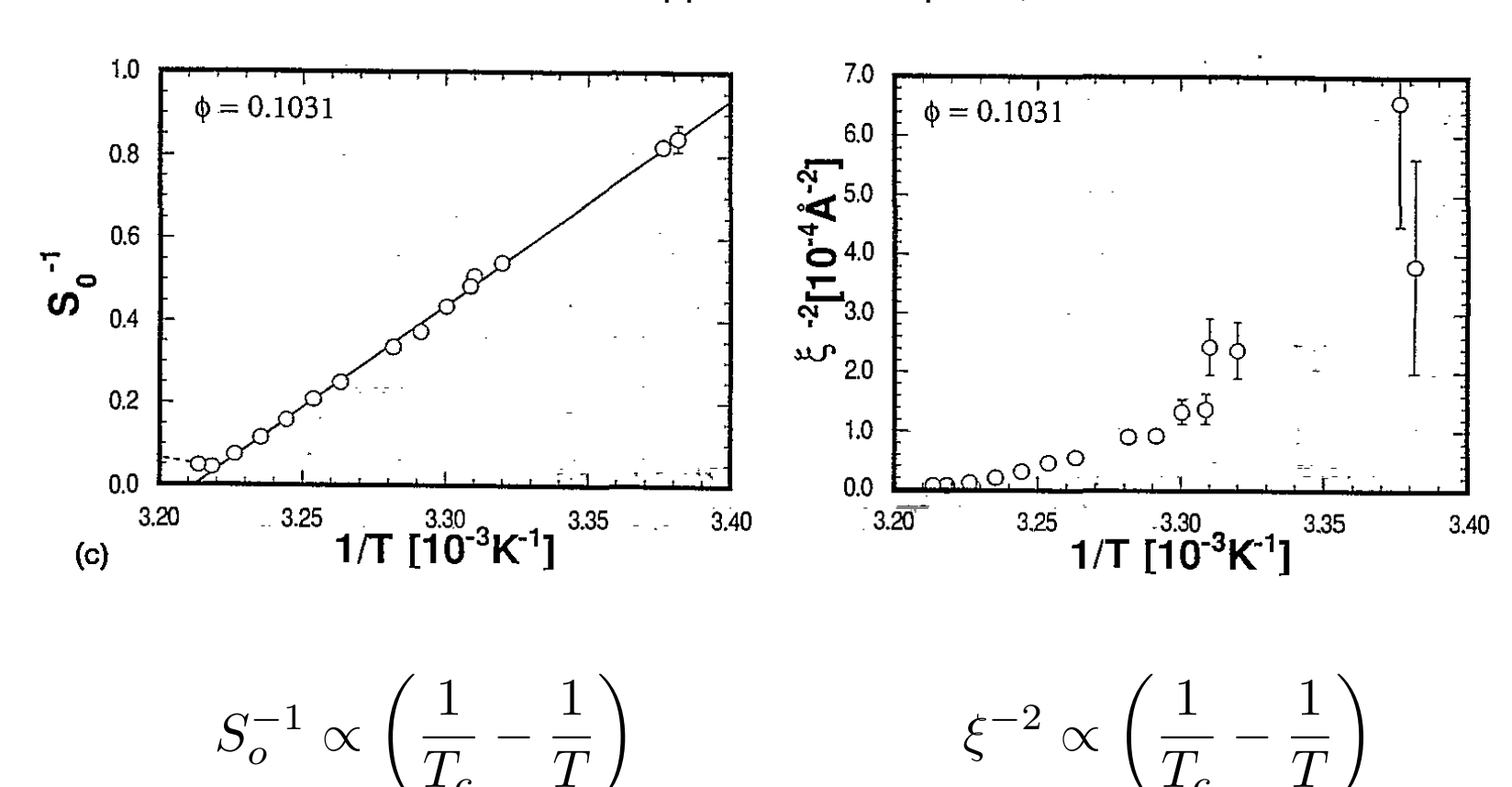
Zimm plot

$$S(Q)^{-1} = 1 + \xi^2 Q^2$$

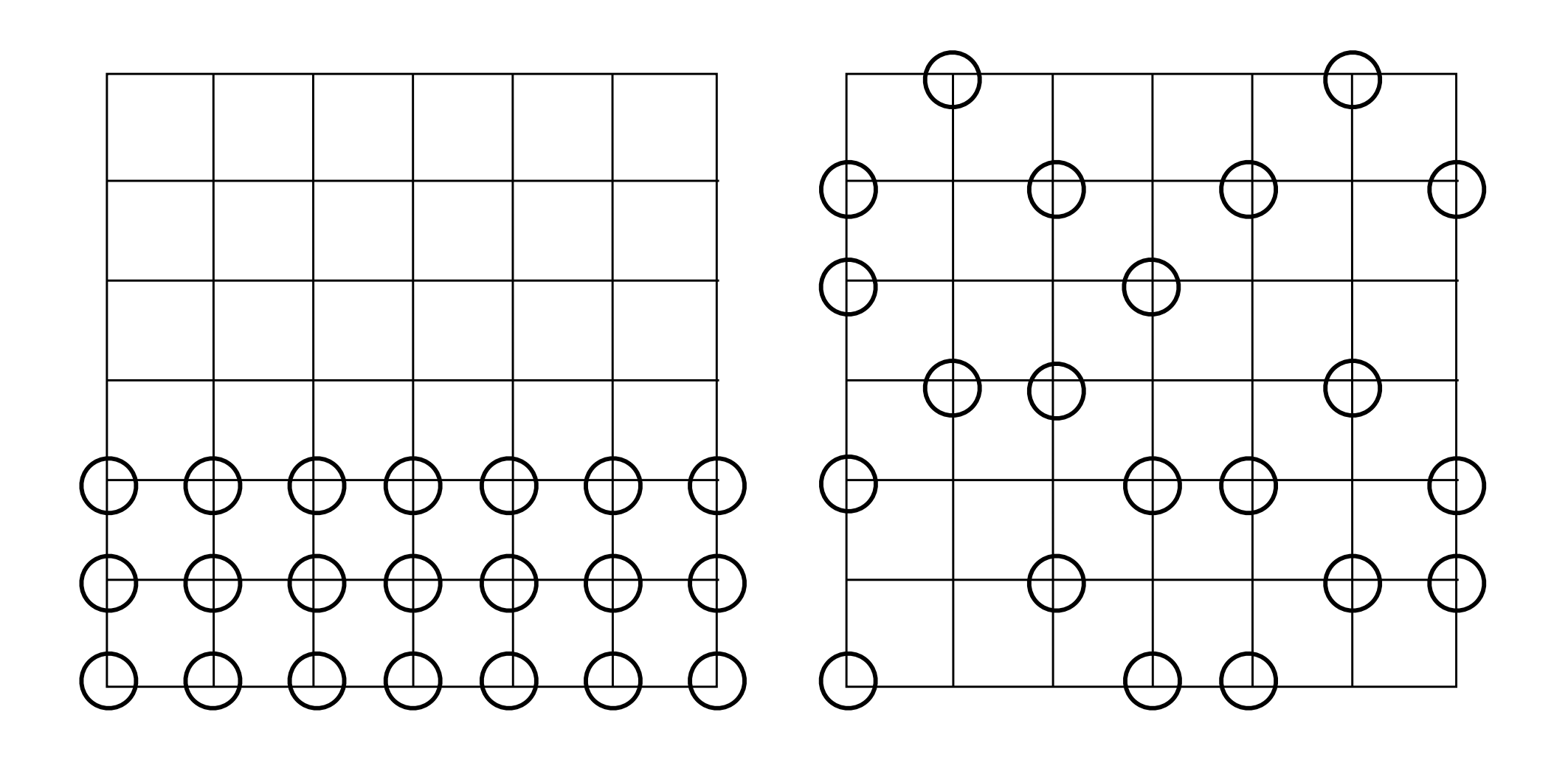
臨界散乱の温度変化

$$\chi = \chi_0 \left| \frac{T - T_c}{T_c} \right|^{-\gamma}$$
 $\xi = \xi_0 \left| \frac{T - T_c}{T_c} \right|^{-\nu}$

Mean Field Approximation: γ=1.0, v=0.5



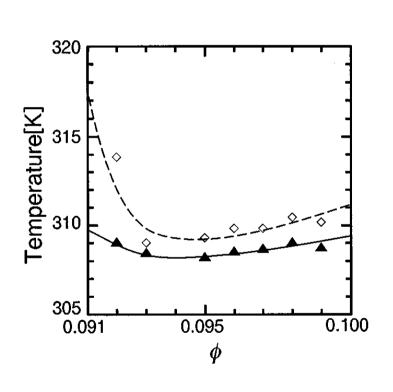
液体の相分離の臨界普遍性

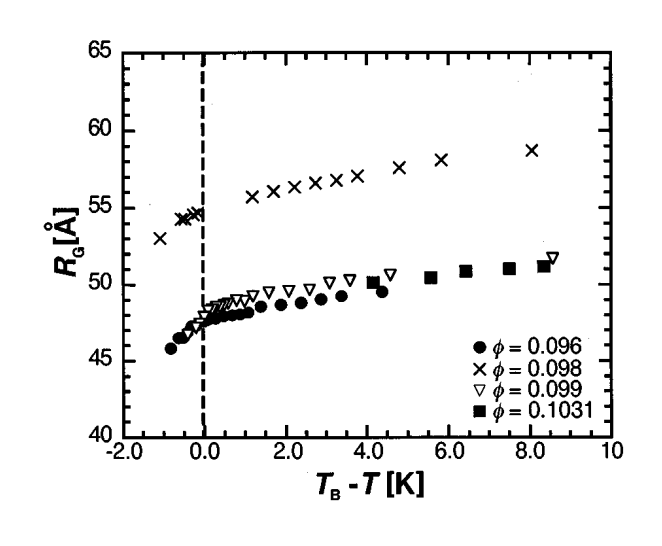


3d-Ising(γ=1.24, v=1.63)になるべき

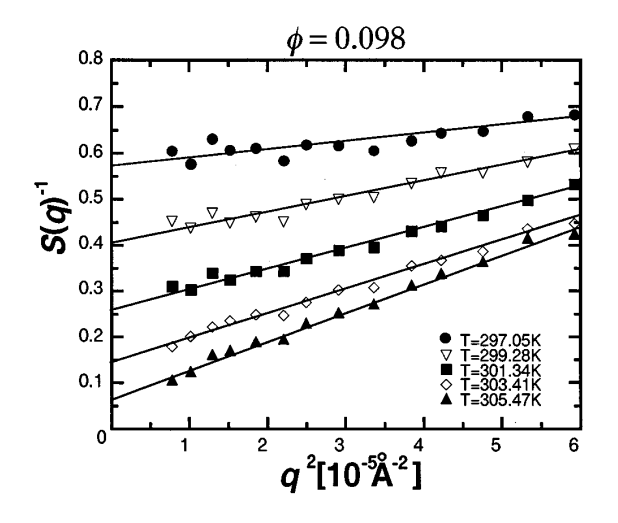
臨界現象を詳細に調べる

H. Seto, et al. Phys. Rev. E, 1996



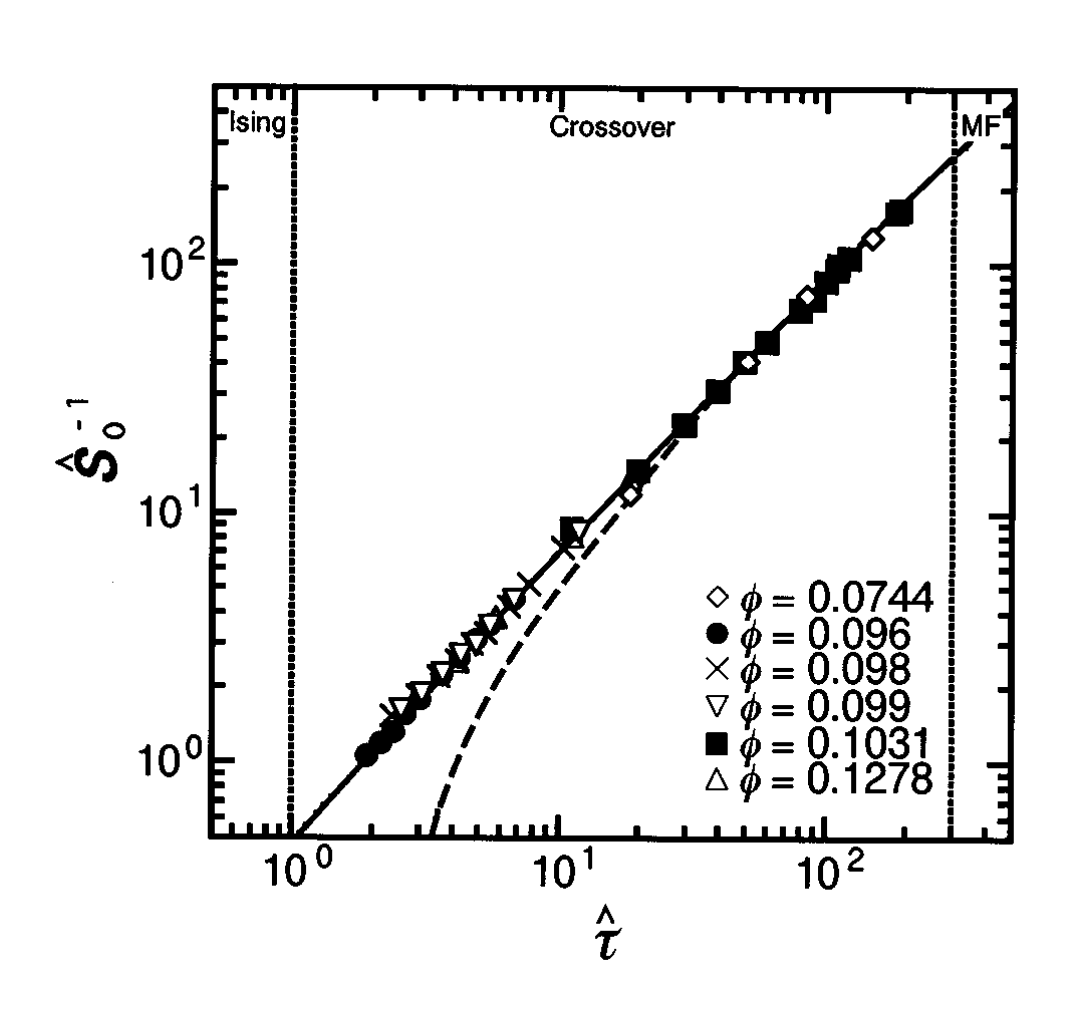


$$P(q) \propto \exp(-R_G^2 q^2/3)$$



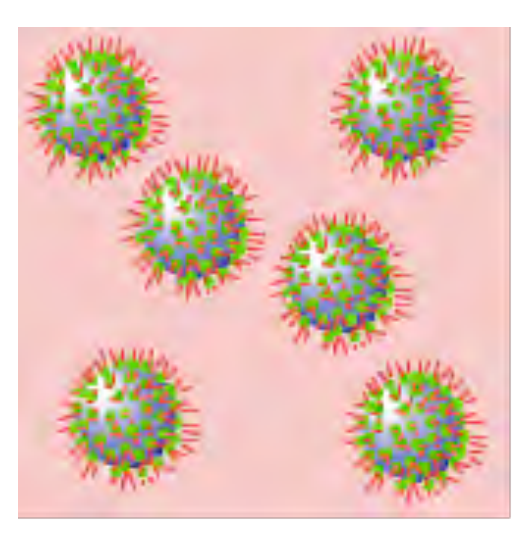
$$S(q) = S_0/(1 + \xi^2 q^2)$$

平均場から3d-Isingへの クロスオーバー



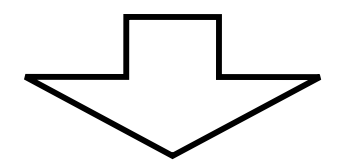
$$\hat{\tau} = (1 + 2.333 \hat{S}_0^{\Delta/\gamma})^{(\gamma - 1)/\Delta} [\hat{S}_0^{-1} + (1 + 2.333 \hat{S}_0^{\Delta/\gamma})^{-\gamma/\Delta}]$$

平均場になる理由

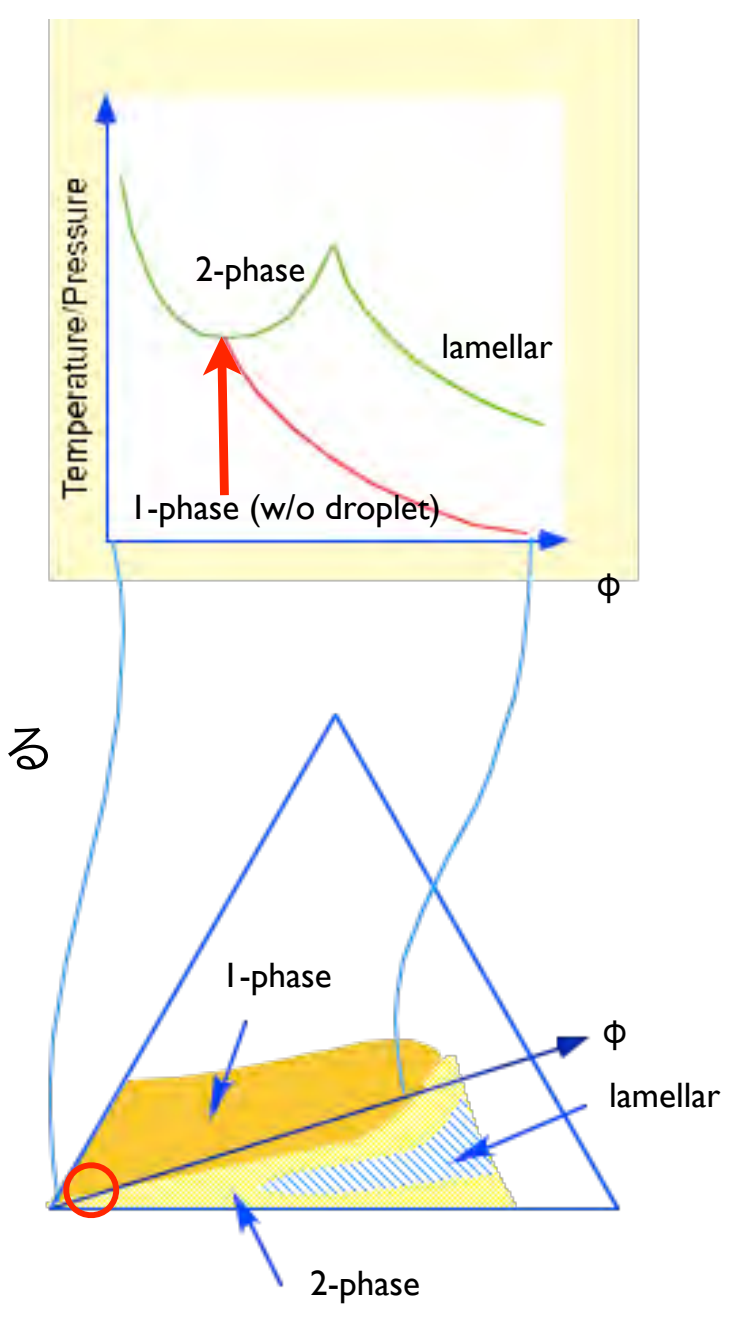


water-in-oil droplet

droplet間には電気的な相互作用が働いている

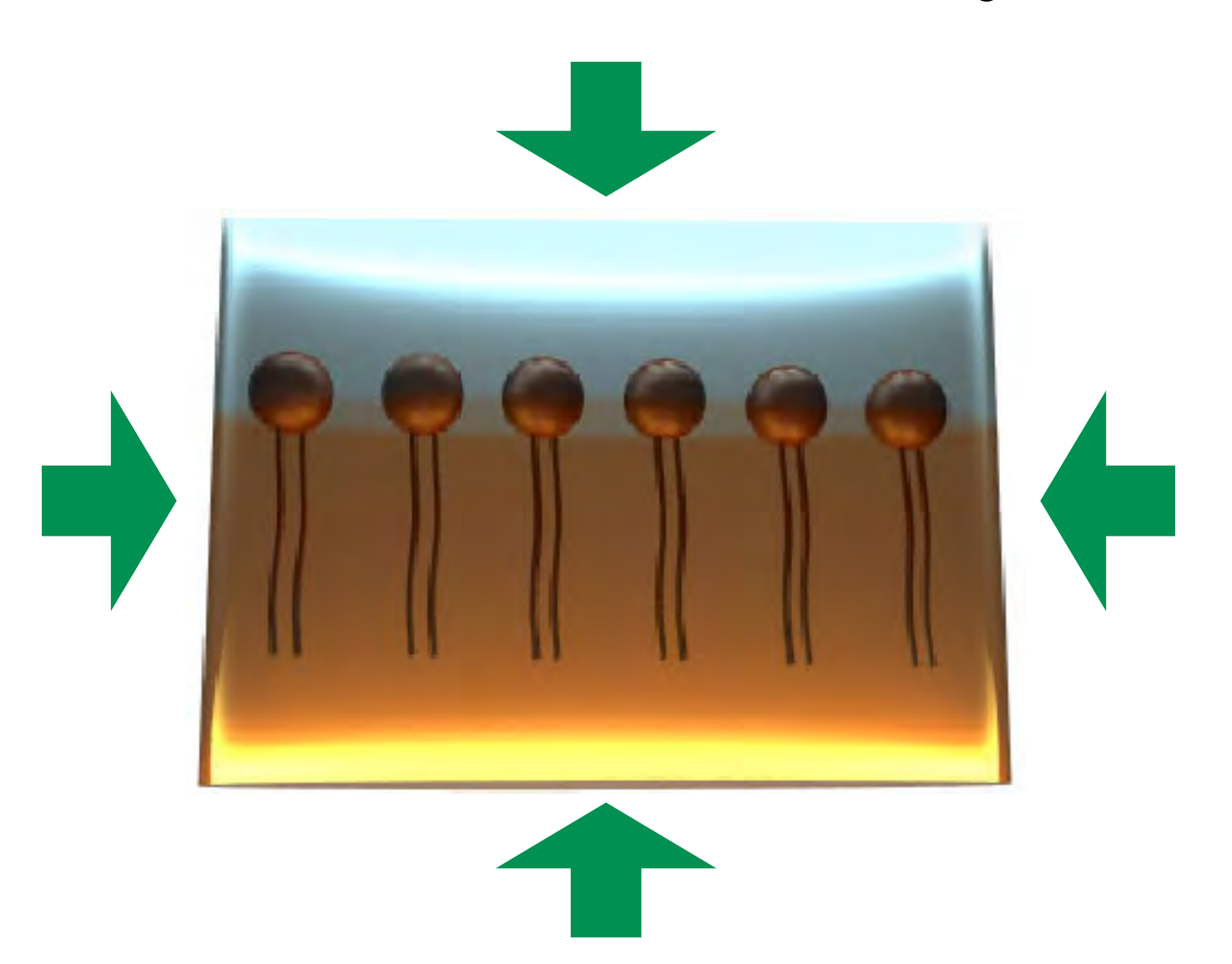


平均場近似:長距離相互作用を仮定

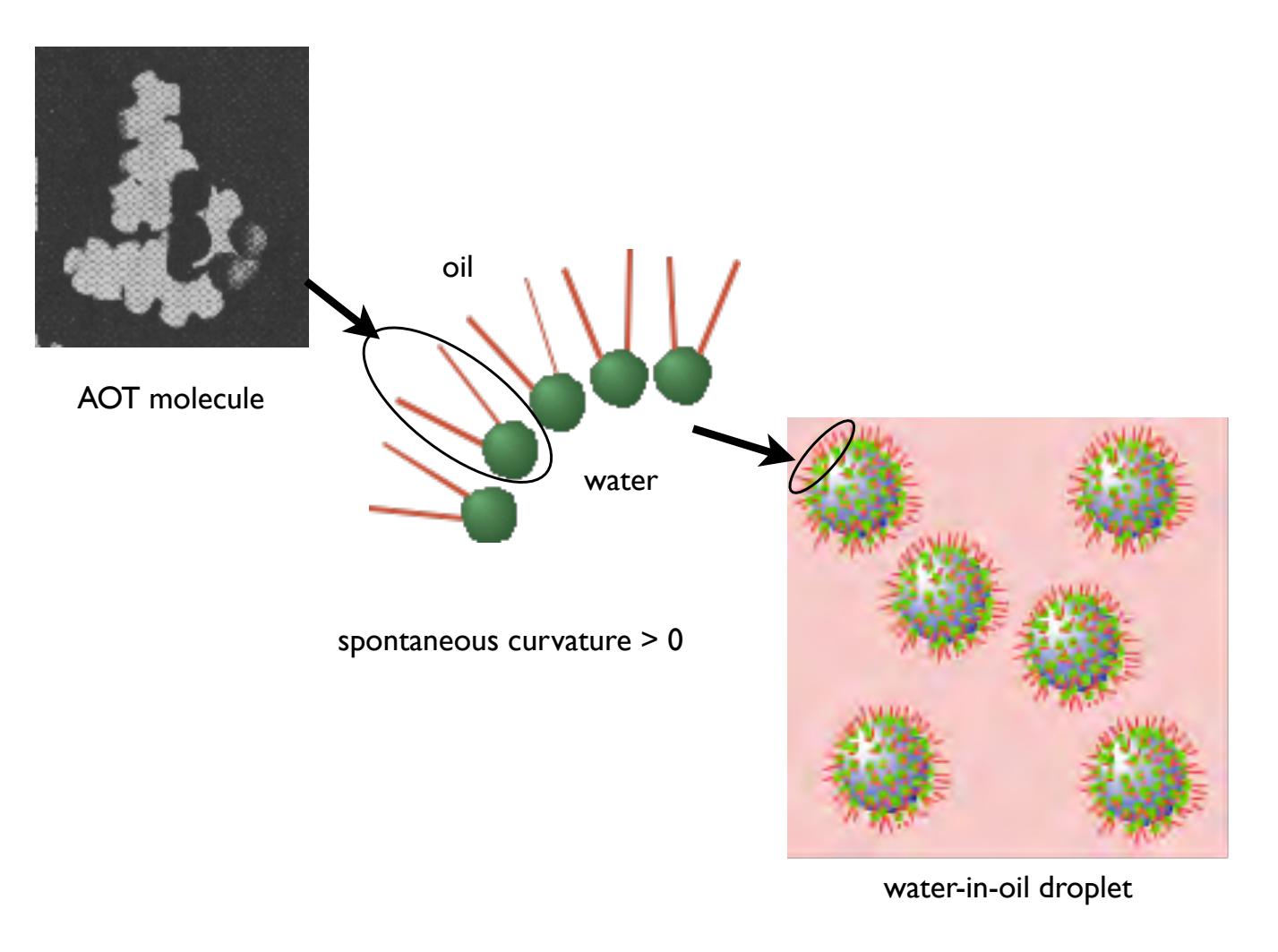


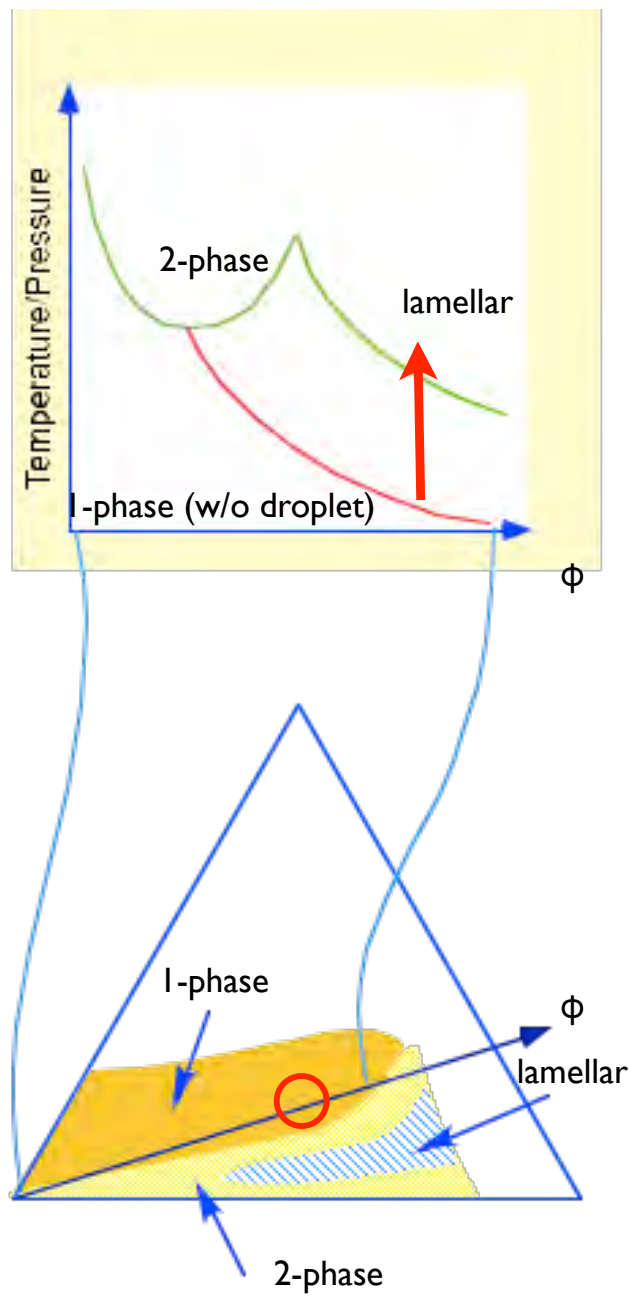
マイクロエマルションの構造の圧力変化

M. Nagao, HS, et al. 1999-2007

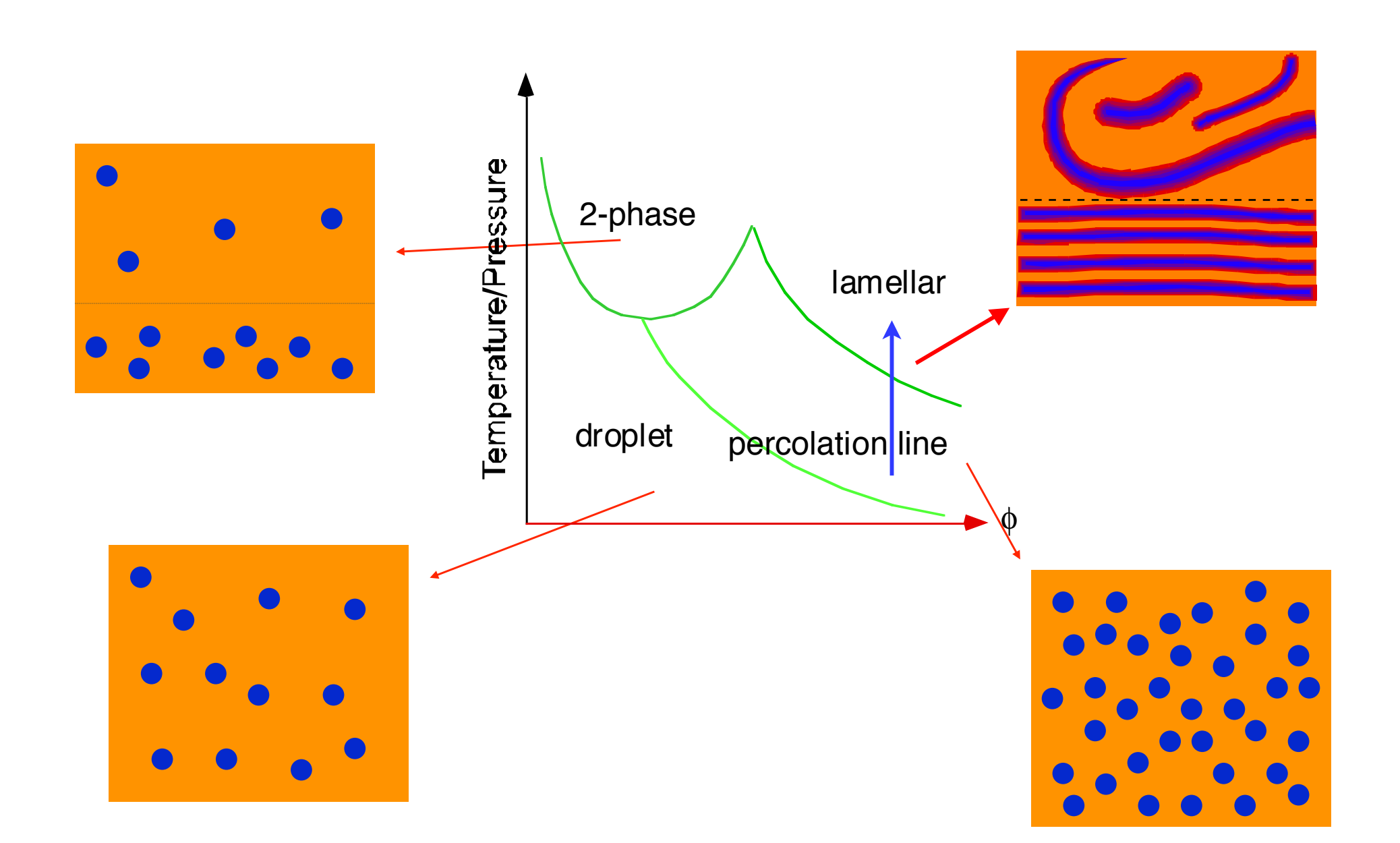


$AOT + D_2O + n$ -decane

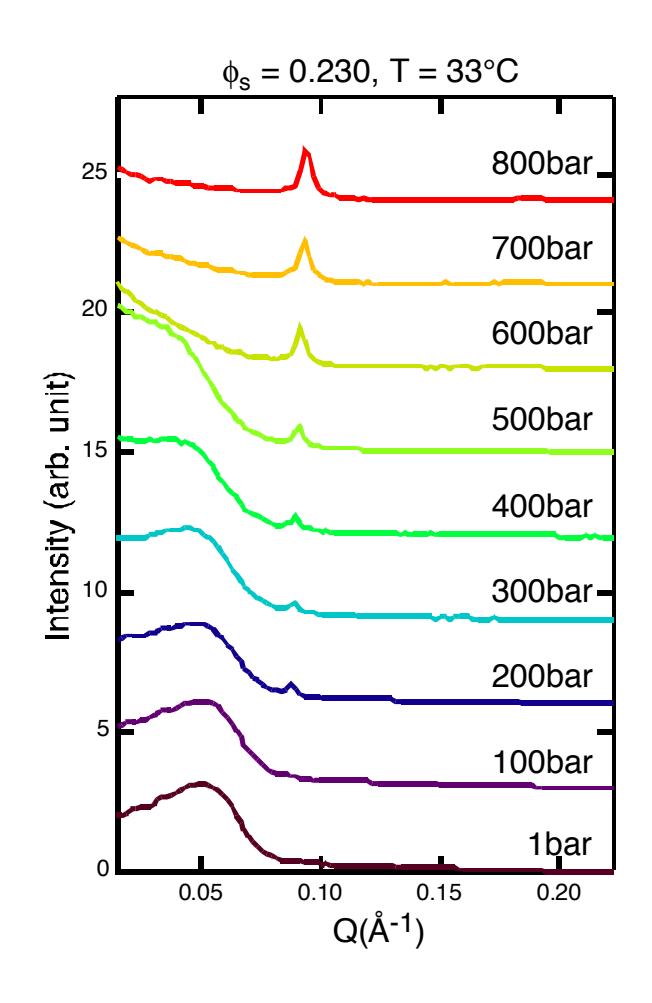


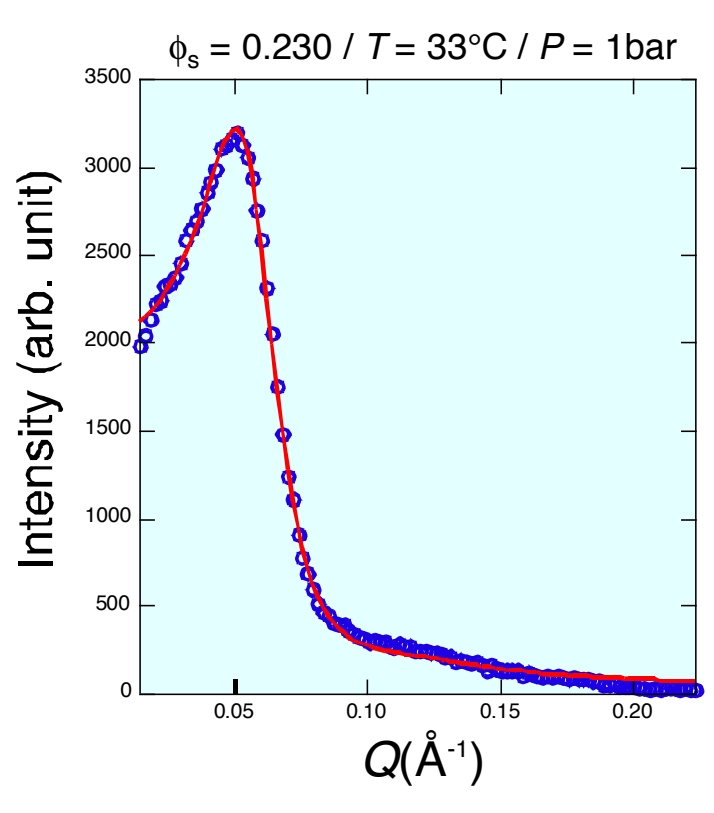


温度の効果=圧力の効果



X線小角散乱の結果

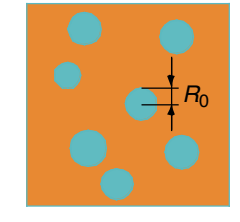




$$I(Q) = P(Q)S(Q)+L(Q)$$

P(Q): form factor of a dropletpolydisperseSchultz size distribution

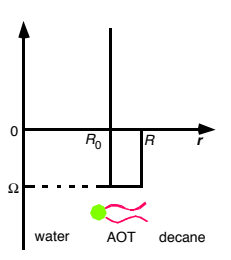
Kotlarchyk and Chen, J. Chem. Phys. 79 (1983) 2461.



S(Q): inter-droplet structure factor

hard-core and short-range attractive potential

Liu, Chen, Huang, Phys. Rev. E54 (1996) 1698.



L(Q): concentration fluctuation

= 1 /
$$(\xi_0^2 Q^2 + 1)$$

形状因子のモデル

Droplet form factor with Schultz size distribution:

$$P(Q) \propto R_0^6 (Z+1)^6 \alpha^{Z+7} G_1(Q),$$
 (1)

$$G_1(Q) = \alpha^{-(Z+1)} - (4+\alpha^2)^{-(Z+1)/2} \cos \left[(Z+1) \tan^{-1} \frac{2}{\alpha} \right]$$
$$+ (Z+2)(Z+1) \left\{ \alpha^{-(Z+3)} + (4+\alpha^2)^{-(Z+3)/2} \right\}$$

$$\times \cos \left[(Z+3) \tan^{-1} \frac{2}{\alpha} \right] - 2(Z+1)(4+\alpha^2)^{-(Z+2)/2}$$

$$\times \sin\left[(Z+2)\tan^{-1}\frac{2}{\alpha}\right],\tag{2}$$

$$\alpha = (Z+1)/QR_0. \tag{3}$$

構造因子のモデル

S(Q) for particles in the form of a hard sphere with an adhesive surface.

$$\frac{V(r)}{k_B T} = \begin{cases} +\infty & \text{for } 0 < r < R' \\ \Omega & \text{for } R' < r < R, \\ 0 & \text{for } R < r \end{cases}$$

Y. C. Liu, S. -H. Chen and J. S. Huang, Phys. Rev. E, 54, 1698 (1996).

Structure factor for the droplet size distribution exists or orientational averaging is necessary,

$$\frac{d\Sigma}{d\Omega}(Q) \propto P(Q)S'(Q)$$

$$S'(Q) = 1 + \beta(Q)[S(Q) - 1],$$

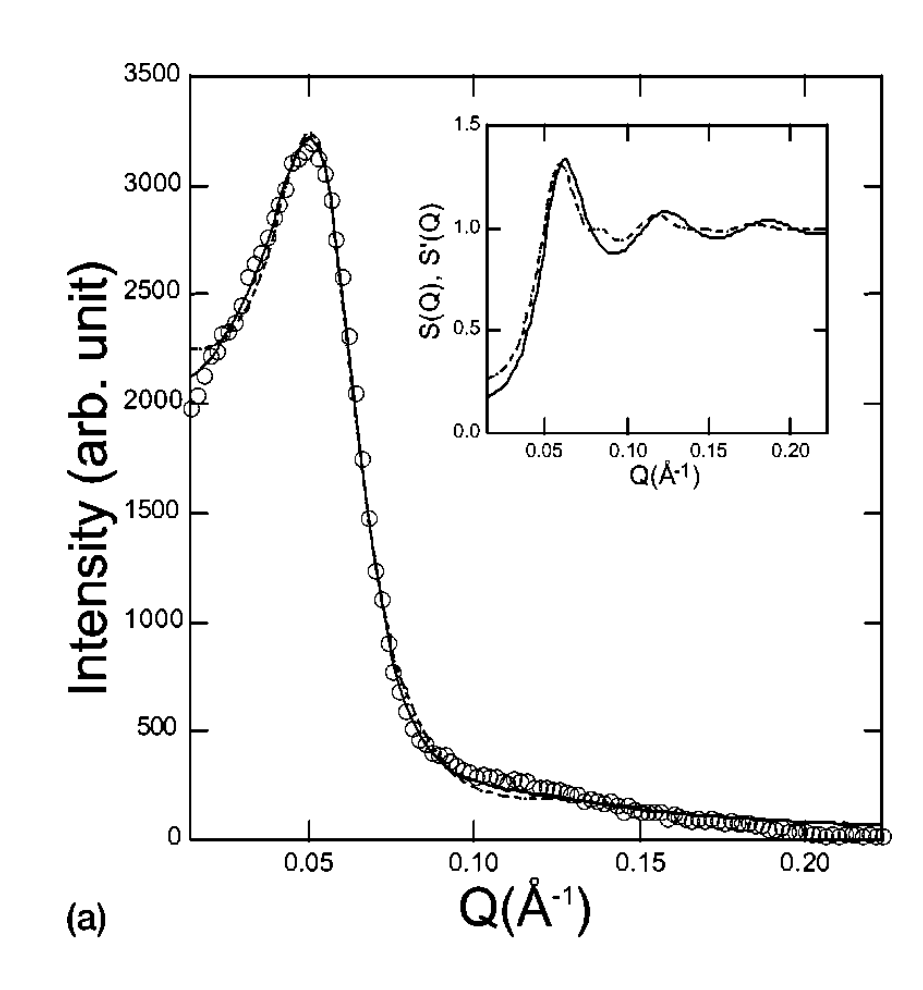
$$\beta(Q) = |\langle F(Q) \rangle|^2 / \langle |F(Q)|^2 \rangle,$$

低圧でのSAXSプロファイル

$$I(Q) = c_0 P(Q) S(Q) + c_2 \frac{\xi_\rho^{-2}}{Q^2 + \xi_\rho^{-2}}$$

droplet

density fluctuation

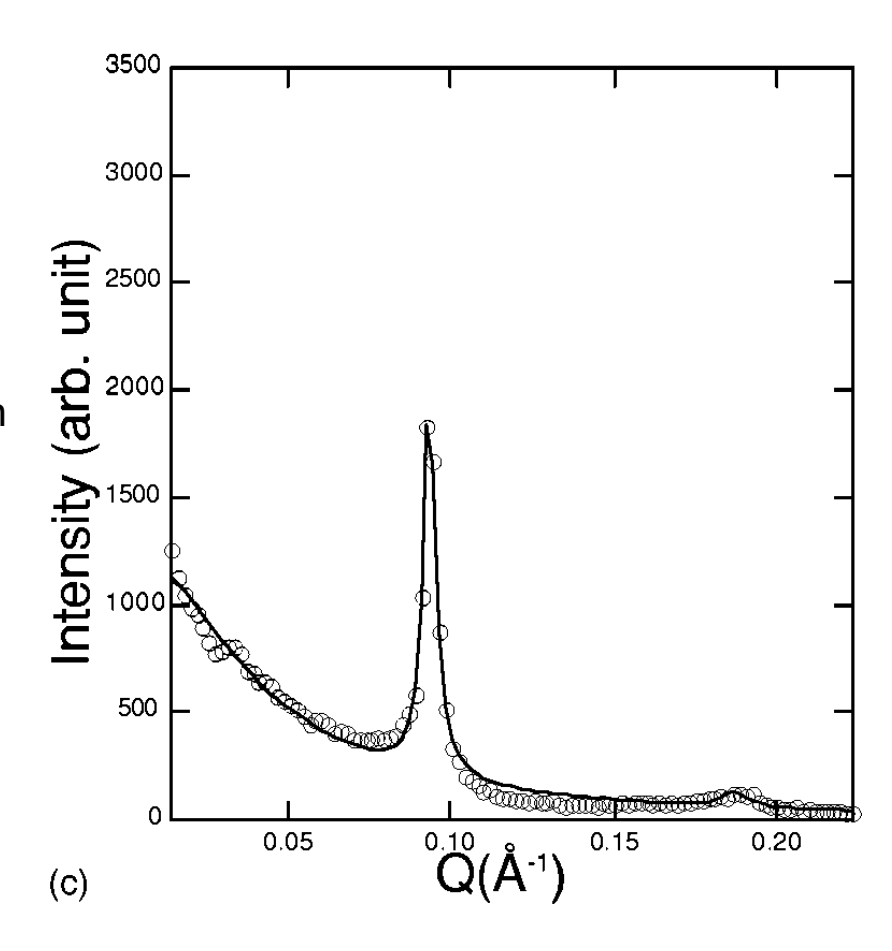


高圧でのSAXSプロファイル

$$I(Q) = c_1 \frac{\xi^{-2}}{\left(Q - \frac{2\pi}{d_L}\right)^2 + \xi^{-2}} + c_2 \frac{\xi_\rho^{-2}}{Q^2 + \xi_\rho^{-2}}$$

lamellar

density fluctuation



相図とdropletサイズの圧力依存性

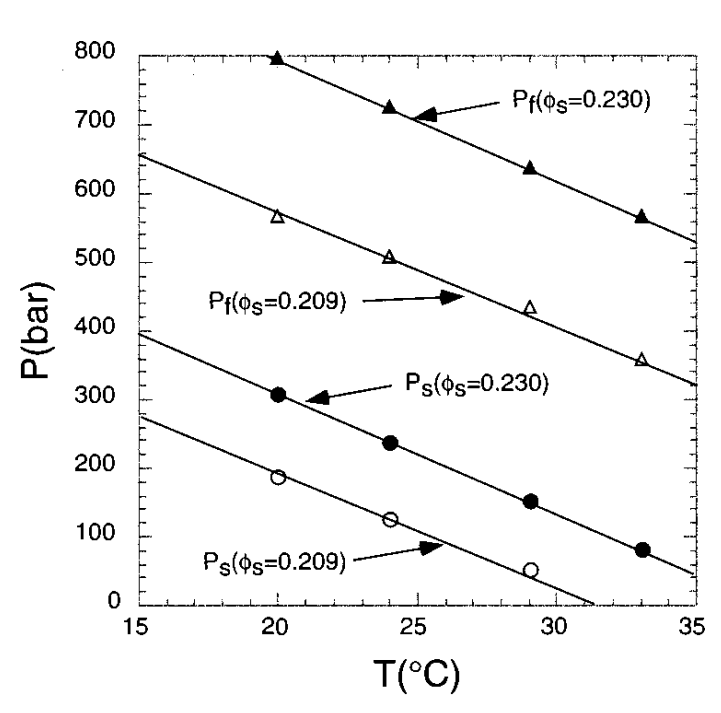


FIG. 5. The P-T phase diagram obtained. Both the slope in the case of P_s and that in the case of P_f were almost the same negative value.

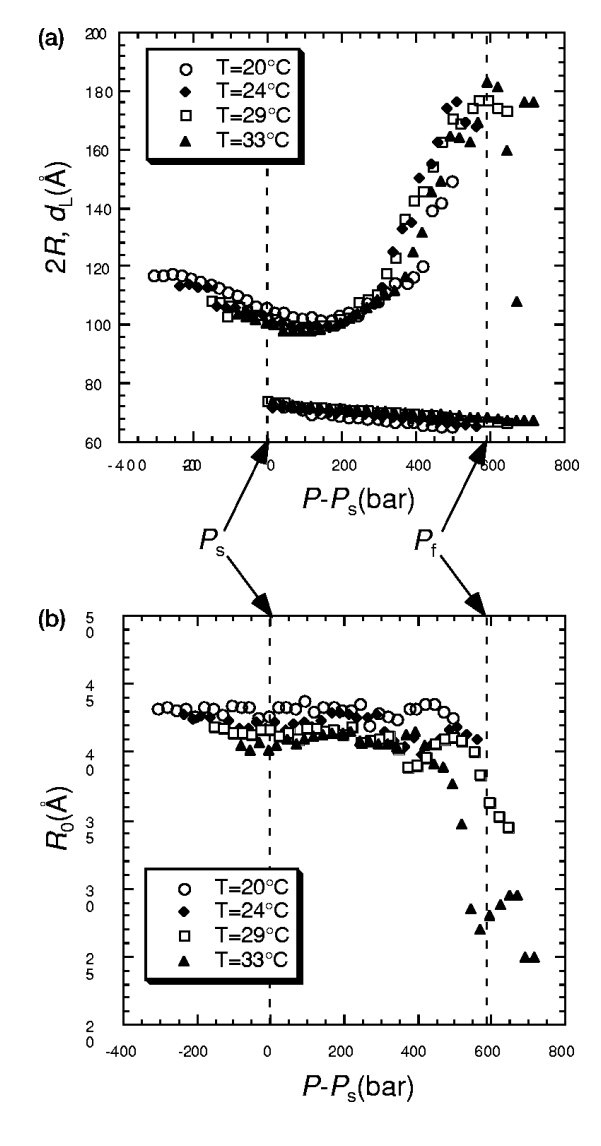
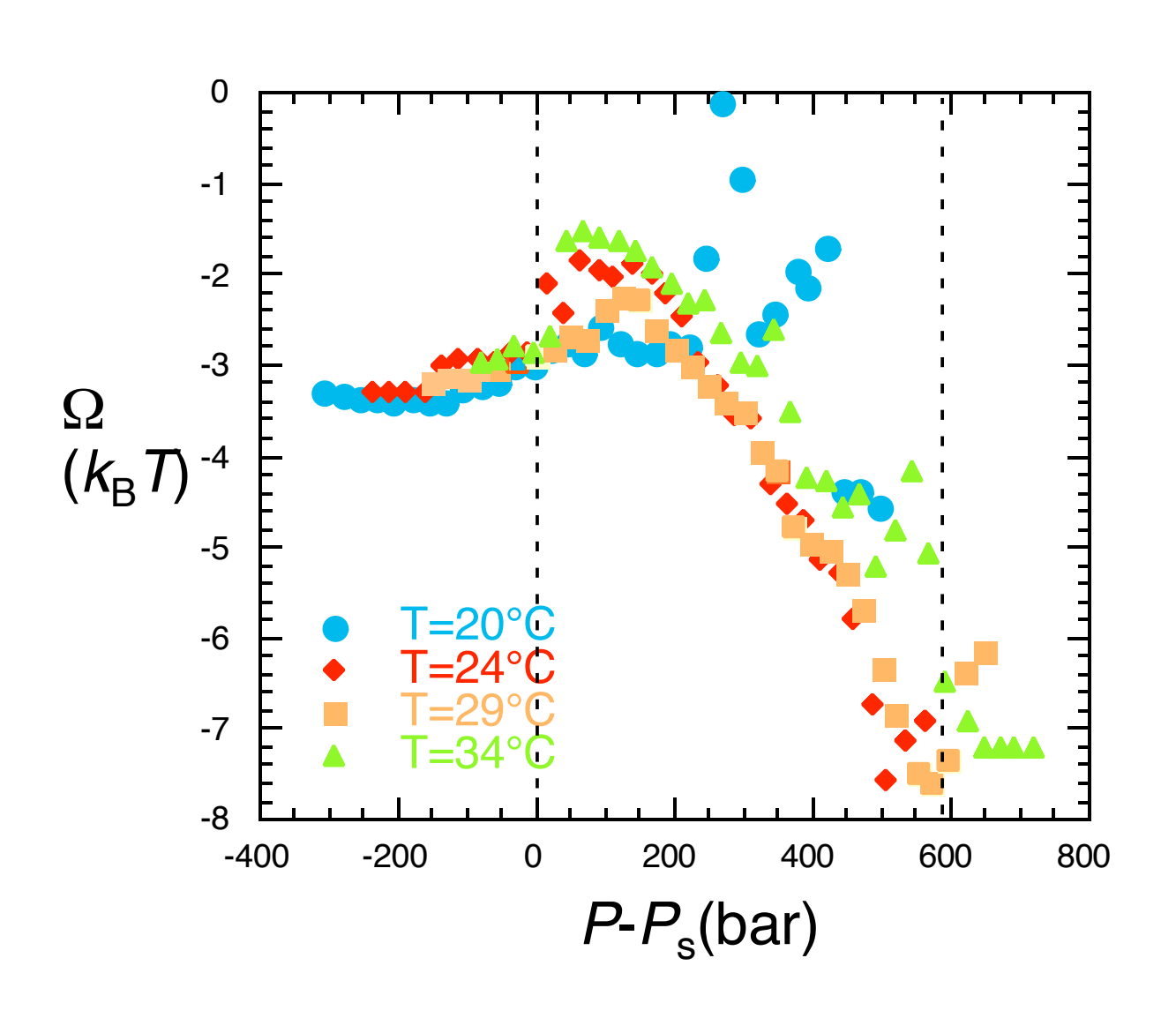
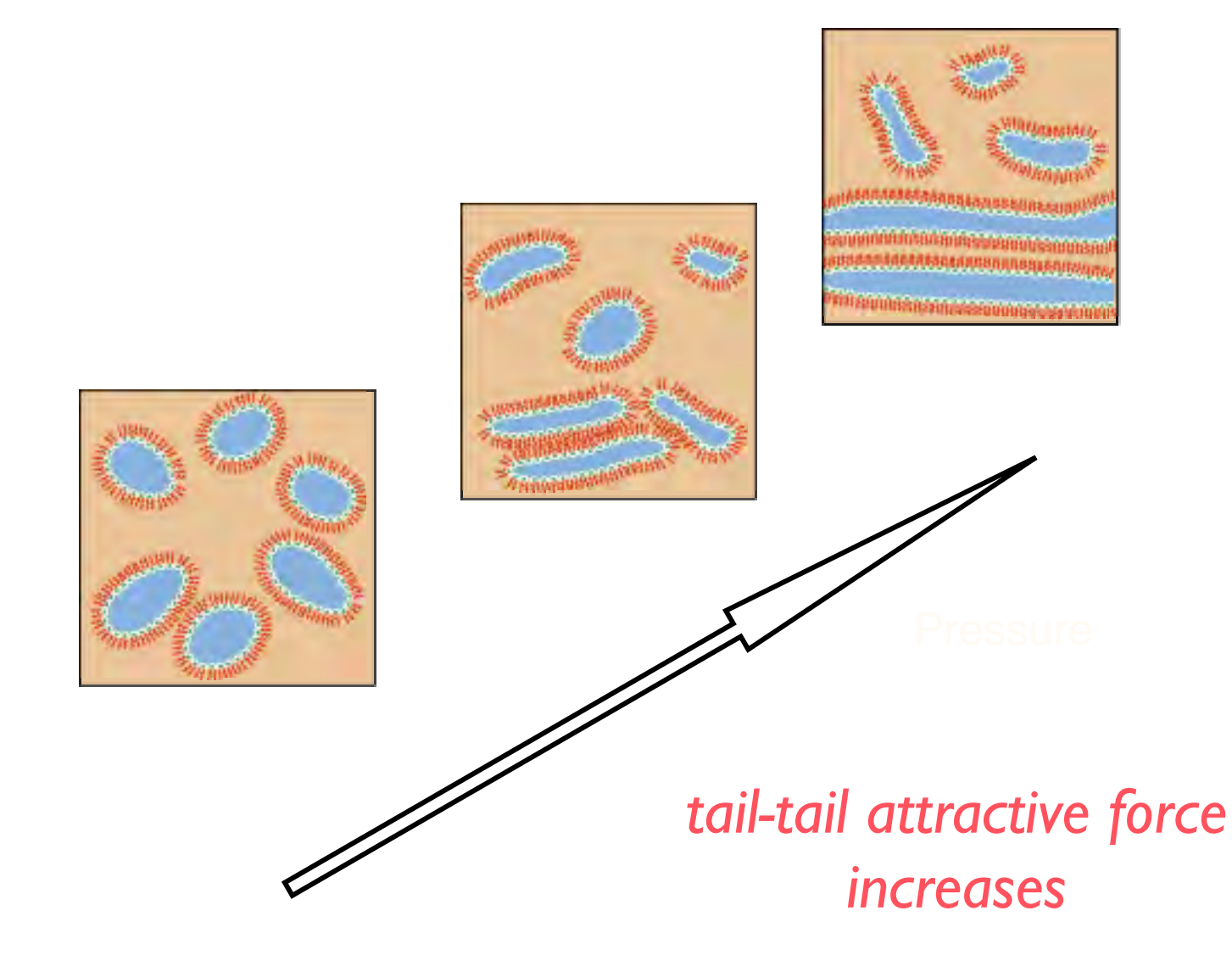


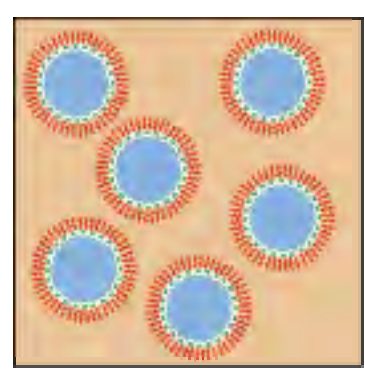
FIG. 6. Summary of the pressure dependence of (a) 2R, d_L and (b) R_0 for ϕ_s =0.230 as a function of $P-P_s$. It is clear that both R and R_0 depended on the temperature and that the pressure dependence of R and R_0 could be normalized as a function of $P-P_s$.

相互作用の圧力依存性

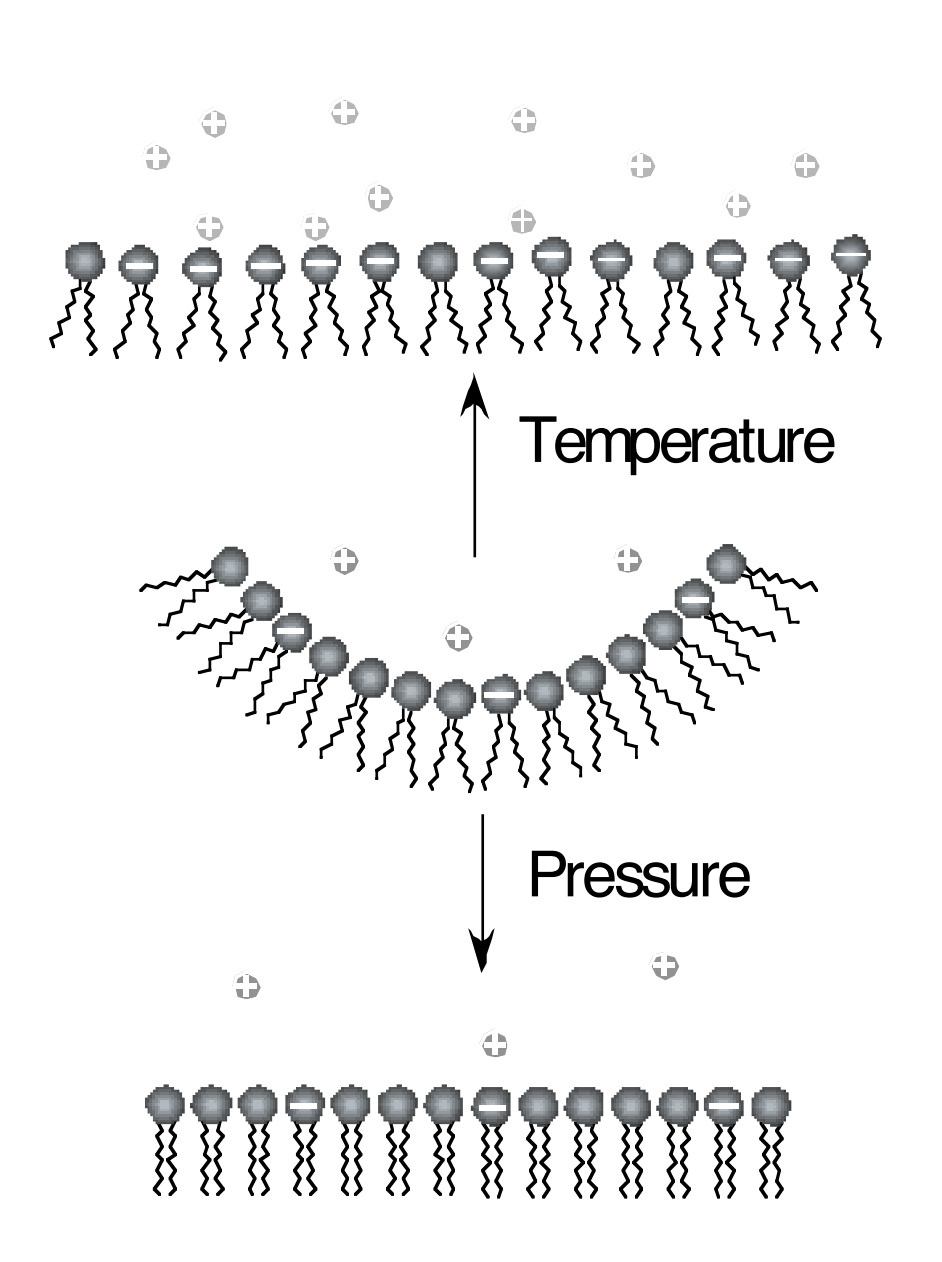


圧力による構造変化





温度変化と圧力変化が同じ理由



counter-ion dissociation

tail-tail interaction

Pressure-induced structural phase transition of dense droplet microemulsions studied by small-angle x-ray scattering

H. Seto, et al. J. Chem. Phys. 115, 9496 (2001)

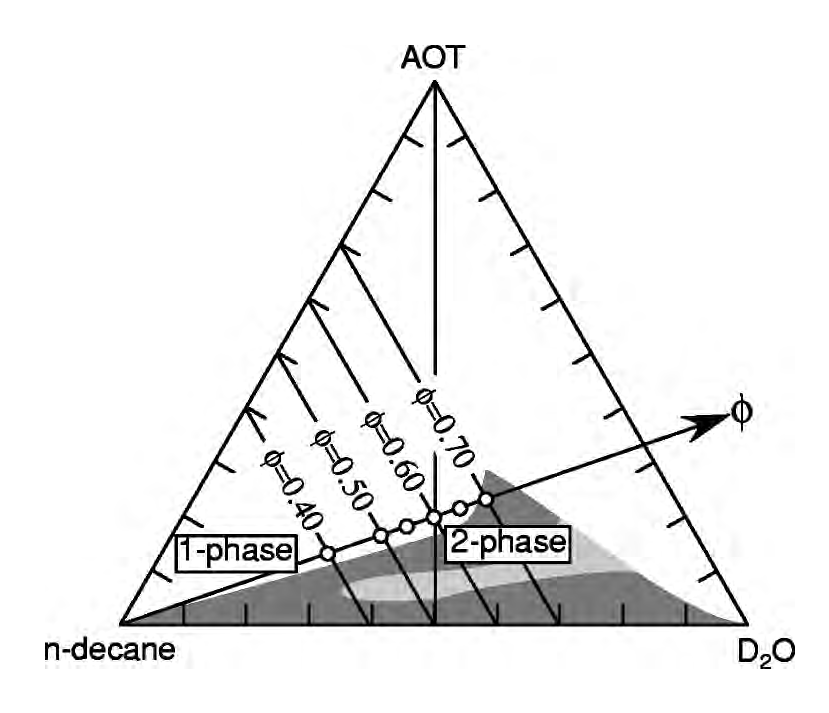


FIG. 1. Schematic phase diagram of a ternary microemulsion $AOT/D_2O/n$ -decane system at ambient pressure. The molar ratio of $[D_2O]/[AOT]$ was fixed at 40.8 on the ϕ -axis. Open circles represent the mixtures of the present study.

$$I(Q) = cP(Q)S(Q) + c_0L_0(Q)$$

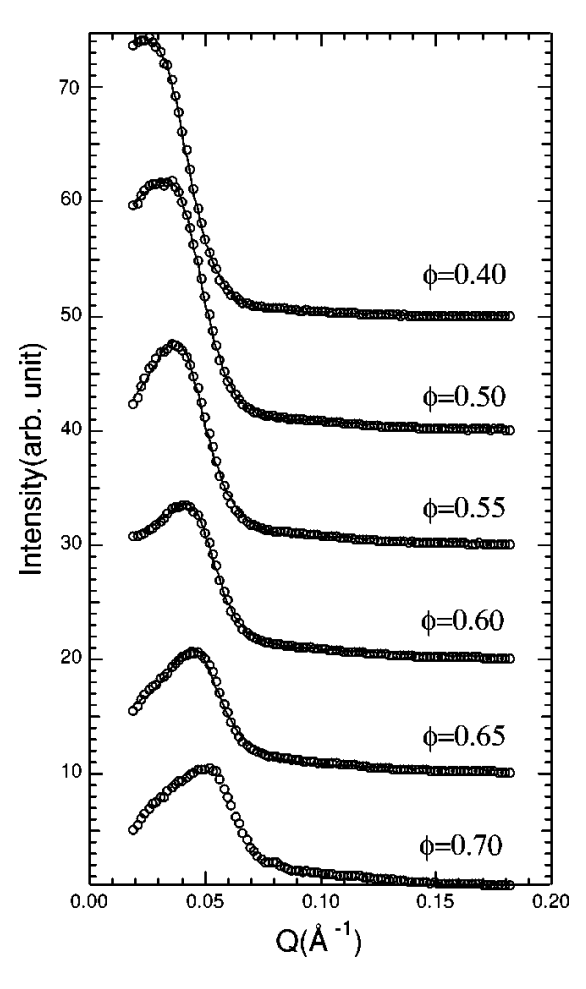
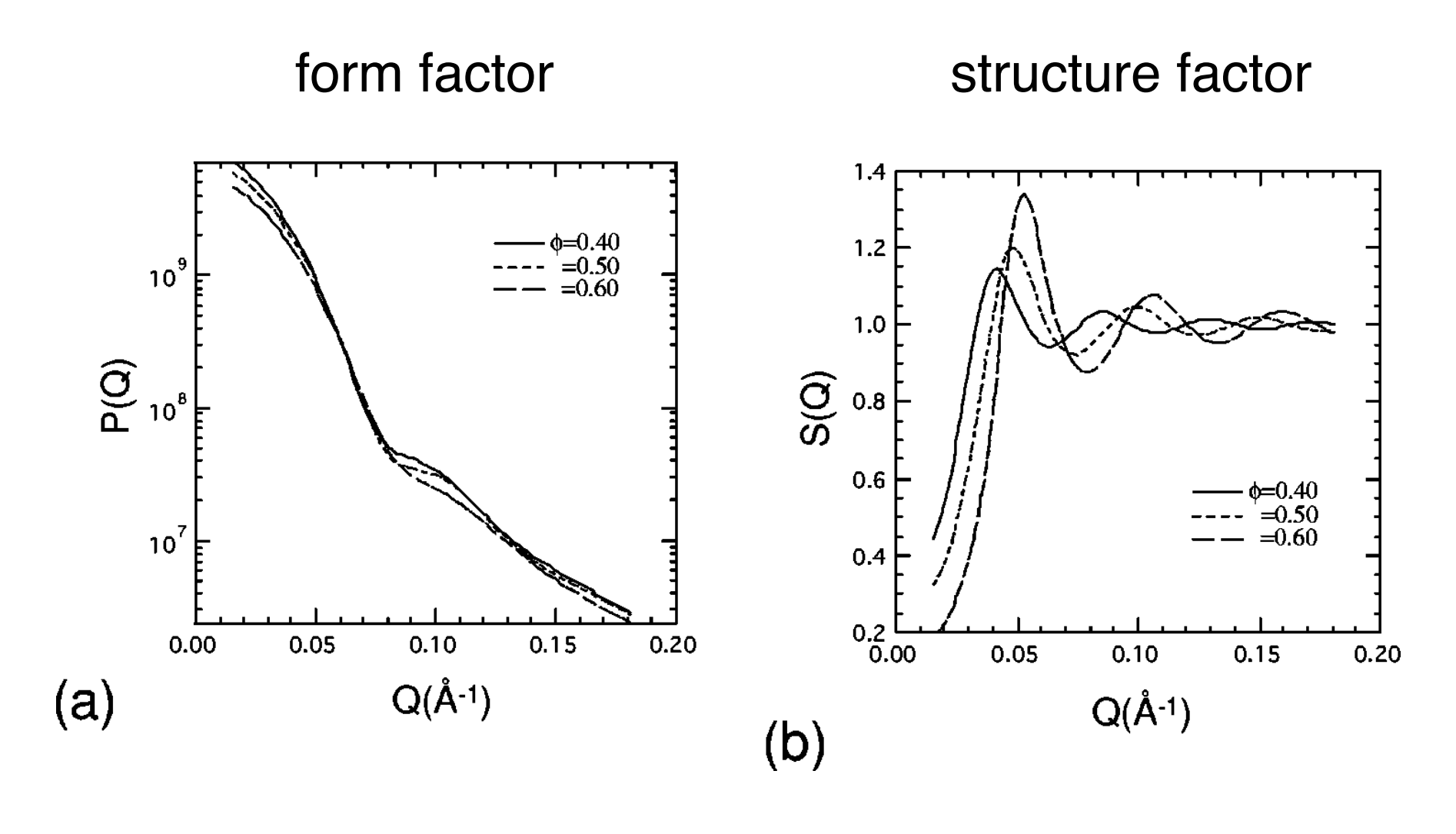


FIG. 2. The droplet volume fraction, ϕ , variation of the SAXS spectra at ambient pressure. All profiles are shifted ten arbitrary units for better visualization. The solid lines are the fit curves to the scattering function of the dense droplet structure.

構造のφ依存性



Droplet濃度のφが増えるに従って平均半径が減少し、多分散性が上がる。

S(Q)を仮定しないで解析する

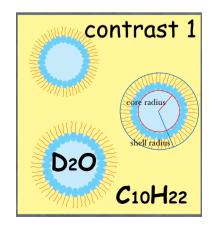
M. Nagao and H. Seto, Phys. Rev. E 75, 061401 (2007)

小角散乱プロファイルは形状因子と構造因子の積で表される。

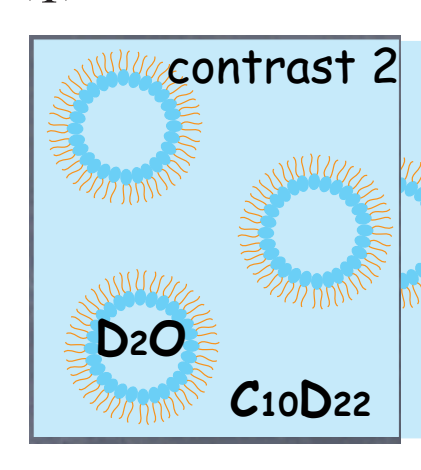
$$I(q) = nF(q)S(q)$$

コントラスト変化によって形状因子は変化するが、構造因子は変化しないはず。そこで「相対形状因子」R(q)を考える。

$$R(q) = \frac{I^b(q)}{I^f(q)} = \frac{F^b(q)}{F^f(q)}$$



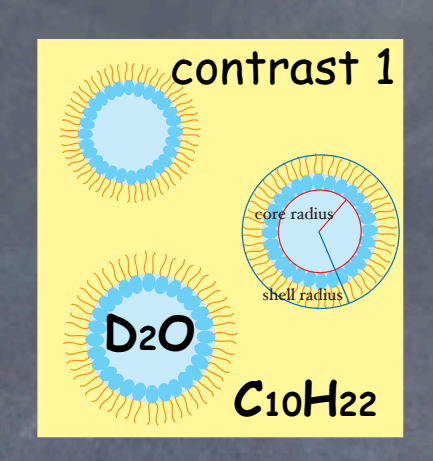


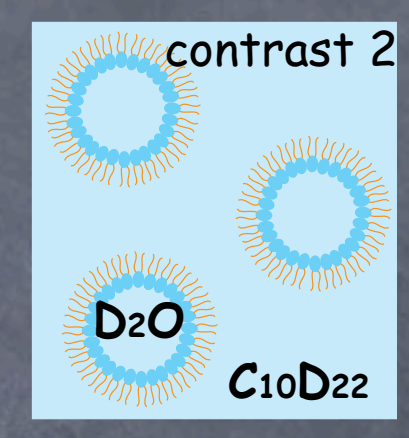


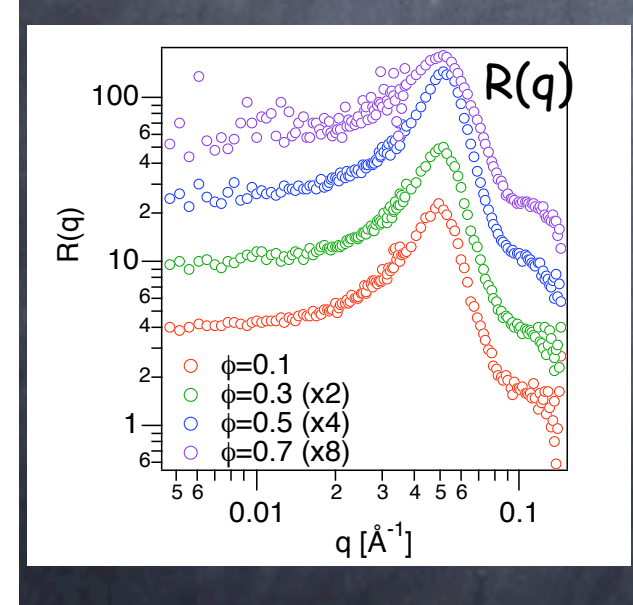
film contrast

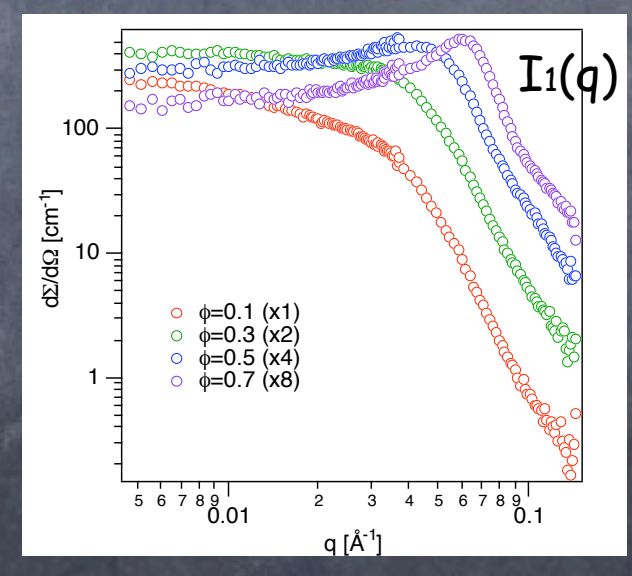
relative form factor analysis in AOT microemulsion

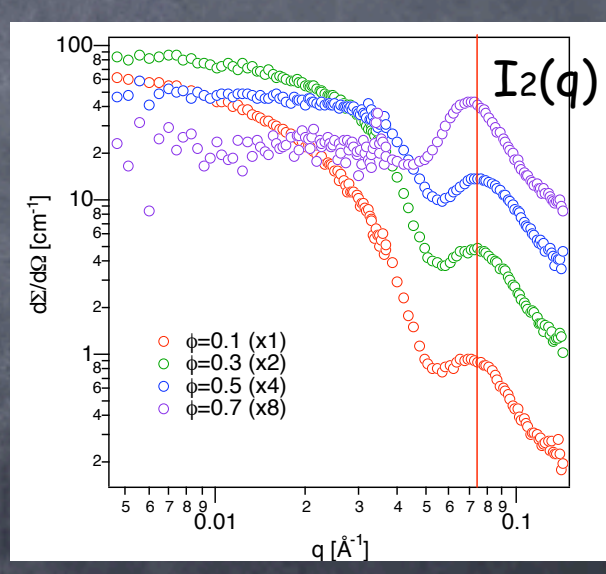
neutron scattering contrast change by deuteration of hydrogen atoms



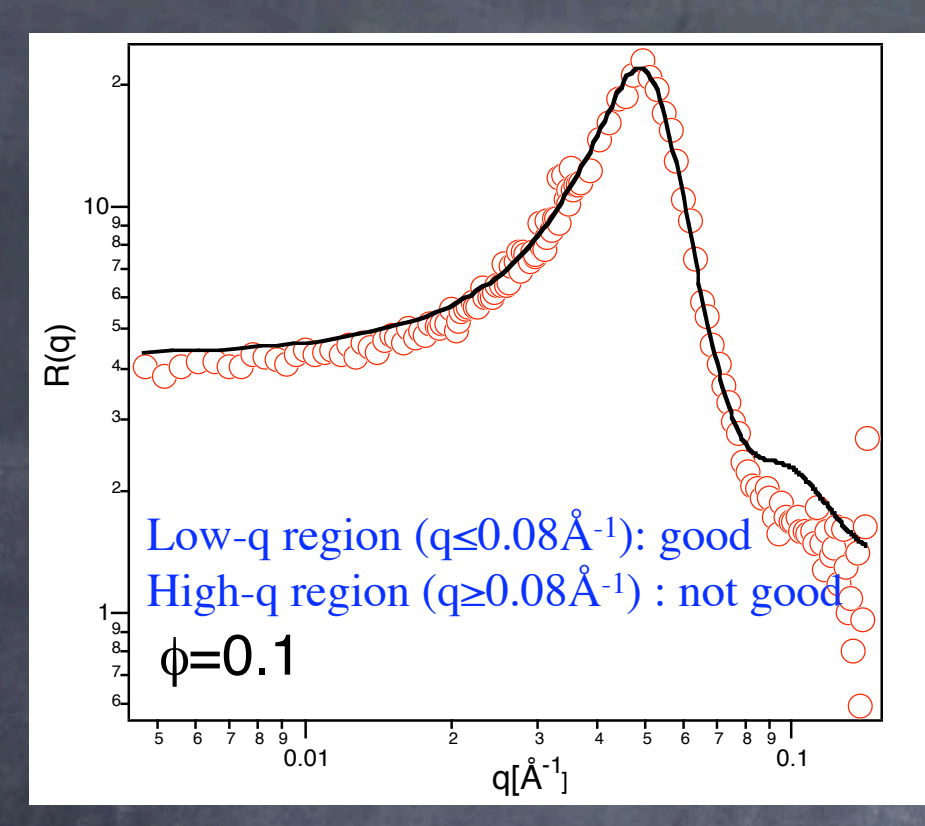








curve fitting of R(q)



fit function

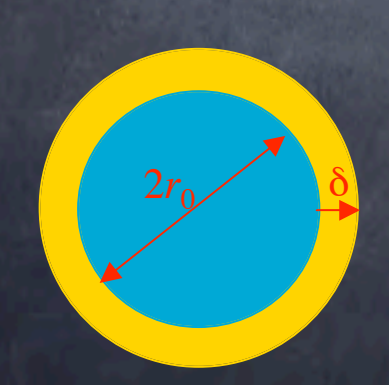
$$R(q) = \frac{F_{\text{bulk}}(q)}{F_{\text{film}}(q)}$$

$$F(q) = \int h(r) |f(q,r)|^2 dr$$

polydisperse sphere

$$h(r) = \frac{I}{\sqrt{2\pi} \Delta r} \exp \left[-\left(\frac{r - \langle r \rangle}{\sqrt{2} \Delta r}\right)^{2} \right]$$

Gaussian distribution



$$f(q,r) = \frac{4\pi}{3} \left(\rho_{\rm w} - \rho_{\rm s} \right) \left[r^3 j_{\rm o}(qr) - \frac{\rho_{\rm o} - \rho_{\rm s}}{\rho_{\rm w} - \rho_{\rm s}} (r + \delta)^3 j_{\rm o} \left\{ q(r + \delta) \right\} \right]$$

$$j_{\circ}(x) = 3 \frac{\sin x - x \cos x}{x^3}$$

$$p = \frac{\Delta r}{\langle r \rangle}$$

解析結果

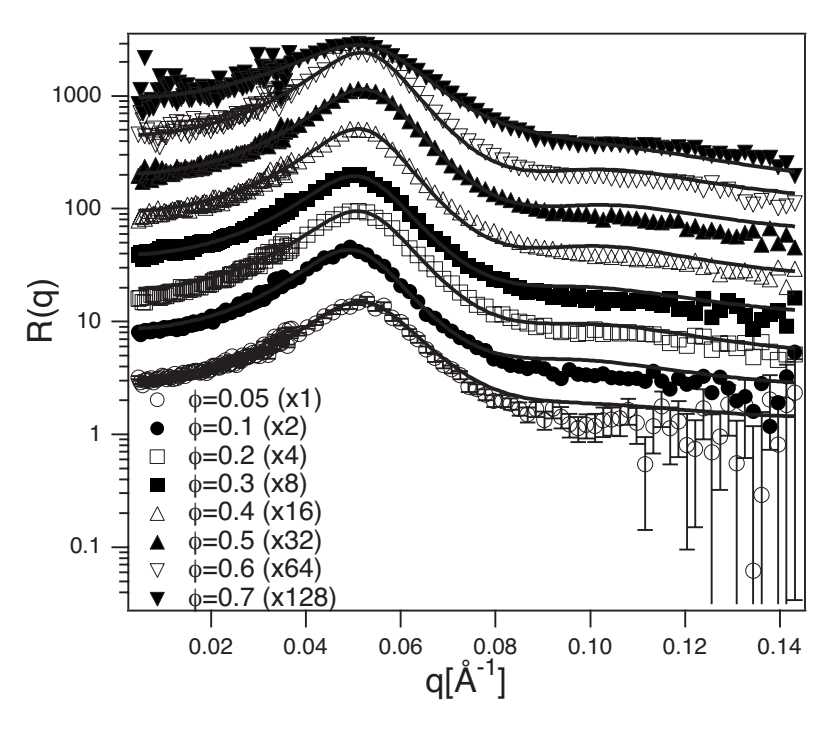


FIG. 2. ϕ dependence of R(q)s. R(q) for ϕ =0.05 is shown as it is and the others are shifted as shown in the legend for better visualization.

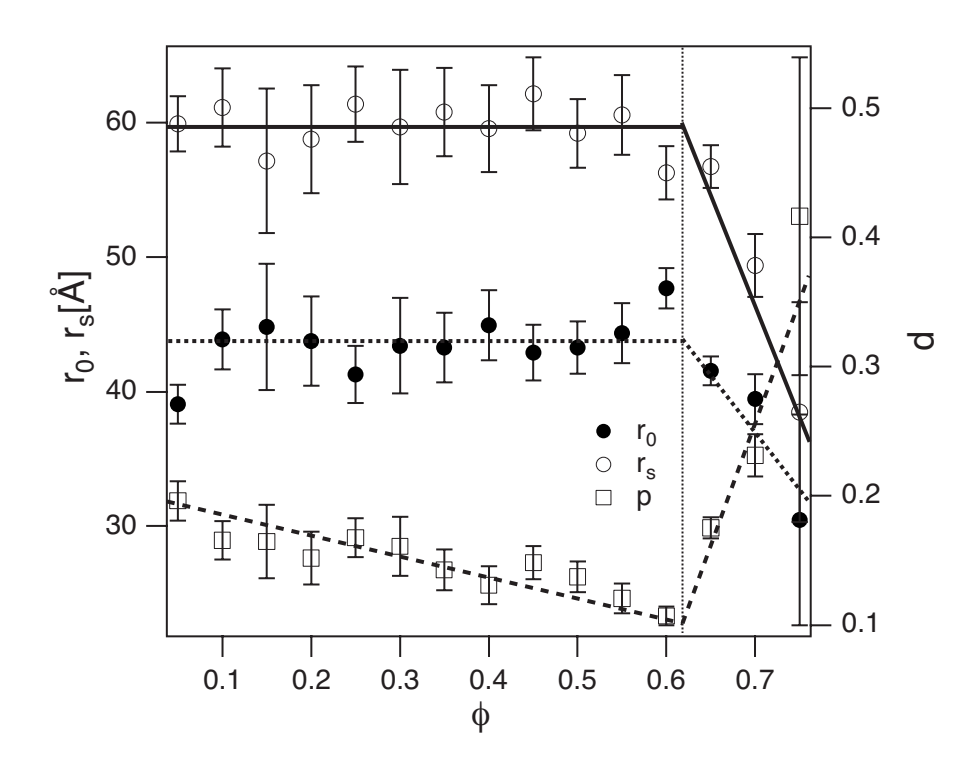
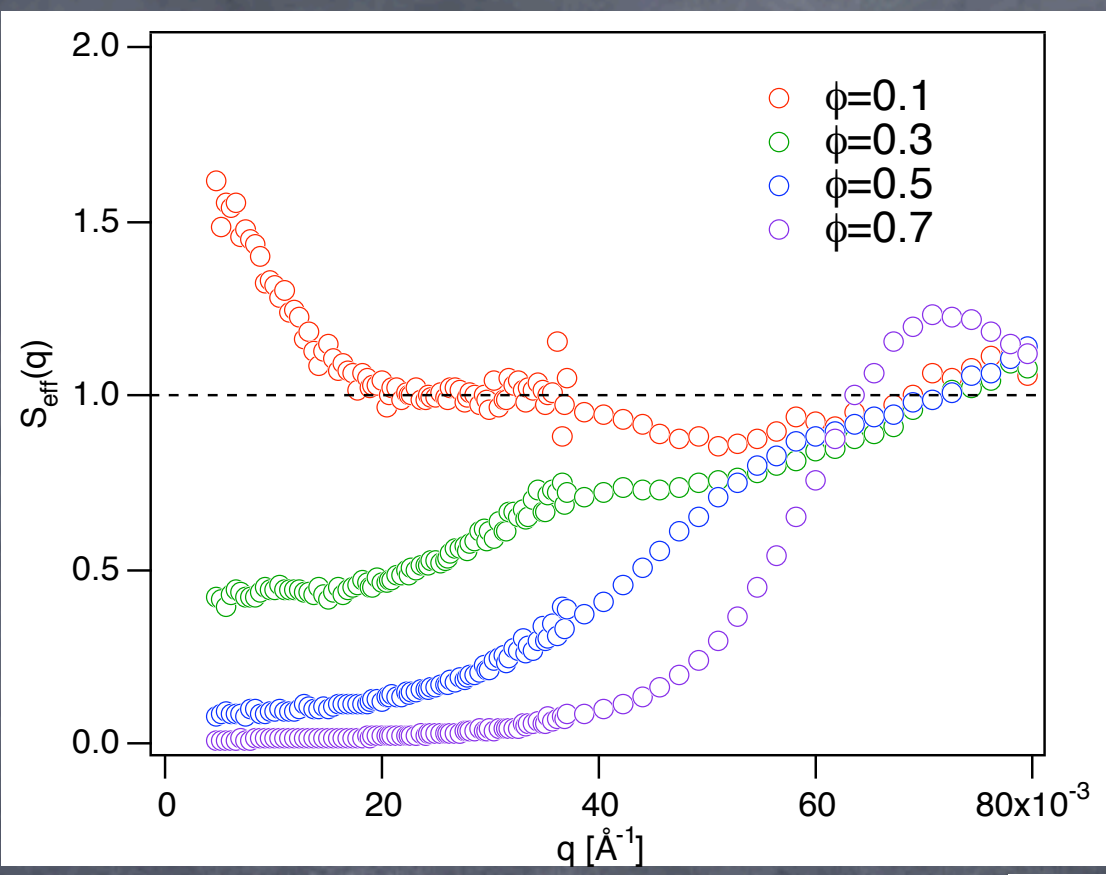


FIG. 3. ϕ dependence of the structural parameters of the droplet shape. r_0 and r_s are indicated with the left vertical axis unit, and p with the right vertical axis unit. The vertical dotted line indicates the concentration of ϕ^* . The solid, dotted, and dashed lines are guides for the eyes.

φによってdroplet半径は変化しない!

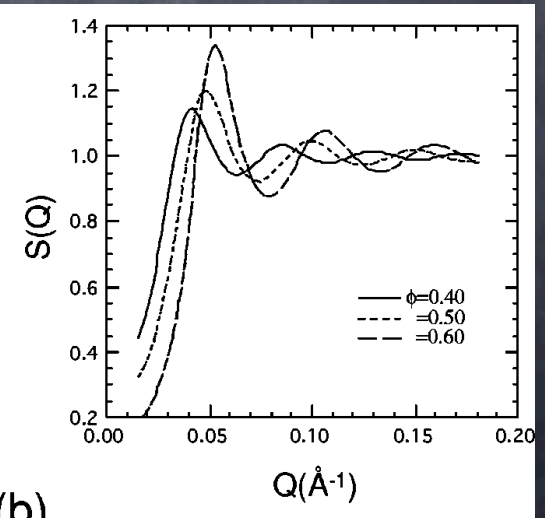
S(q)=I(q)/nF(q)



Concentration dependence of S(low- ϕ : upturn at low-q attractive interaction between dropl

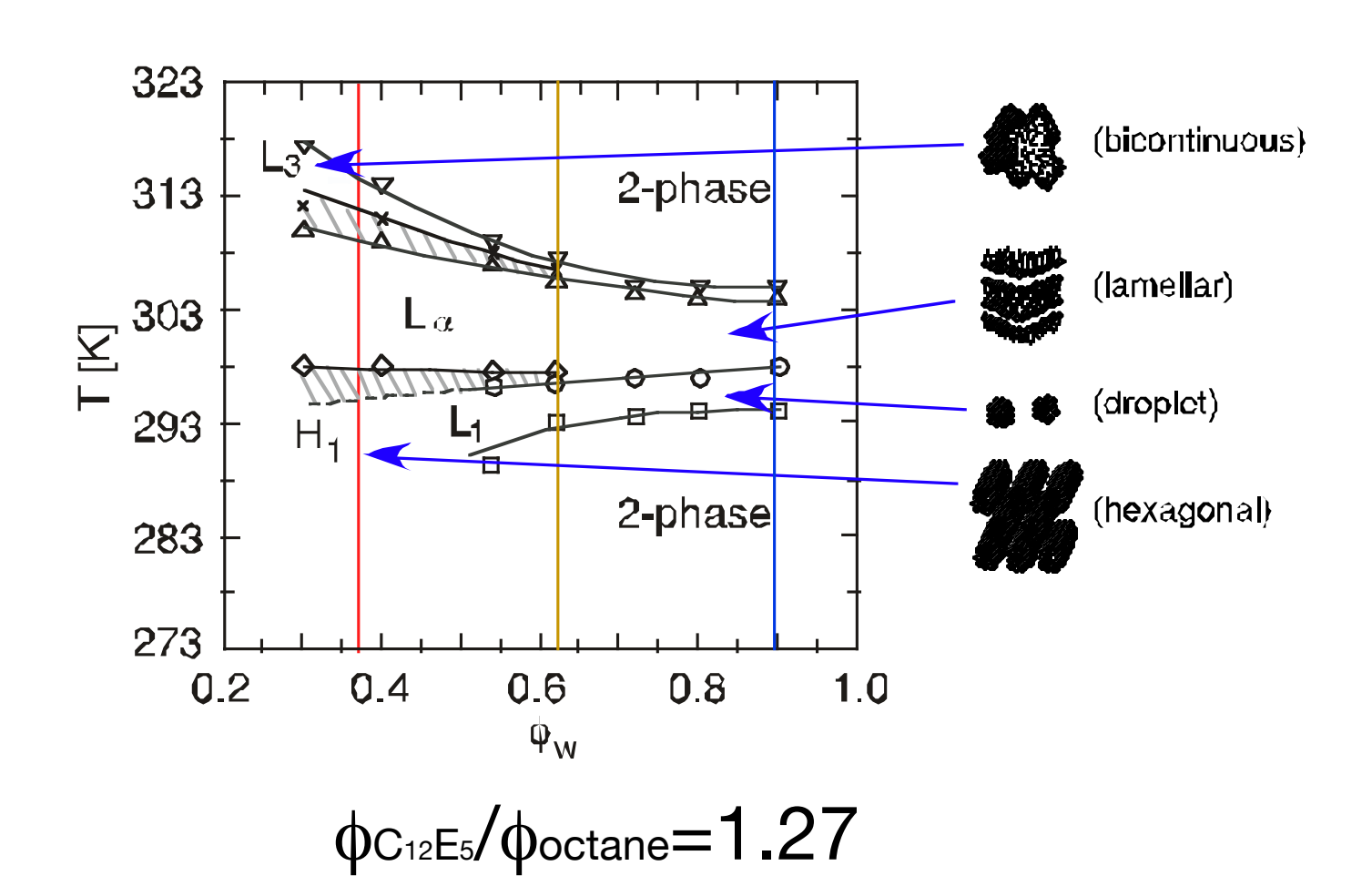
with increasing ϕ : S(q=0) becomes small repulsive interaction between drople

M. Nagao, H. Seto, and N. L. Yama (b)

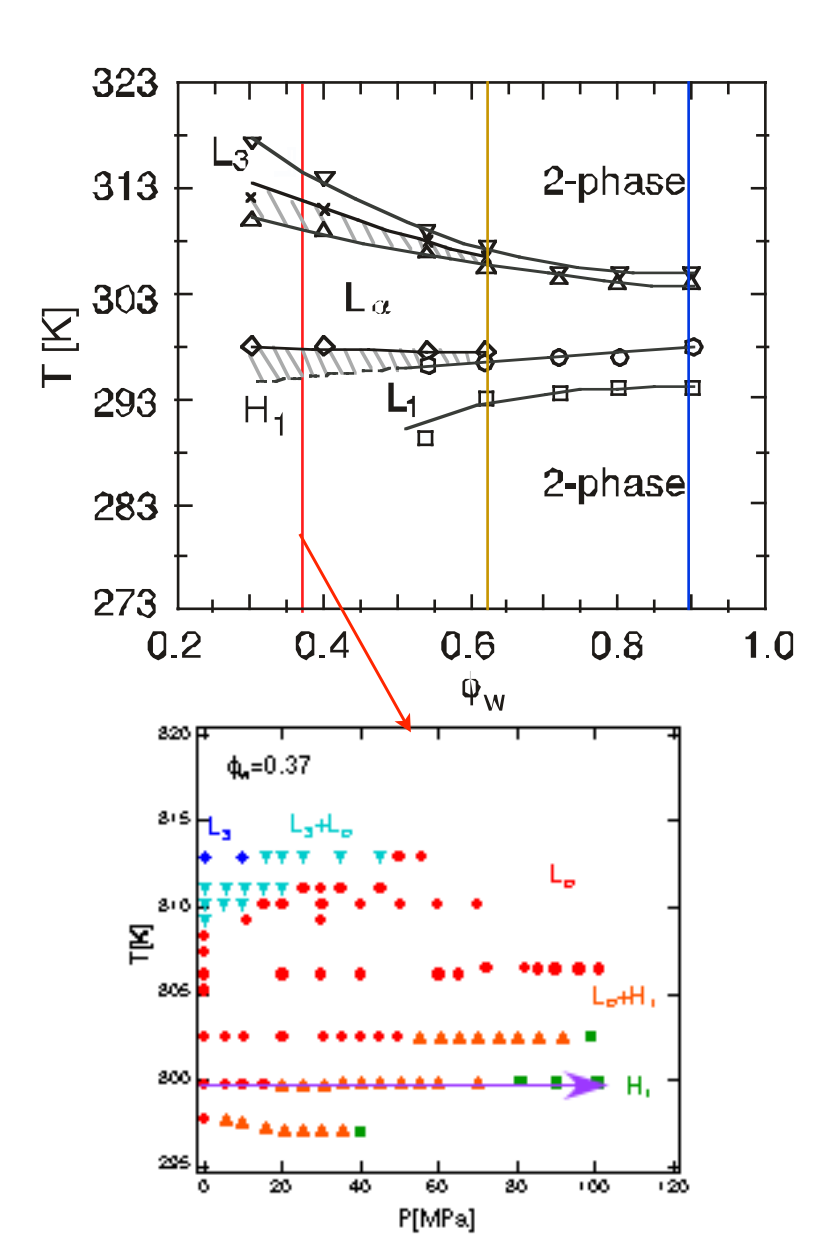


非イオン性界面活性剤の構造の圧力依存性

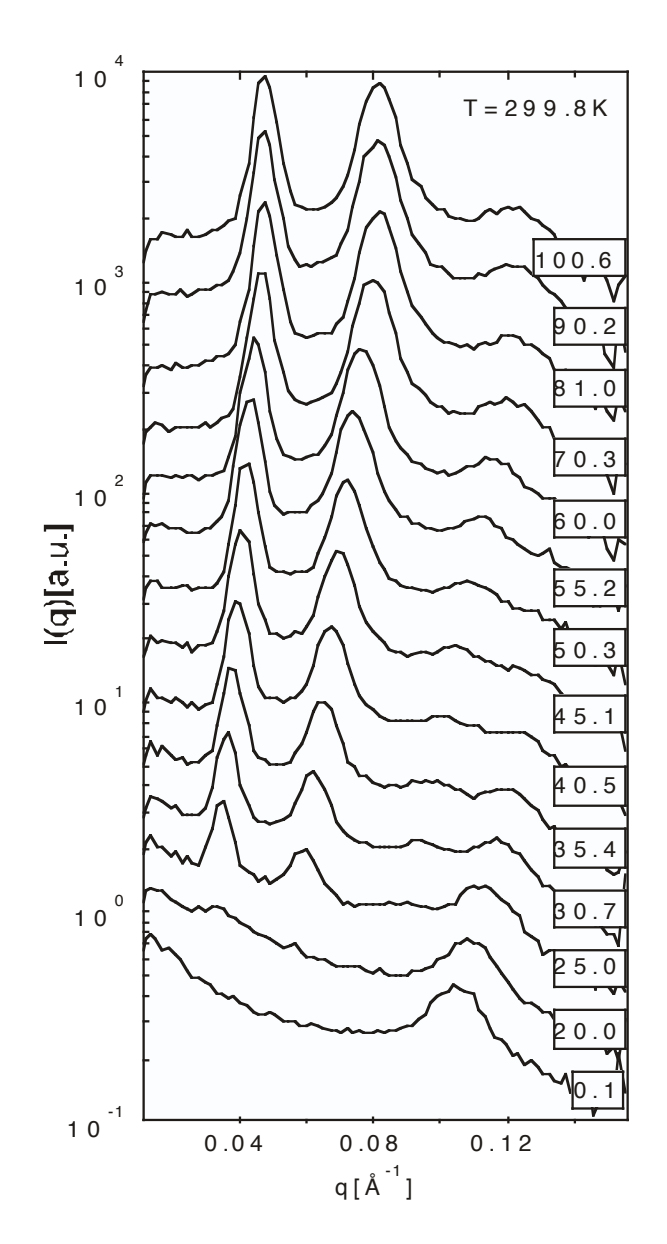
(C12E5/water/octane)



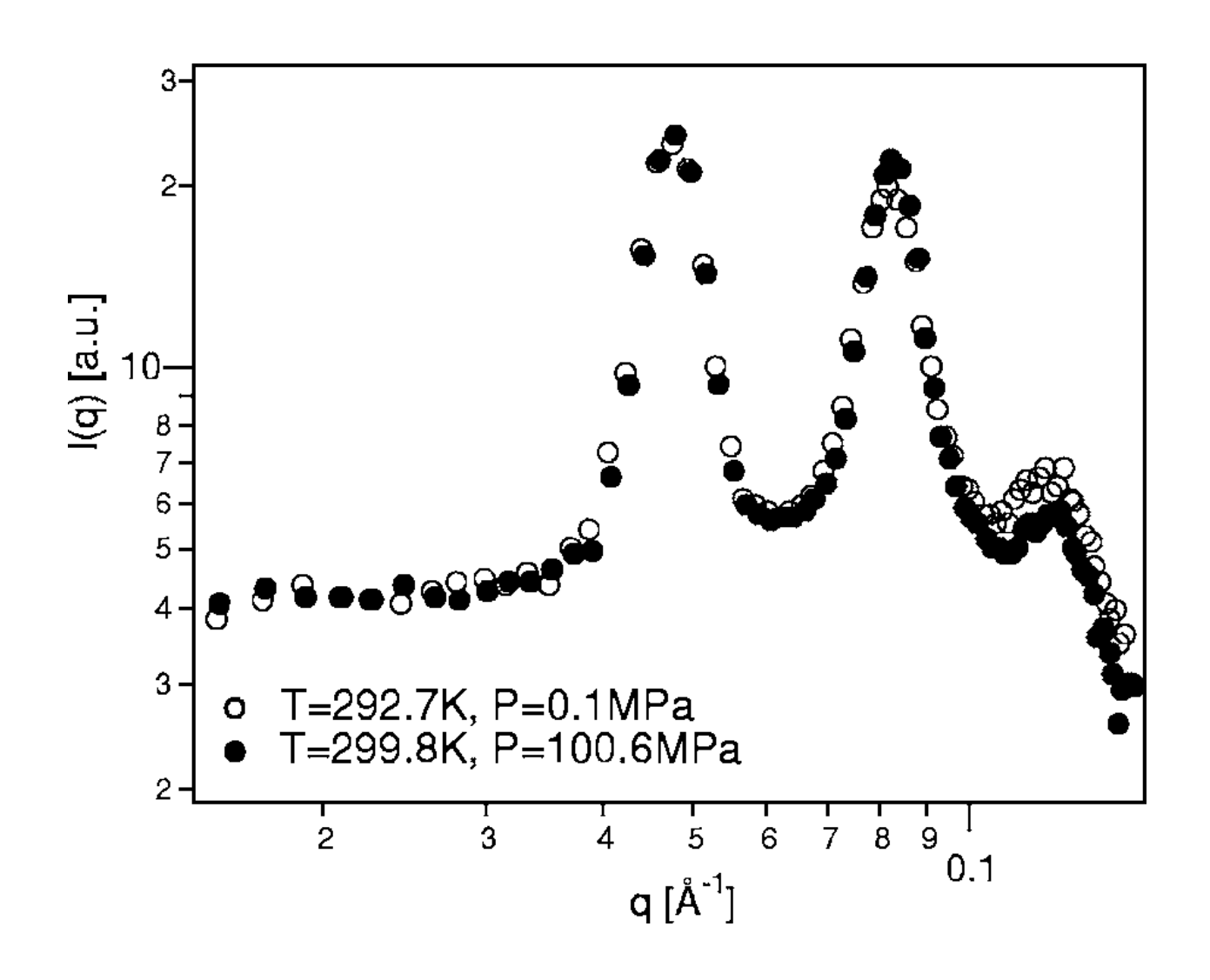
$\phi w = 0.37$

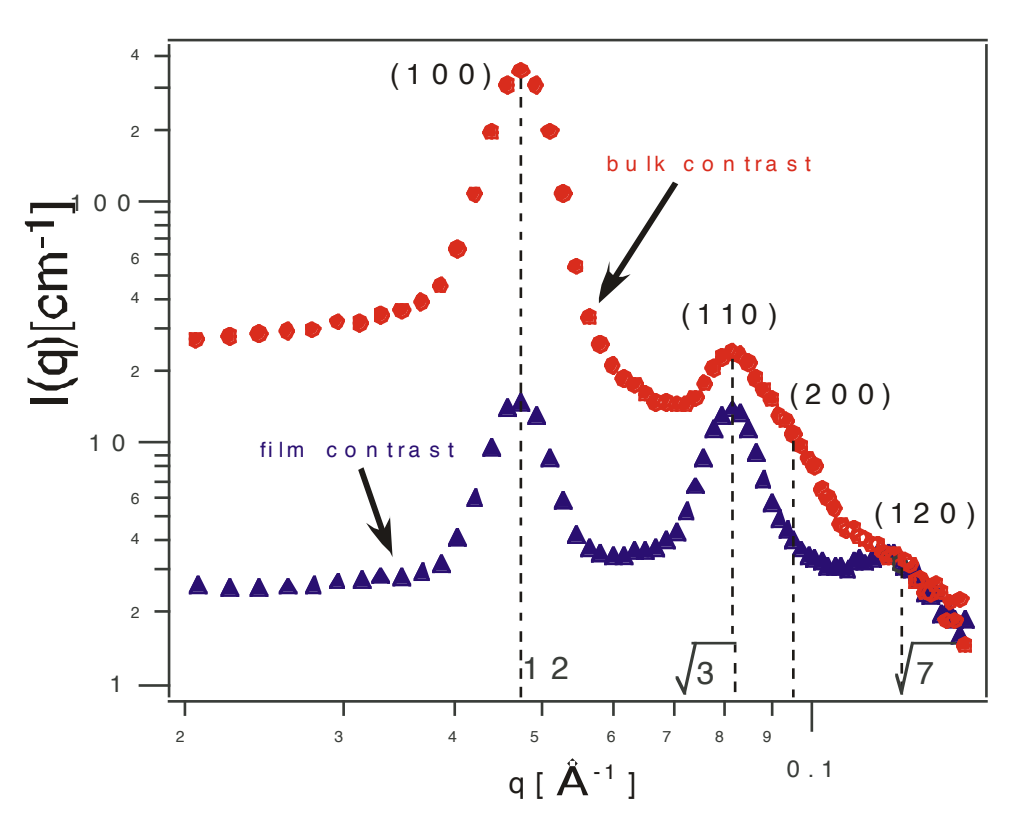


SANS experiment (SANS-U, JRR-3M, JAERI, Japan)



低温相と高圧相





$$d_{H} = \frac{4\pi}{\sqrt{3}q_{hk0}} \sqrt{h^{2} + k^{2} + hk}, \qquad (1) \qquad P(q) = \frac{\text{scale}}{V_{\text{sh}}} \int_{0}^{\pi/2} f^{2}(q, \alpha) \sin \alpha d\alpha, \qquad (5)$$

$$R_c = d_H \sqrt{\frac{\sqrt{3}}{2\pi} \phi_c}, \qquad (2) \qquad f(q, \alpha) = 2(\rho_c - \rho_{\rm sh}) V_c j_0(qH \cos \alpha) \frac{J_1(qr \sin \alpha)}{qr \sin \alpha}$$

$$t_c = \frac{\phi_s}{2\phi_c} R_c.$$

$$(3)$$

$$+ 2(\rho_{sh} - \rho_{so}) V_{sh} j_0 \{ q(H + t_c) \cos \alpha \}$$

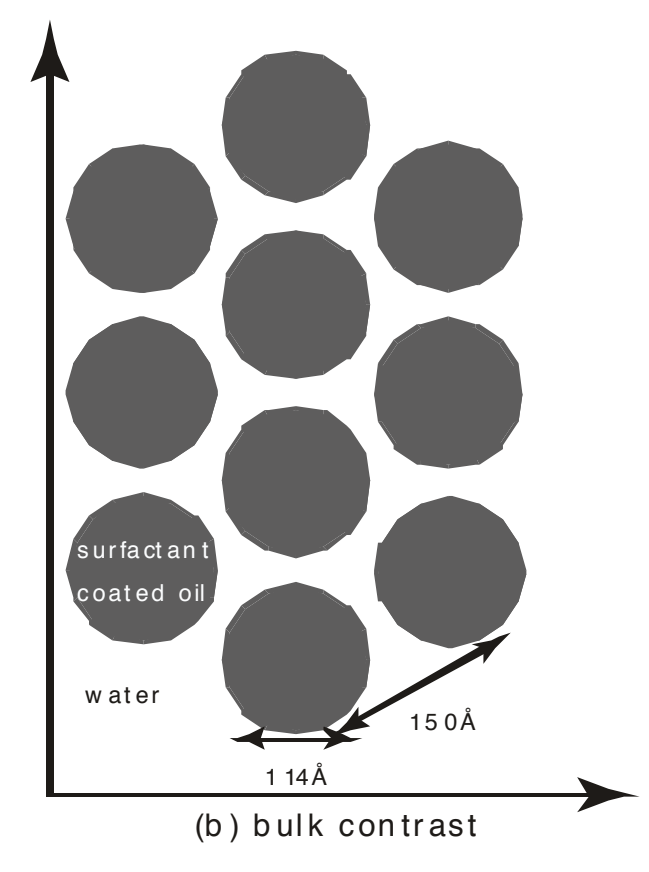
$$\times \frac{J_1(qR_c \sin \alpha)}{qR_c \sin \alpha},$$

$$(6)$$

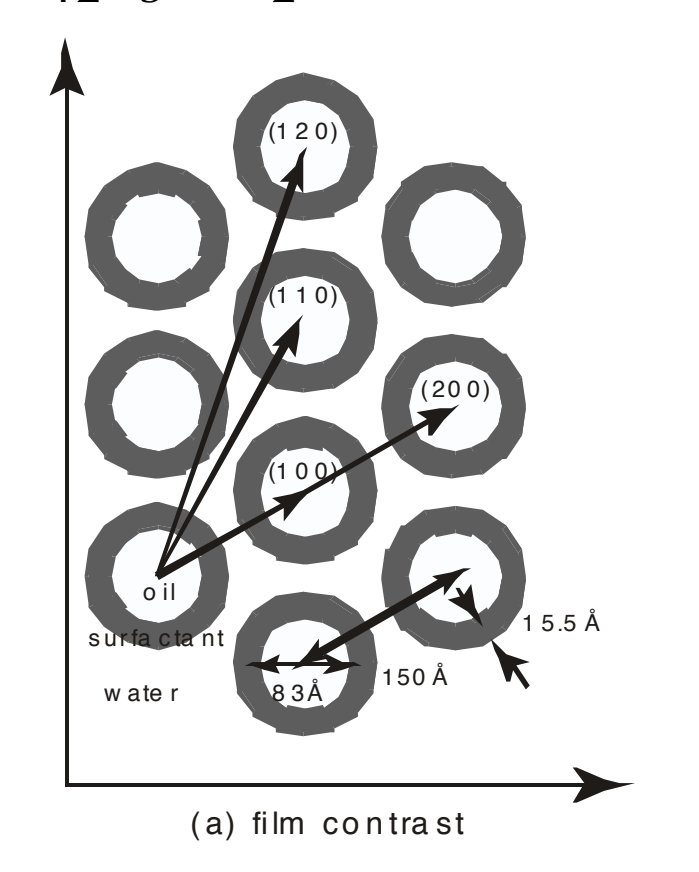
$$S(hk0) = 1 + \exp\left[-2\pi i\left(\frac{\sqrt{3}}{2}h + \frac{1}{2}k\right)\right] + \exp\left[-2\pi ik\right] + \exp\left[-2\pi i\left(-\frac{\sqrt{3}}{2}h + \frac{1}{2}k\right)\right],\tag{4}$$

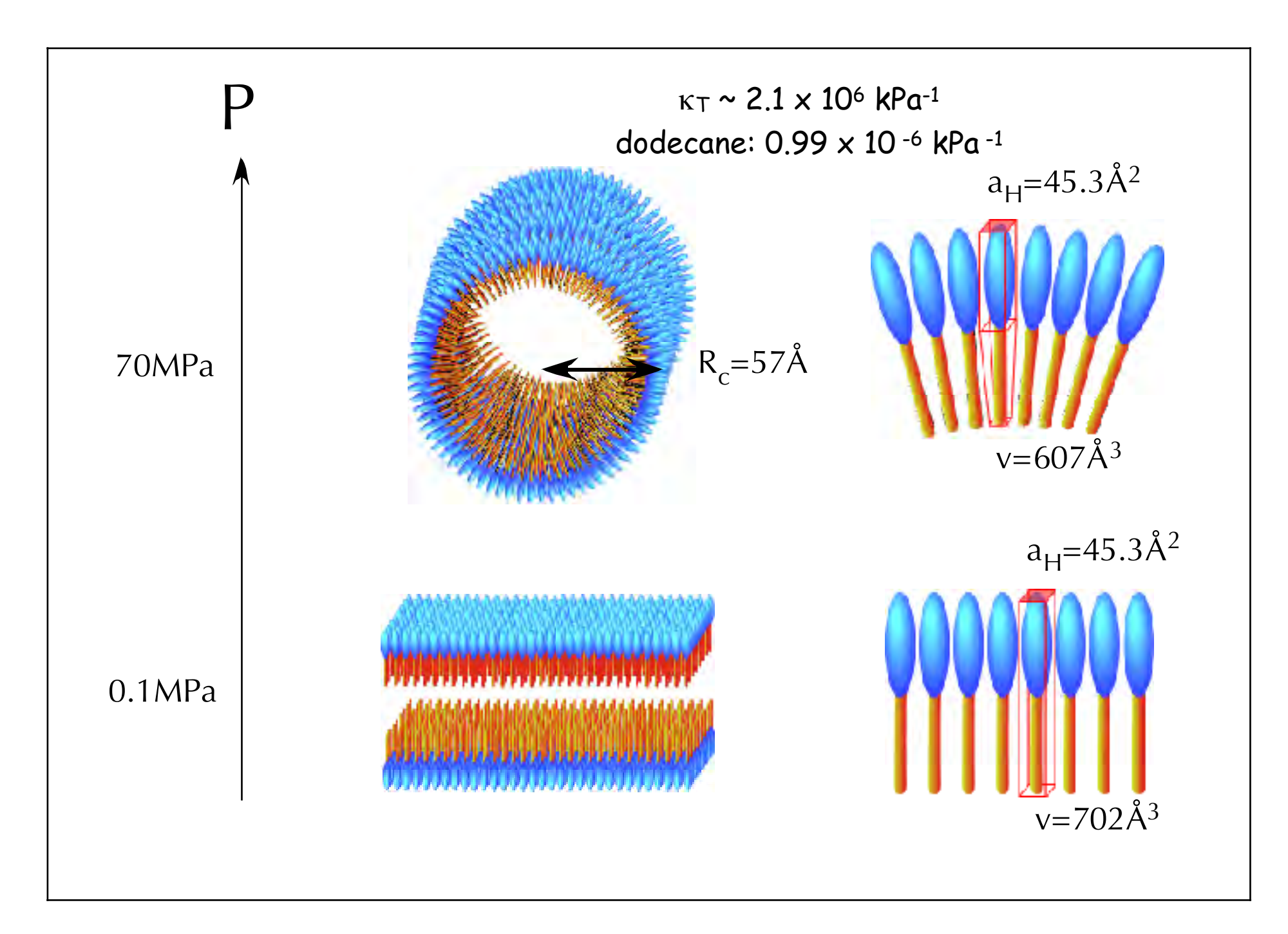
解析結果

bulk contrast (C₁₂E₅ / D₂O / octane)

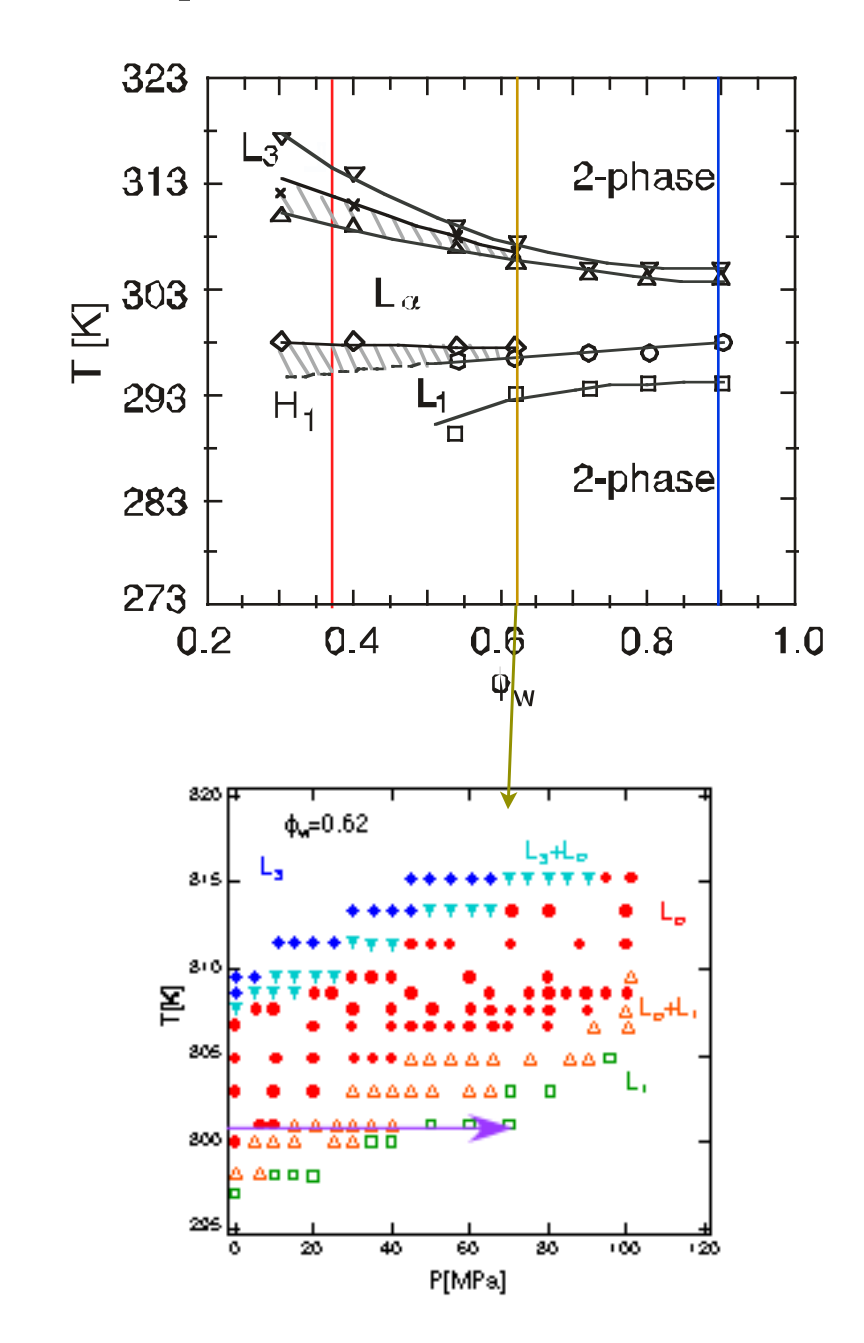


film contrast $(C_{12}E_5 / D_2O / d\text{-octane})$

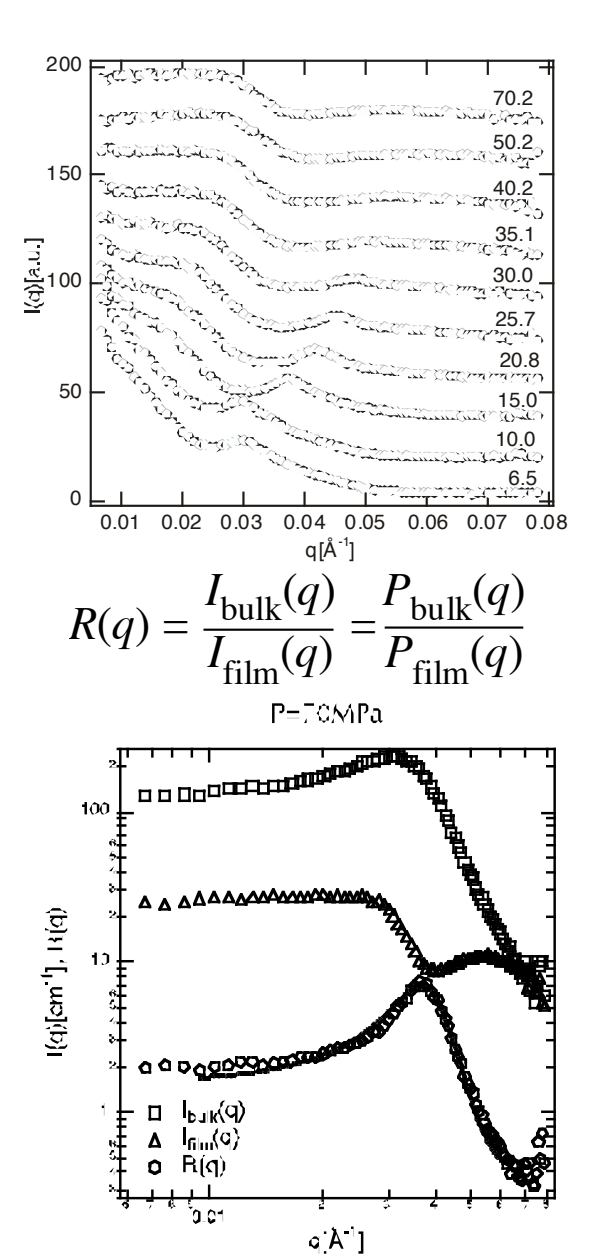


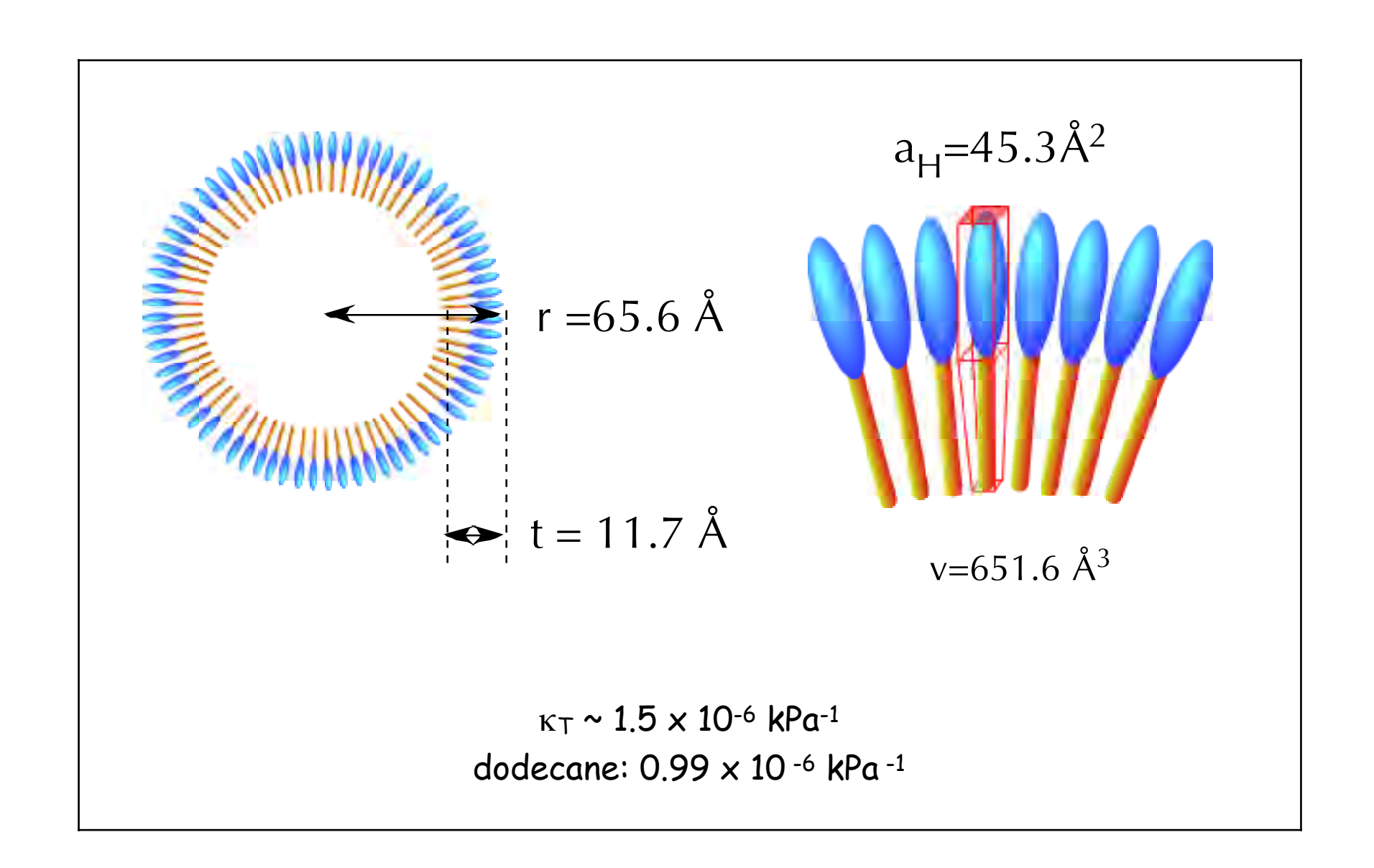


$\phi w = 0.62$



SANS experiment (SANS-U, JRR-3M, JAERI, Japan)



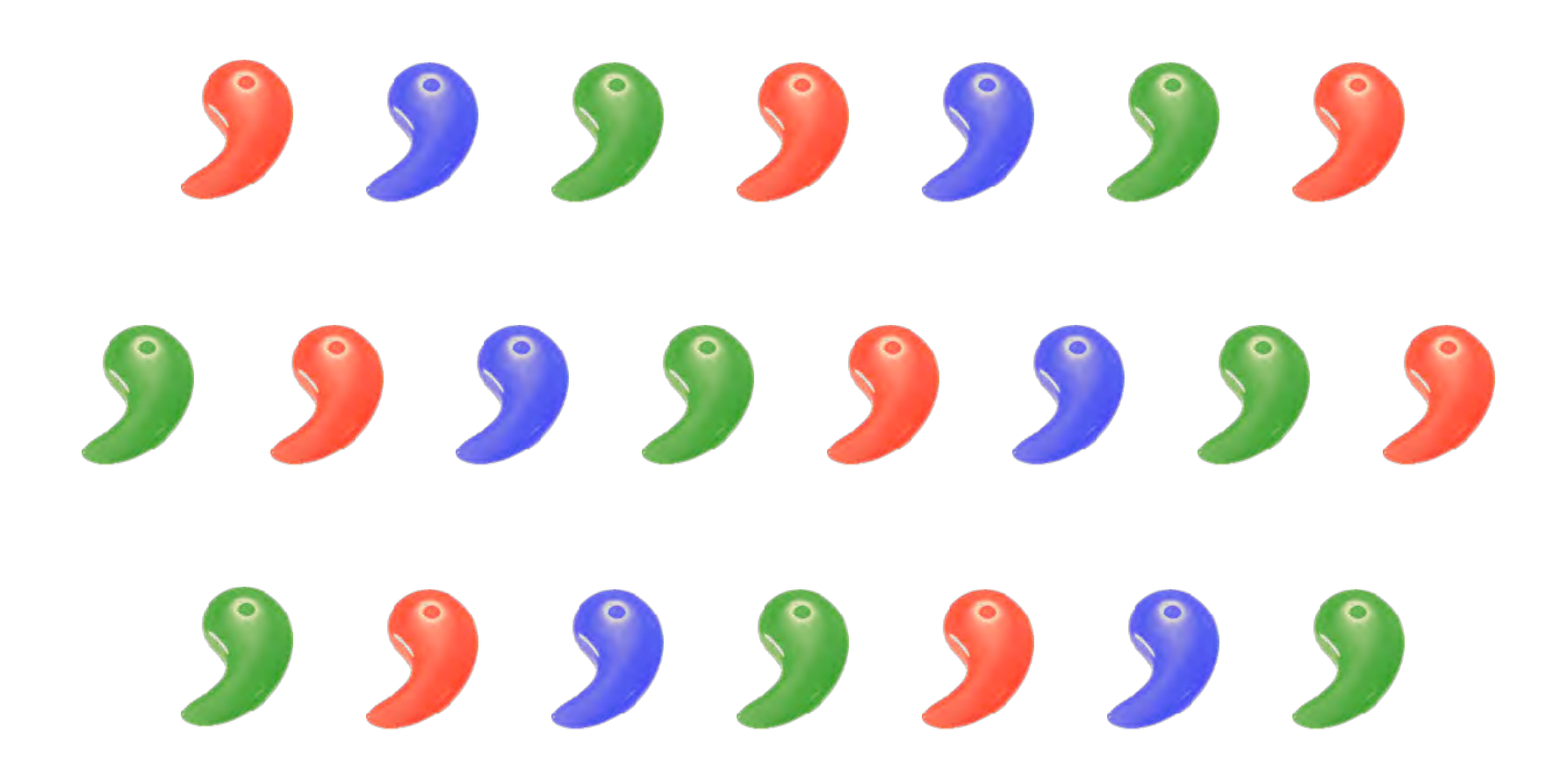


研究例-2

Polymer Gel

コントラスト変調法による多成分解析

散乱体が多成分系の場合、観測される散乱強度は複雑となる.



コントラスト変調法による多成分解析

A:

B: _____

C:

 $S_{ii}(Q)$: 部分散乱関数

 $\Delta
ho_{i}$: 散乱コントラスト

$$I(Q) = \Delta \rho_A^2 S_{AA}(Q) + \Delta \rho_B^2 S_{BB}(Q) + \Delta \rho_C^2 S_{CC}(Q)$$
$$+2\Delta \rho_A \Delta \rho_B S_{AB}(Q) + 2\Delta \rho_B \Delta \rho_C S_{BC}(Q) + 2\Delta \rho_A \Delta \rho_C S_{AC}(Q)$$

コントラスト変調法による多成分解析

A: **)**

B:

C:

 $S_{ii}(Q)$: 部分散乱関数

 $\Delta \rho_i$: 散乱コントラスト

$$I(Q) = \Delta \rho_A^2 S_{AA}(Q) + \Delta \rho_B^2 S_{BB}(Q) + \Delta \rho_C^2 S_{CC}(Q)$$
$$+2\Delta \rho_A \Delta \rho_B S_{AB}(Q) + 2\Delta \rho_B \Delta \rho_C S_{BC}(Q) + 2\Delta \rho_A \Delta \rho_C S_{AC}(Q)$$

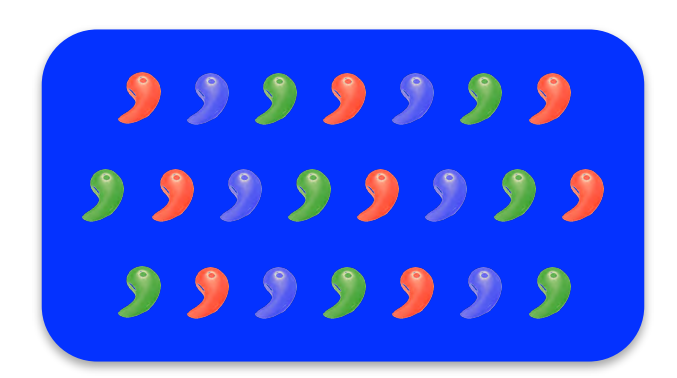
- ・コントラスト変調法とは、多成分系における全ての部分散乱関数を分離する実験手法である。
- ・重水素等の同位体置換を利用することで変化させる。
- ・N成分系におけるコントラスト変調実験は、最低 $_{N+1}C_2$ のコントラストの異なる実験が必要である.
- ・実験的に対相関関数が得られる唯一の方法。

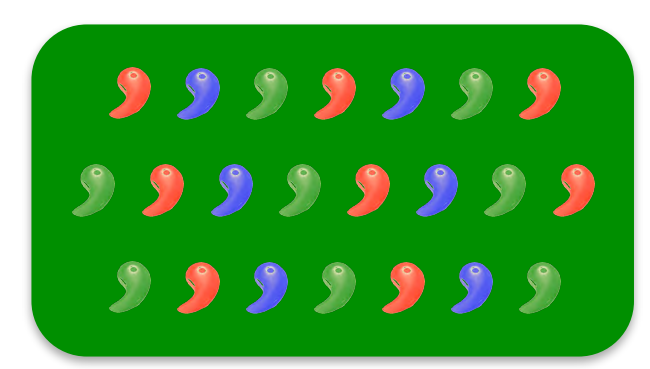
溶媒のコントラスト変化

溶媒のコントラストをある成分に合わせると、その成分からの散乱を消す事が出来る.

⇒ コントラストマッチング法



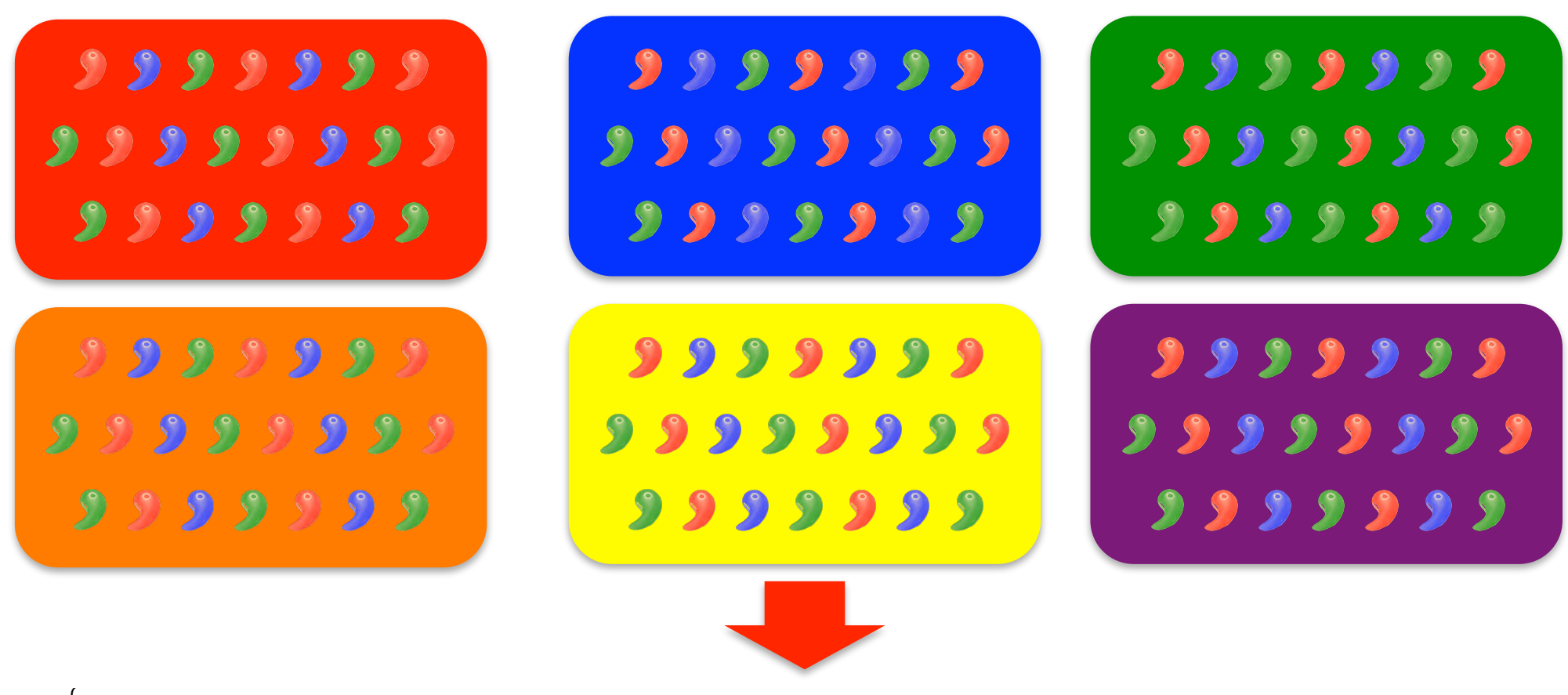




コントラストマッチング法は、ある特定の(一つの)部分散乱関数を抽出する手法である.

散乱体が2成分の系には適用が容易だが、3成分以上になると、単純には適用出来ない.

部分散乱関数



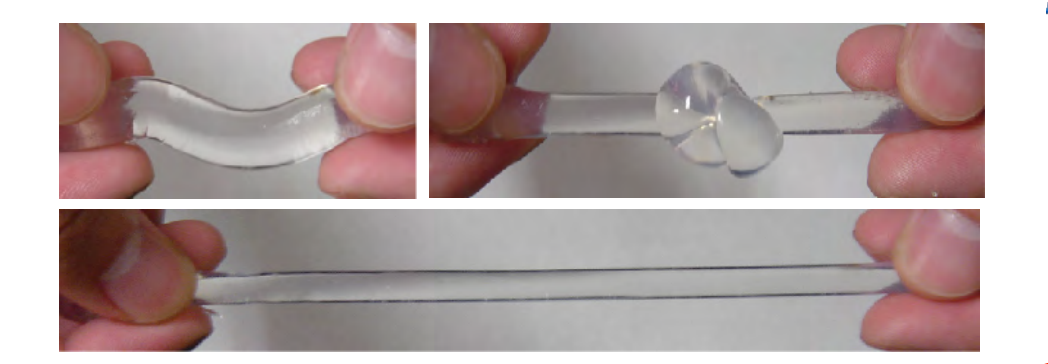
$$\begin{cases} I_{1}(Q) &= \Delta^{1}\rho_{A}^{2}S_{AA}(Q) + \Delta^{1}\rho_{B}^{2}S_{BB}(Q) + \Delta^{1}\rho_{C}^{2}S_{CC}(Q) + 2\Delta^{1}\rho_{A}\Delta^{1}\rho_{B}S_{AB}(Q) + 2\Delta^{1}\rho_{B}\Delta^{1}\rho_{C}S_{BC}(Q) + 2\Delta^{1}\rho_{A}\Delta^{1}\rho_{C}S_{AC}(Q) \\ I_{2}(Q) &= \Delta^{2}\rho_{A}^{2}S_{AA}(Q) + \Delta^{2}\rho_{B}^{2}S_{BB}(Q) + \Delta^{2}\rho_{C}^{2}S_{CC}(Q) + 2\Delta^{2}\rho_{A}\Delta^{2}\rho_{B}S_{AB}(Q) + 2\Delta^{2}\rho_{B}\Delta^{2}\rho_{C}S_{BC}(Q) + 2\Delta^{2}\rho_{A}\Delta^{2}\rho_{C}S_{AC}(Q) \\ \vdots \\ I_{6}(Q) &= \Delta^{6}\rho_{A}^{2}S_{AA}(Q) + \Delta^{6}\rho_{B}^{2}S_{BB}(Q) + \Delta^{6}\rho_{C}^{2}S_{CC}(Q) + 2\Delta^{6}\rho_{A}\Delta^{6}\rho_{B}S_{AB}(Q) + 2\Delta^{6}\rho_{B}\Delta^{6}\rho_{C}S_{BC}(Q) + 2\Delta^{6}\rho_{A}\Delta^{6}\rho_{C}S_{AC}(Q) \end{cases}$$

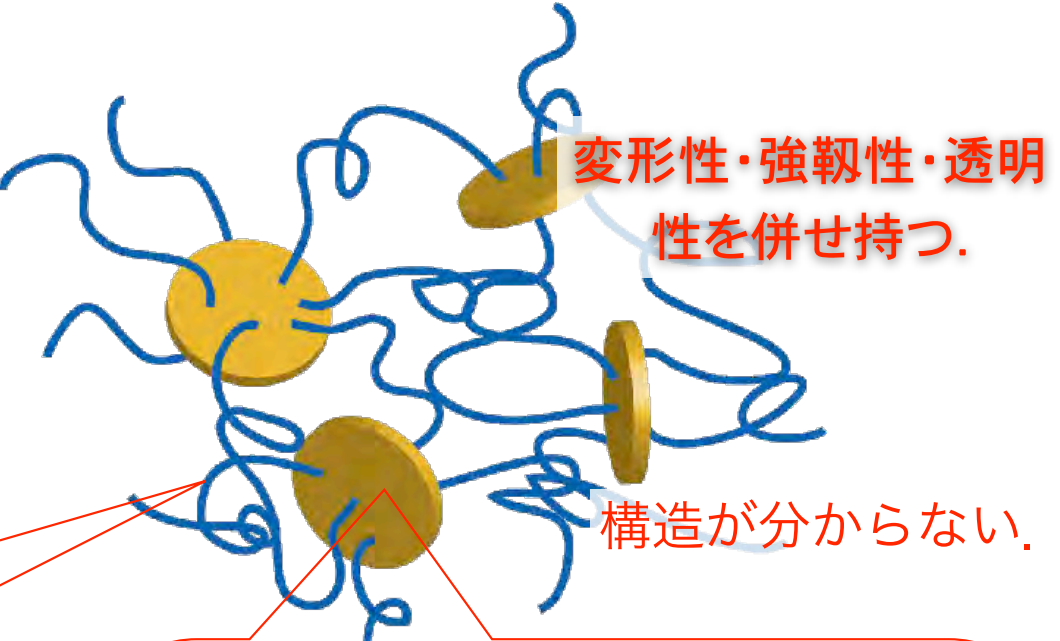
6元1次方程式を解けば、各部分散乱関数を得られる.

NCゲルの構造解析

ナノコンポジット (NC) ゲル

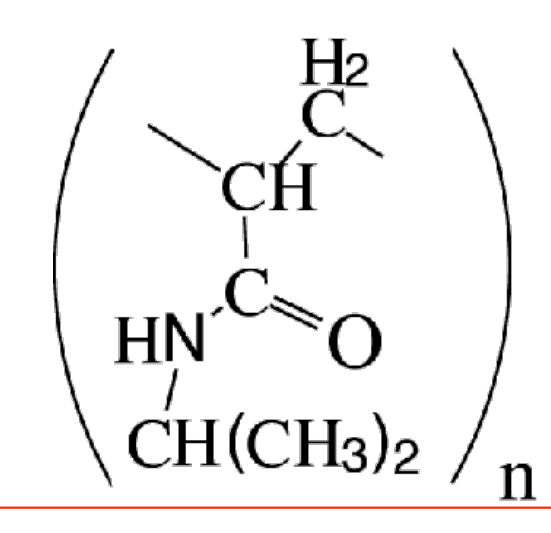
川村理化学研究所・原口和敏博士グループ開発.

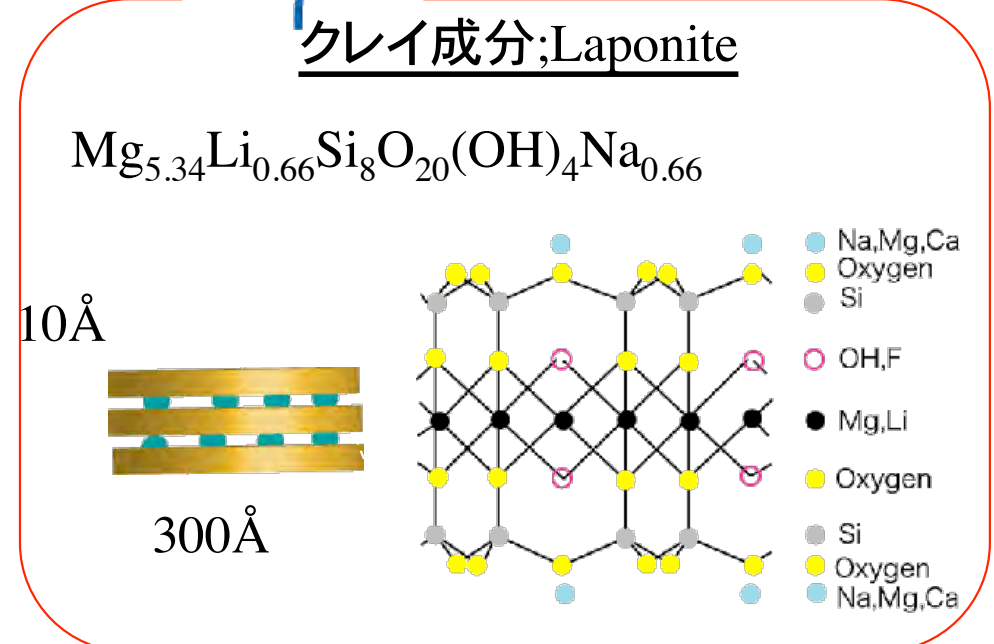




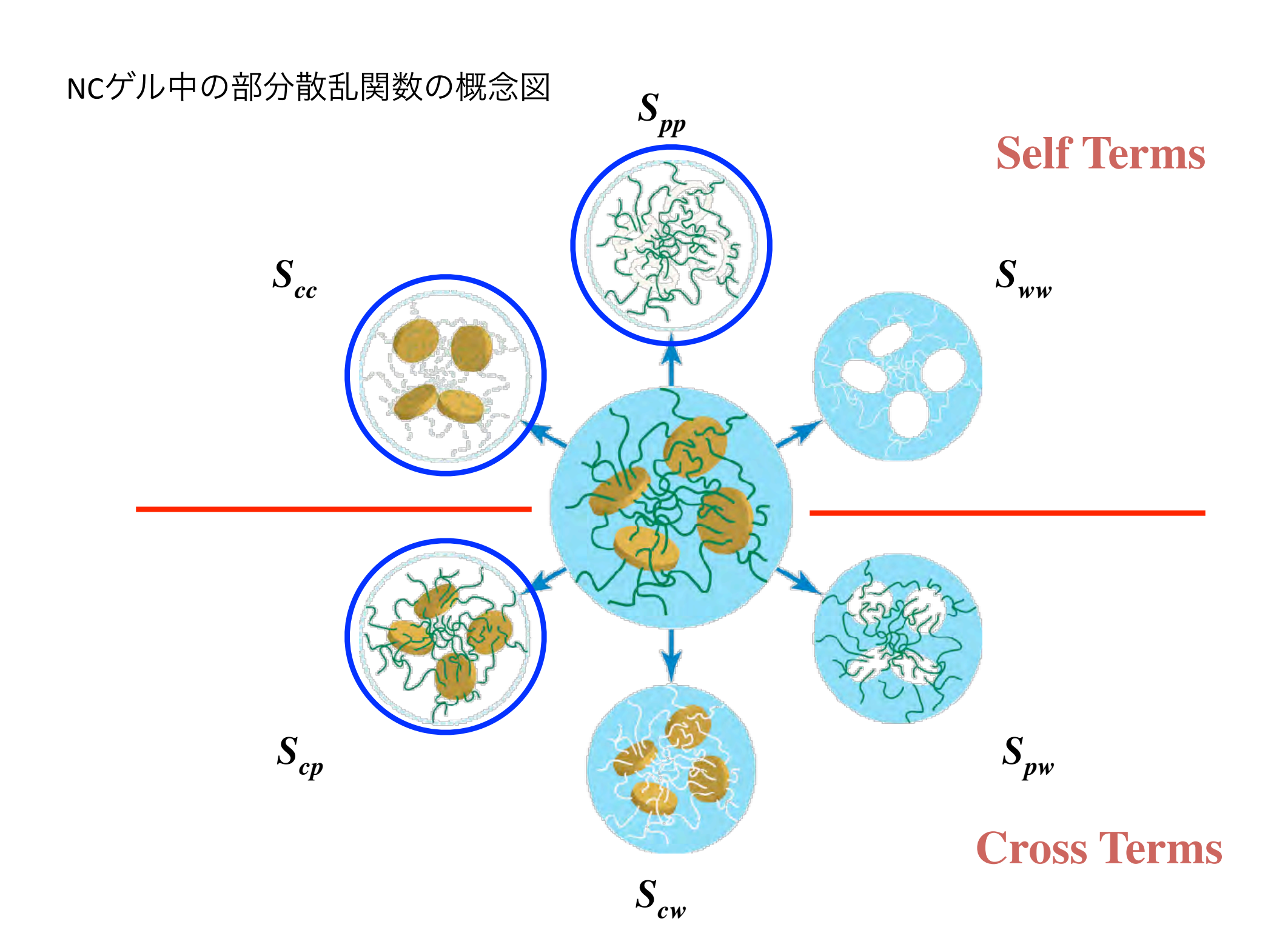
東大物性研・柴山G

高分子:ポリNIPAm





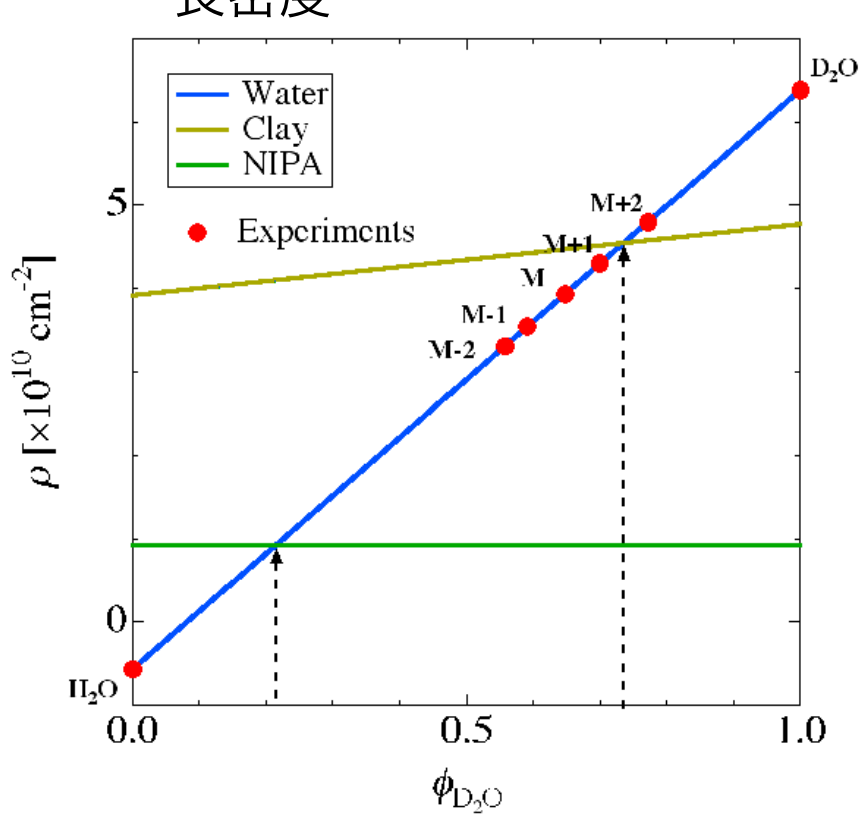
Haraguchi et al. Macromolecules, 2002, 35, 10162



NCゲルを用いたコントラスト変調実験.

D₂O/H₂O比と各成分の散乱



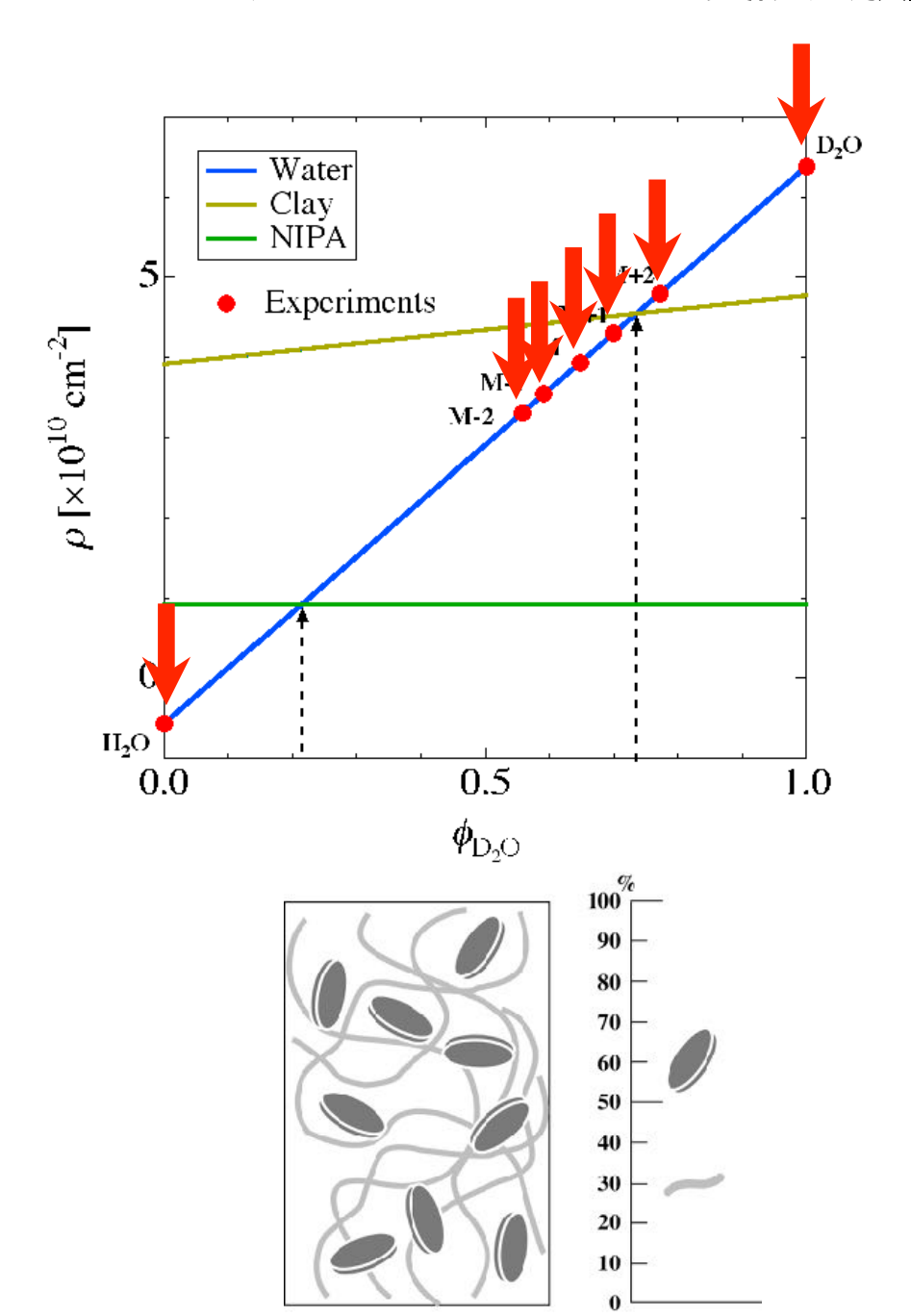


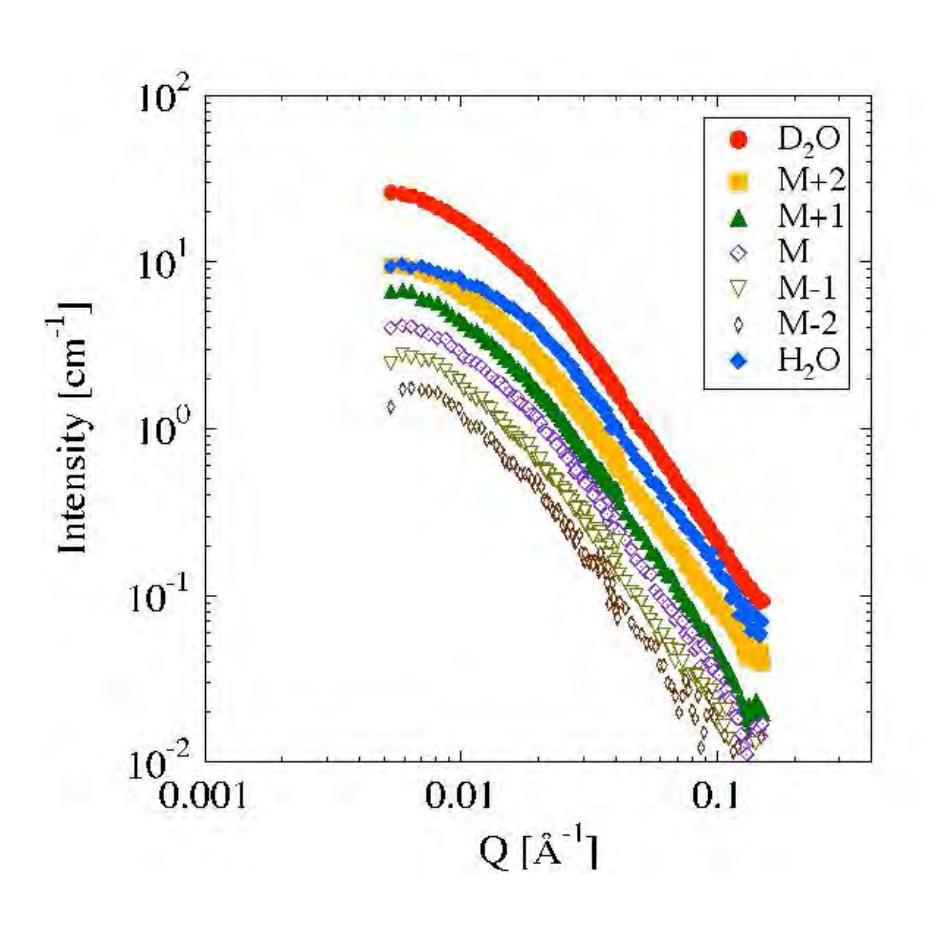
NCゲル

クレイの体積分率: $\phi_{Clay} = 0.013$ 高分子の体積分率: $\phi_{Polymer} = 0.042$

クレイを分散させた水溶液中でラジカル重合を行う.

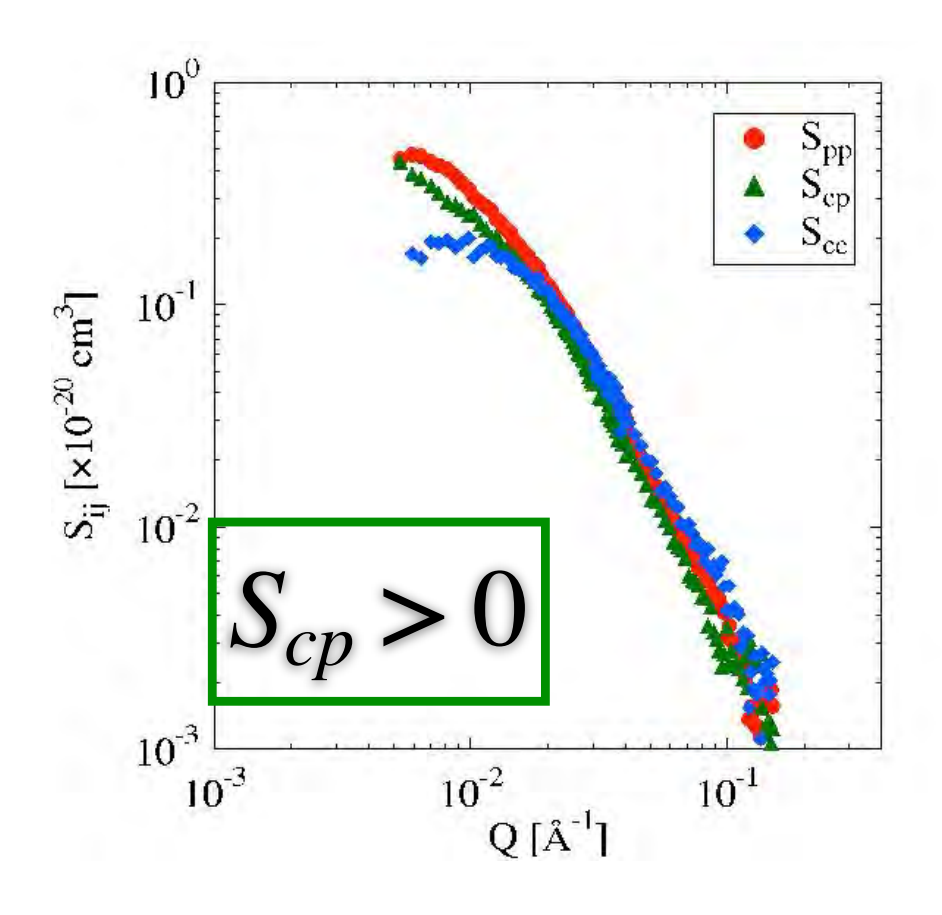
NCゲルを用いたコントラスト変調実験.



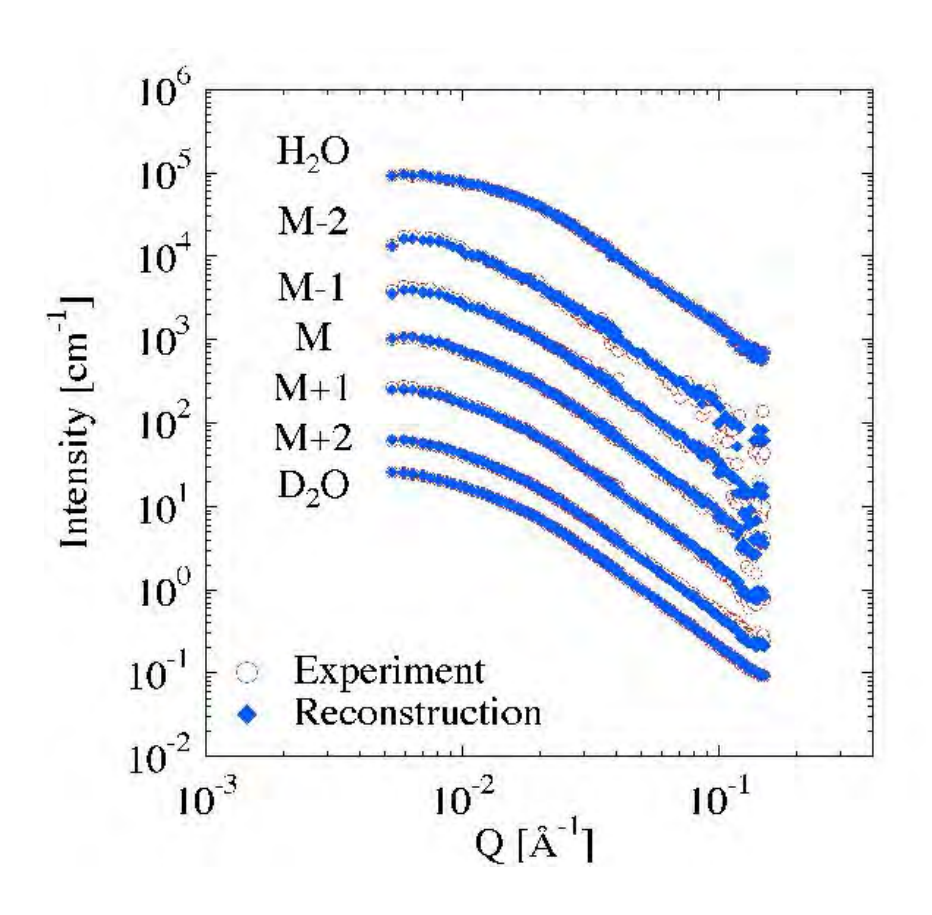


各コントラストで得られた 散乱強度

NCゲルを用いたコントラスト変調実験.

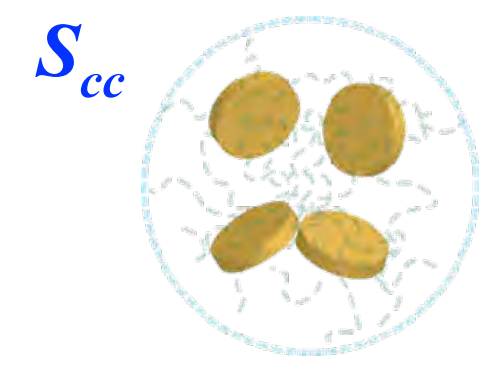


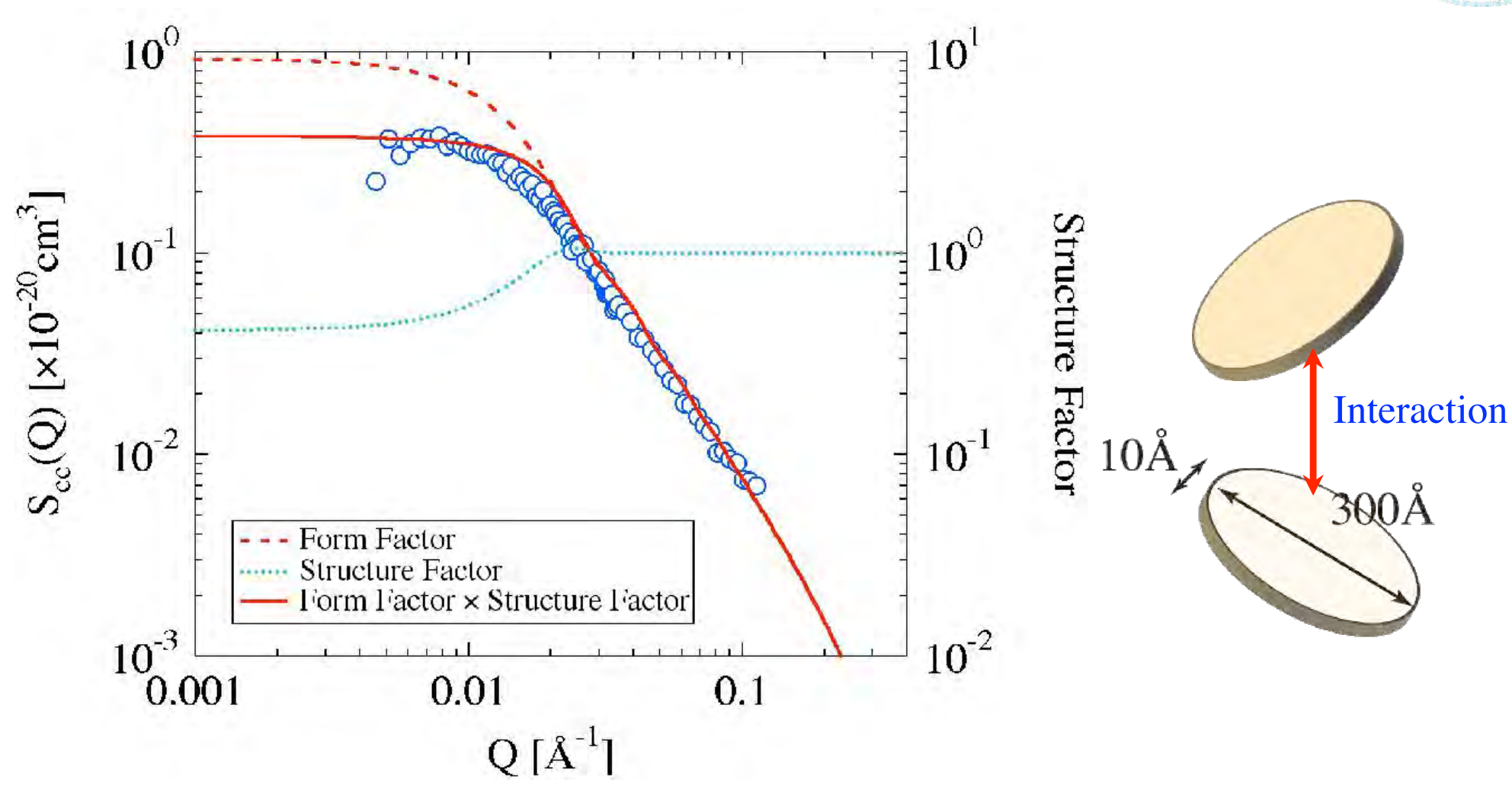
分離した部分散乱関数



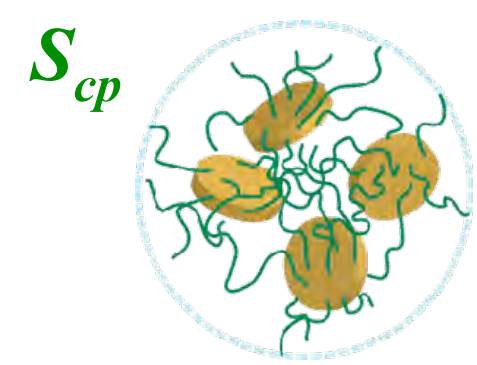
実験値と再構築した強度との比較

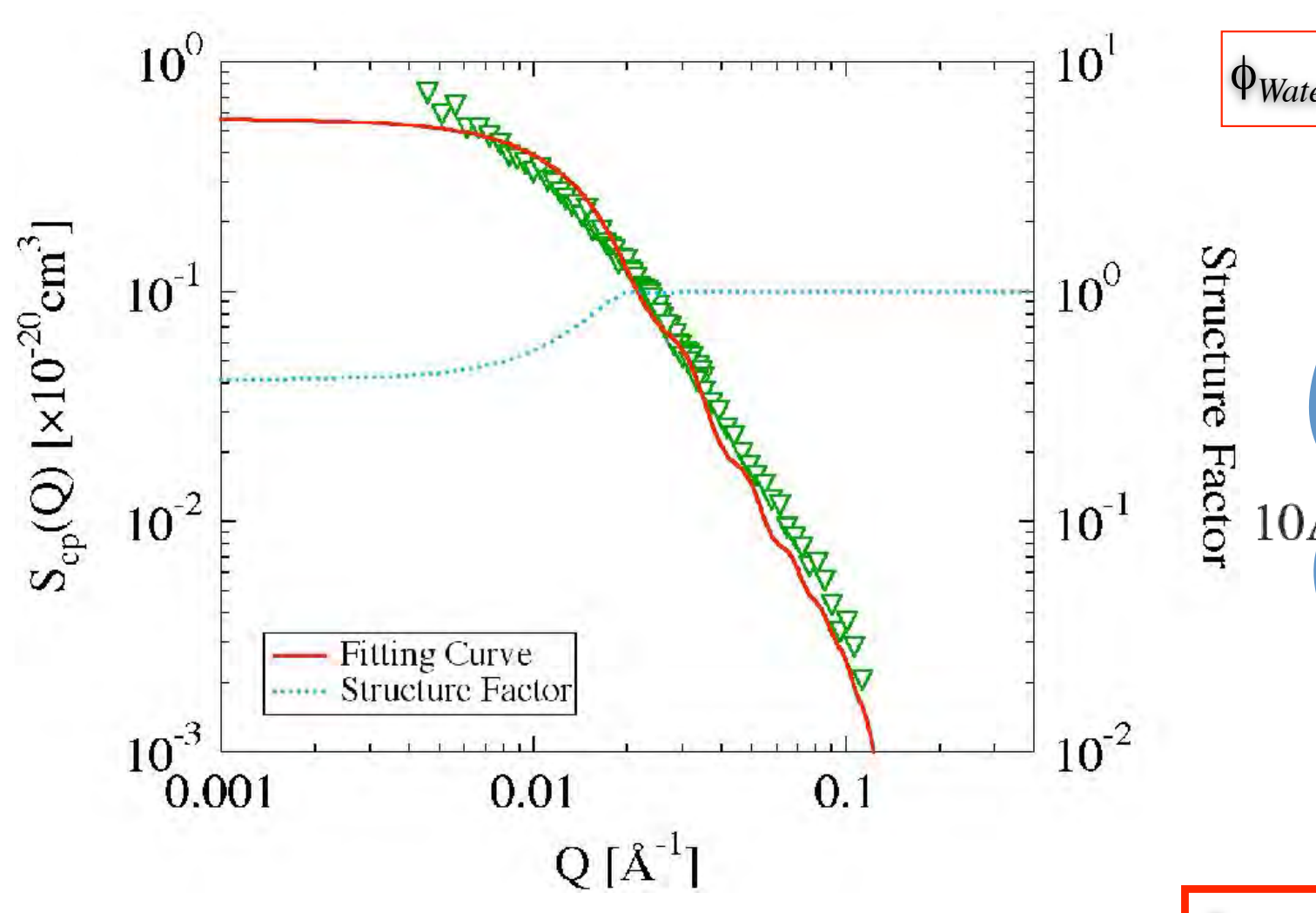
部分散乱関数の解析.

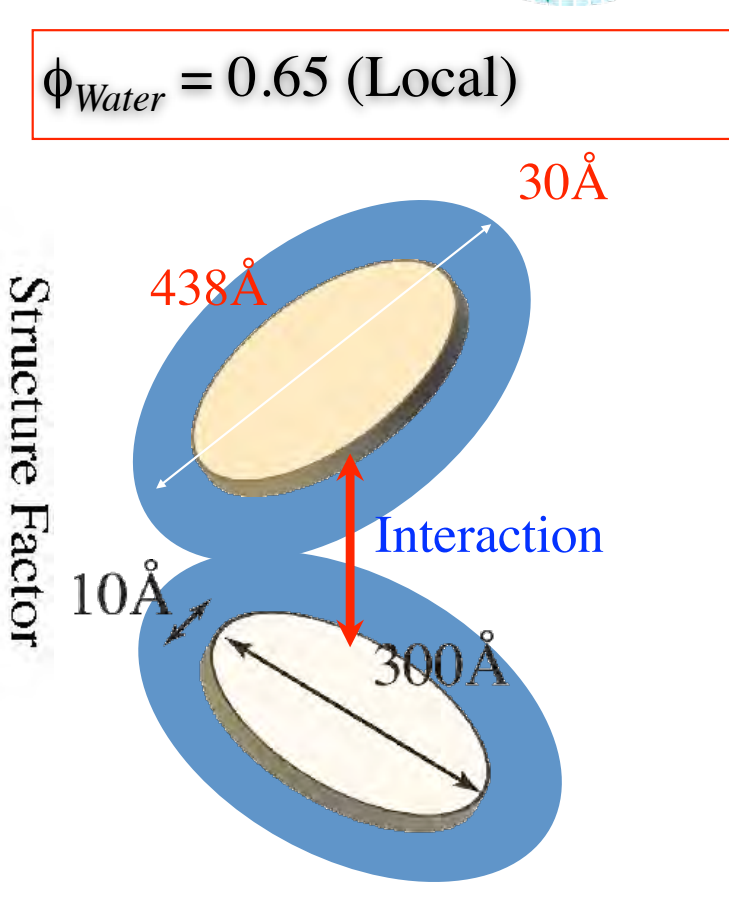




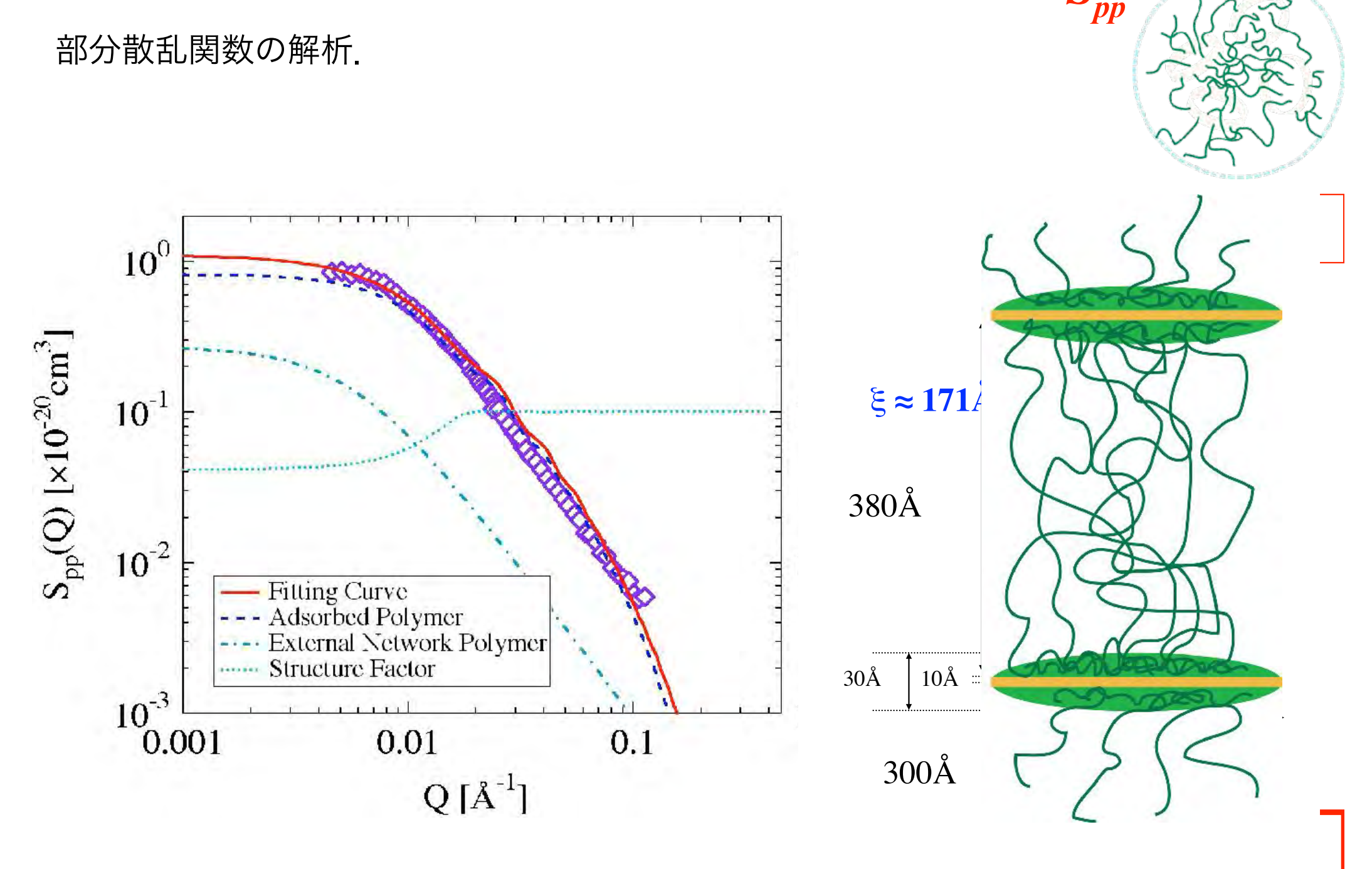
部分散乱関数の解析.







$$\Phi_{Water} = 0.95 \text{ (Overall)}$$



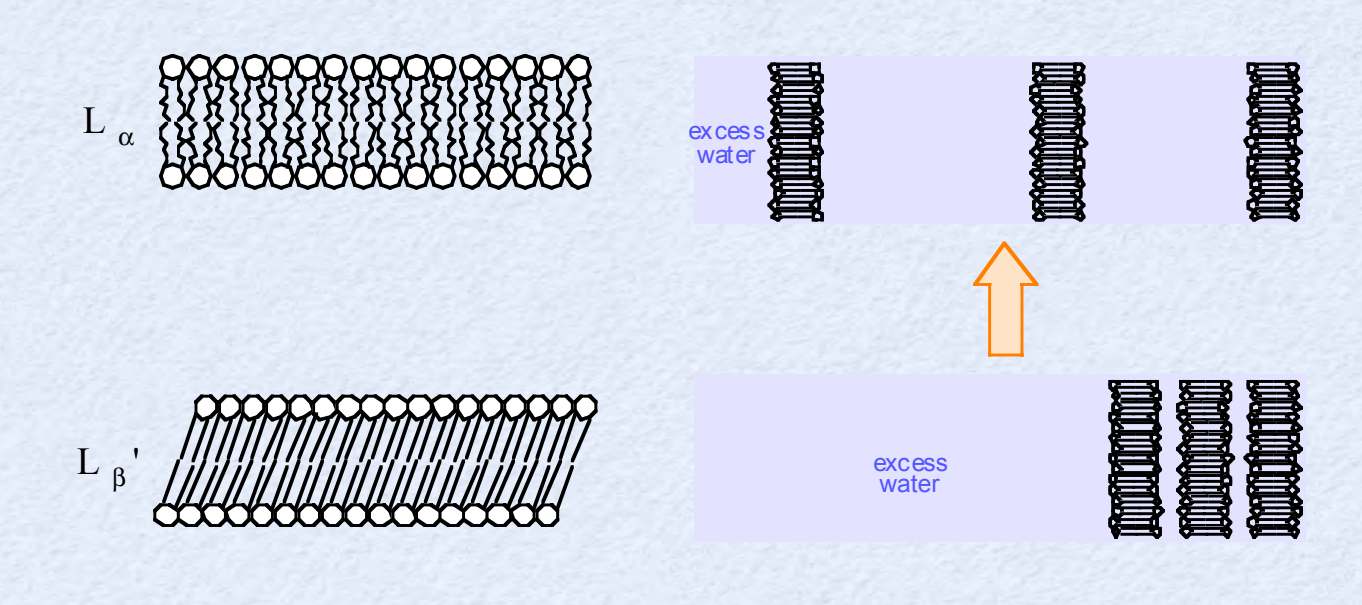
Endo et al. Macromolecules, 2008, 41, 5406

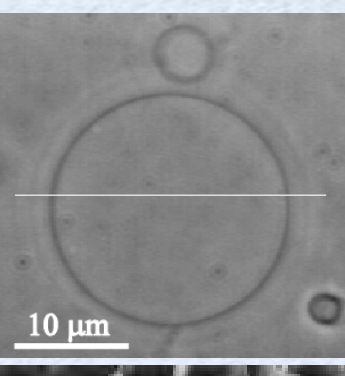
研究例3

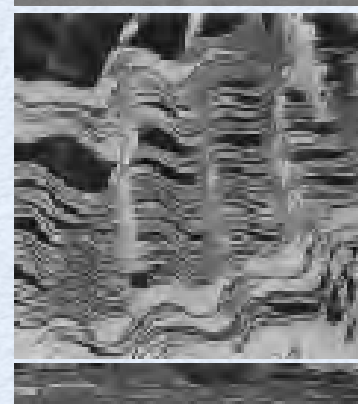
Unbinding of a lipid bilayer

リン脂質二重膜の作る構造

unilamellar/multilamellar unbinding transition

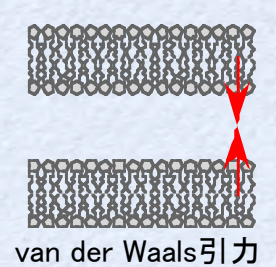




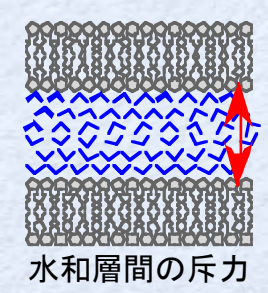




Inter-bilayer interaction







$$f = f_{vdW} + f_{Ca} + f_{hyd} + f_{st},$$

$$f_{vdW} = -\frac{H}{12\pi} \left\{ \frac{1}{d_w^2} - \frac{2}{(d_w + d_l)^2} + \frac{1}{(d_w + 2d_l)^2} \right\},$$

$$f_{Ca} = \bar{f}_{Ca}(d_w) - \bar{f}_{Ca}(\infty),$$

$$f_{hyd} = P_h \lambda \exp\left[-\frac{d_w}{\lambda}\right],$$

$$f_{st} = 0.42 \frac{(k_B T)^2}{K_c d_w^2},$$

$$10^3 - \frac{30\text{mM}}{40\text{mM}} - \frac{50\text{mM}}{60\text{mM}} - \frac{50\text{mM}}{70\text{mM}} - \frac{60\text{mM}}{10^3} - \frac{70\text{mM}}{10^3} - \frac{1000}{1000}$$

$$t_{w}(z)$$

unbinding transition = 2nd order transition

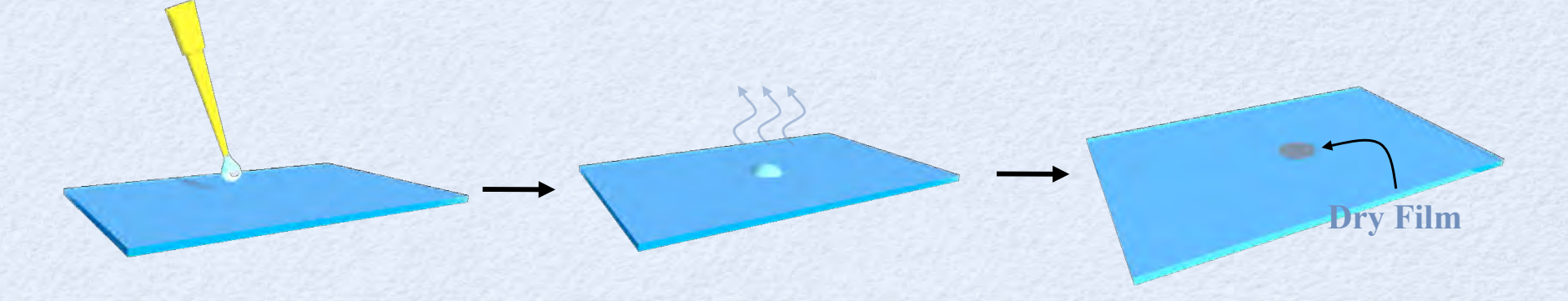
Natural swelling method

Lipid Dry film

(1) Lipids are solved in an organic solvent.

(2) The organic solvent are evaporated.

(3) Dry lipid film remains on a solid substrate.



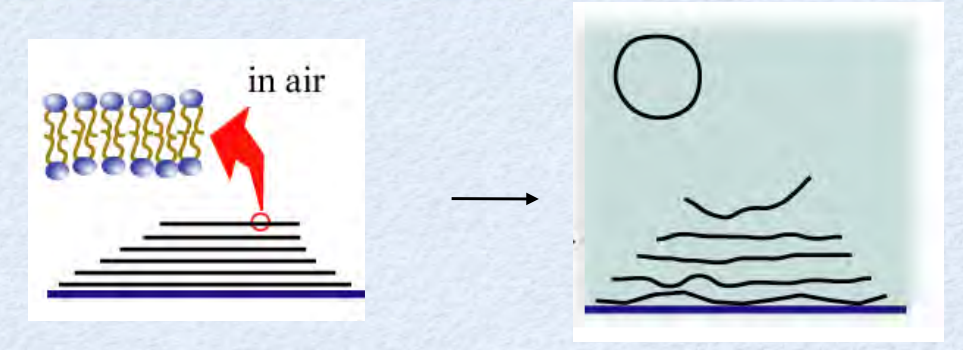
Hydration

(4) After the hydration, Giant Vesicles are formed spontaneously.

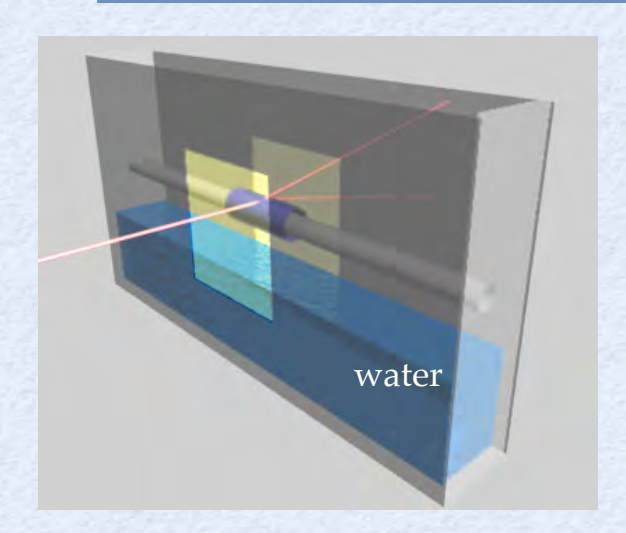
** A.D. Bangham et al., J. Mol. Biol. 13 (1965) 238. ** N. Magome, T. Takemura, K. Yoshikawa, Chem. Lett. 26 (1997) 205.

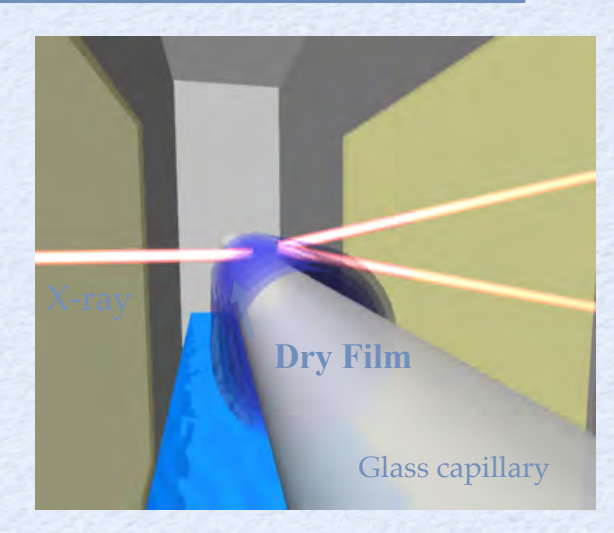
SAXSによる時分割測定

Hishida et al., Chem. Phys. Lett. 2008



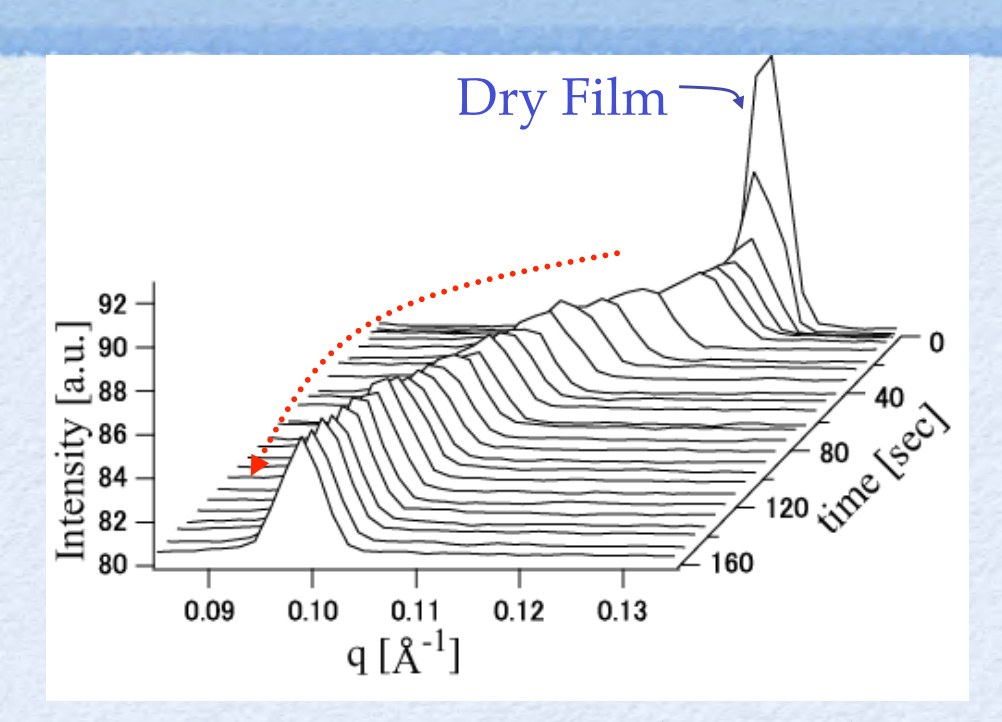
Time-resolved SAXS measurement

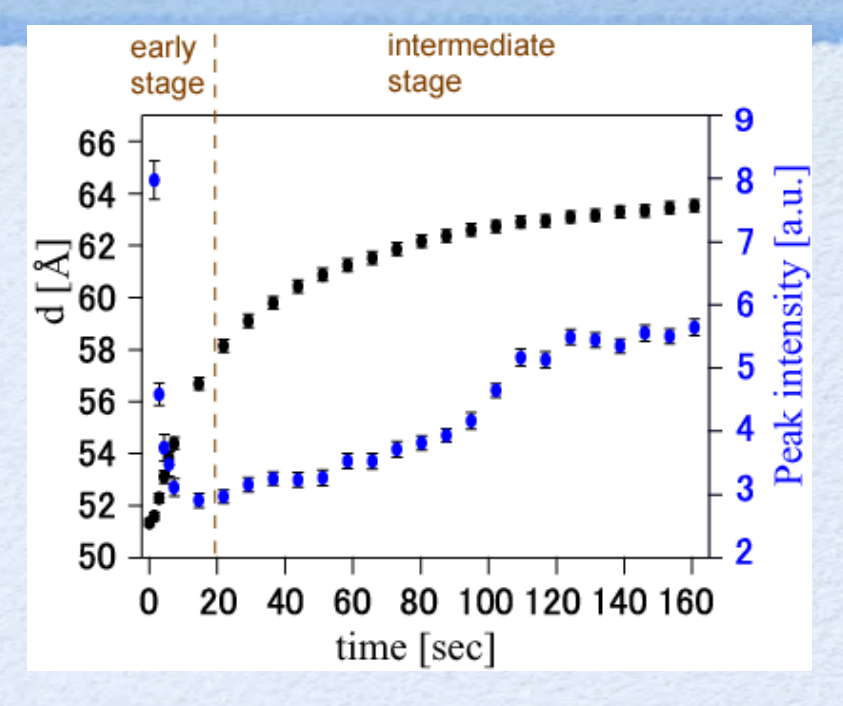




SPring-8, BL40B2 λ=1Å, Camera-length=1m, Detector: CCD room temperature

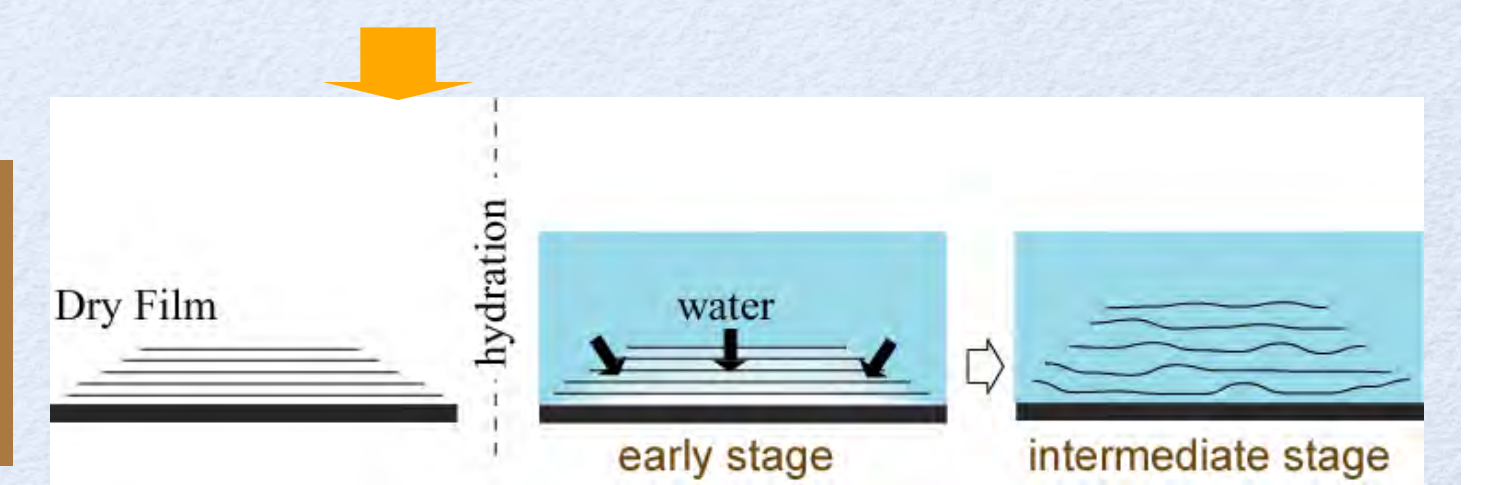
The early stage (0~20s) and the intermediate stage (20~200s)



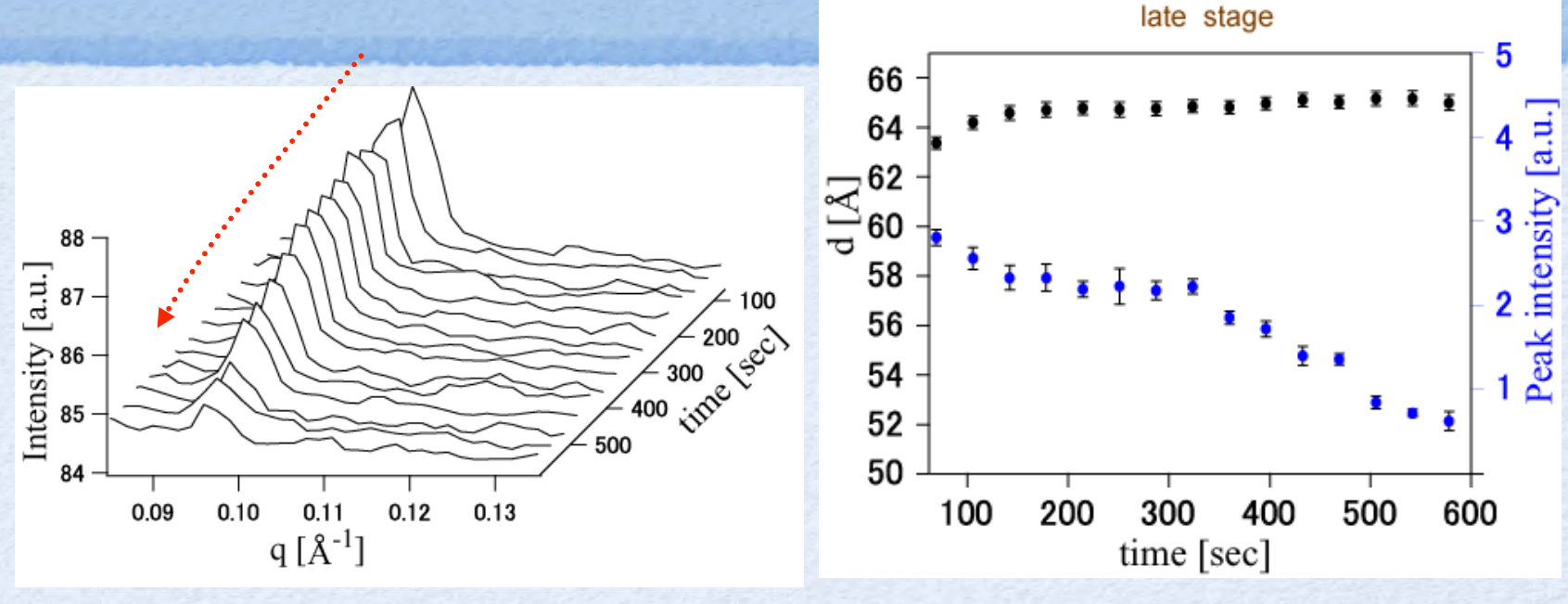


- Repeat distance between layers "d" increases inverse-exponentially.
- The peak intensity decreases in the early stage, and recovers in the intermediate stage.

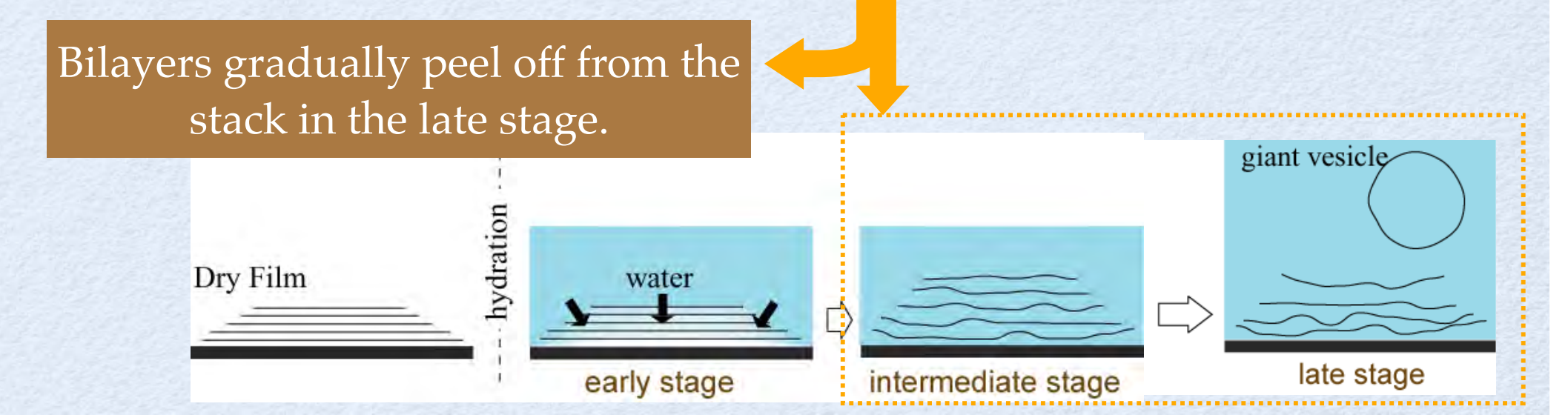
Penetration of water &
Relaxation to be a quasi-stable state

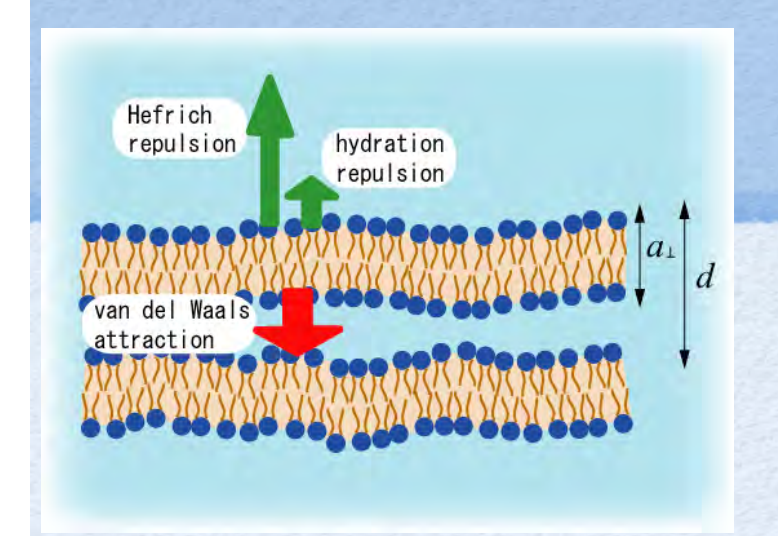


The late stage (100 - 600 s)



- "d" is almost constant ($\approx 64 \text{ Å}$).
- The peak intensity decreases monotonically. (The peak width is almost constant.)





*H.I. Petrache et al., Phys. Rev. E 57 (1998) 7014 **W. Helfrich, Z. Naturforsch 33a (1978) 305

Free energy profile per unit area as a function of "d"

$$F(d) = F_{vdW}(d) + F_{hyd}(d) + F_{Ste}(d)$$

van der Waals interaction*

$$F_{vdW}(d) = -\frac{H}{12\pi} \left[\frac{1}{(d - a_{\perp})^2} - \frac{2}{(d)^2} + \frac{1}{(d + a_{\perp})^2} \right]$$

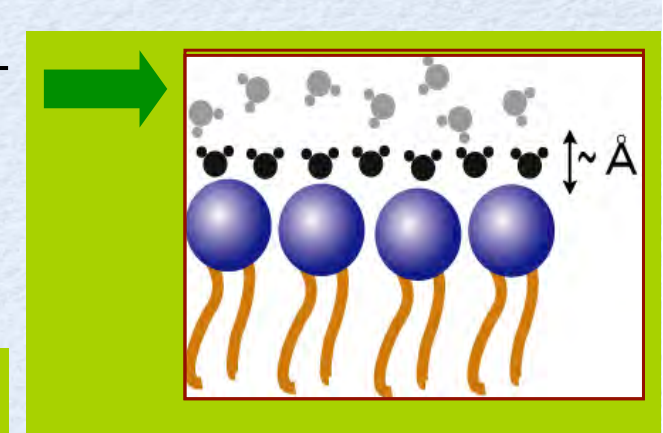
<u>Hydration repulsion</u>* $F_{hyd}(d) = P_{hyd}\lambda \exp\left(-\frac{(d-a_{\perp})}{\lambda}\right)$

Steric repulsion**
(Helfrich repulsion)
$$F_{Ste}(d) = 0.42 \frac{(k_B T)^2}{K_c (d - a_\perp)^2}$$



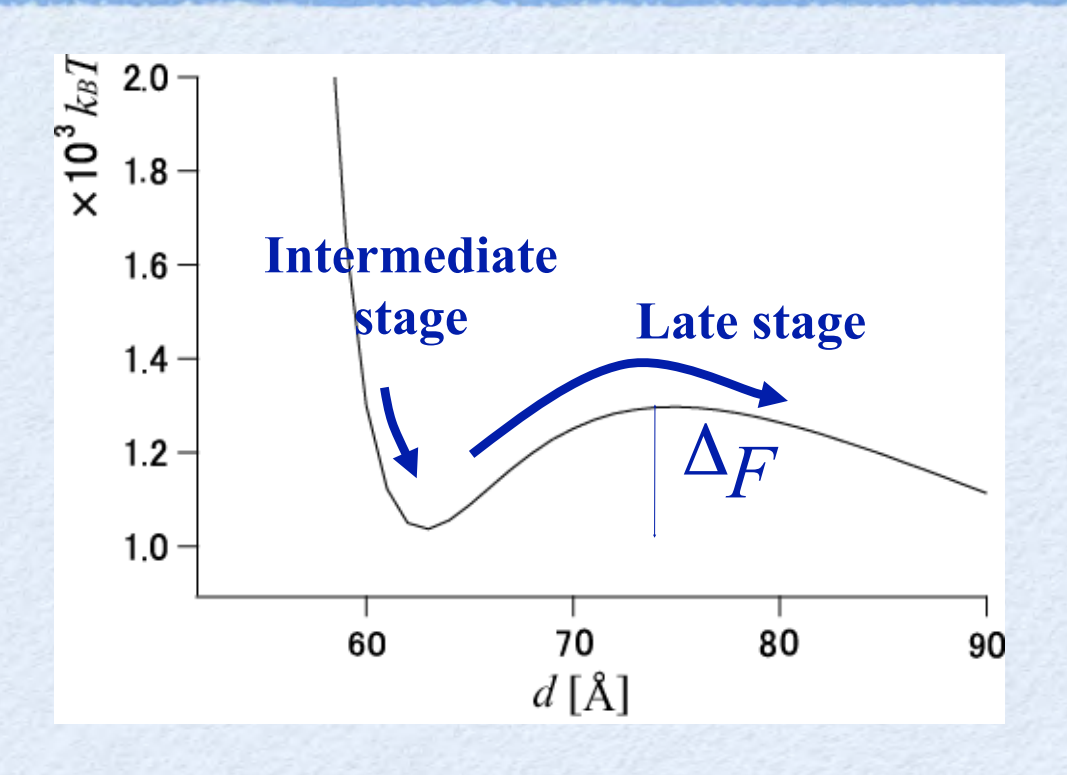
Steric repulsion originates from thermal fluctuation

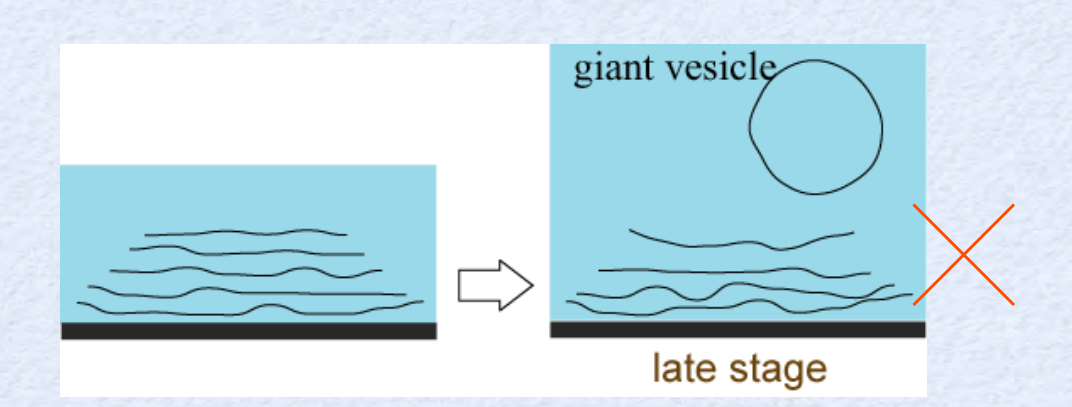
Long-range repulsion $\sim 10^{-1} \mu m$



Short-range repulsion

This process should be the 1st order transition





The energy barrier

 $\Delta F \sim 10^2 - 10^3 k_B T$

Diffusion (peeling-off) is too slow to observe.

→ Bilayers remain stacked and giant vesicles are not formed. One side of the outermost bilayers is not restricted by other bilayers.

$$F(d) = F_{vdW}(d) + F_{hyd}(d) + A F_{Ste}(d)$$

van der Waals interaction

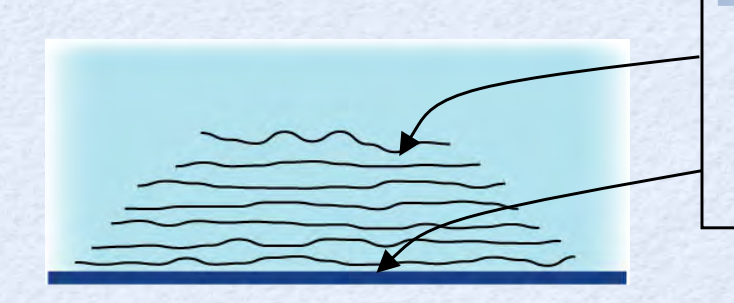
Hydration repulsion

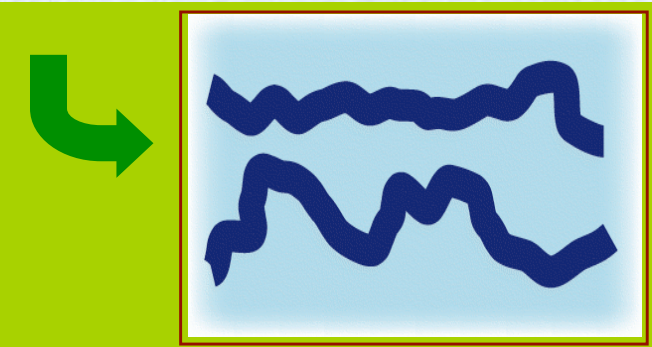
Steric repulsion

A : Effective Steric repulsion

The outermost layer: A>1

The inner layer: A=1

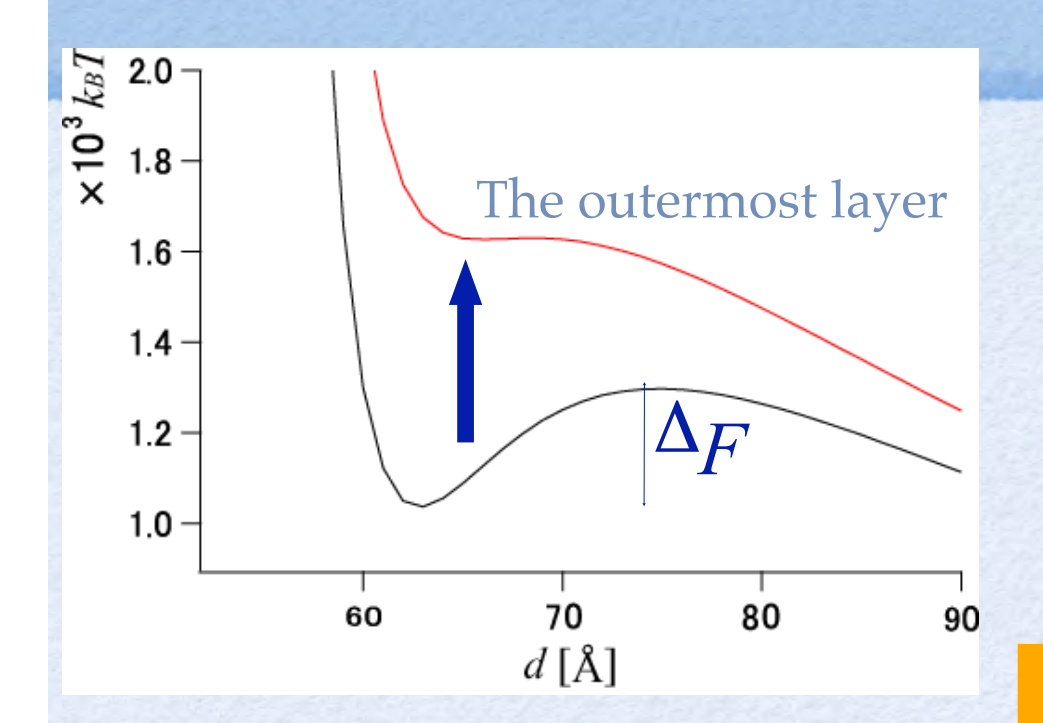




Steric repulsion originates from thermal fluctuation

Long-range repulsion ~10-1 µm

Unbinding kinetics of the outermost bilayer



Inner layers: $\Delta F \sim 10^2 - 10^3 k_B T$

 \rightarrow Diffusion is too slow to observe.



→ Bilayer is unbound by thermal fluctuation to form a giant vesicle.

Fokker-Planck equation (Smoluchowski equation)

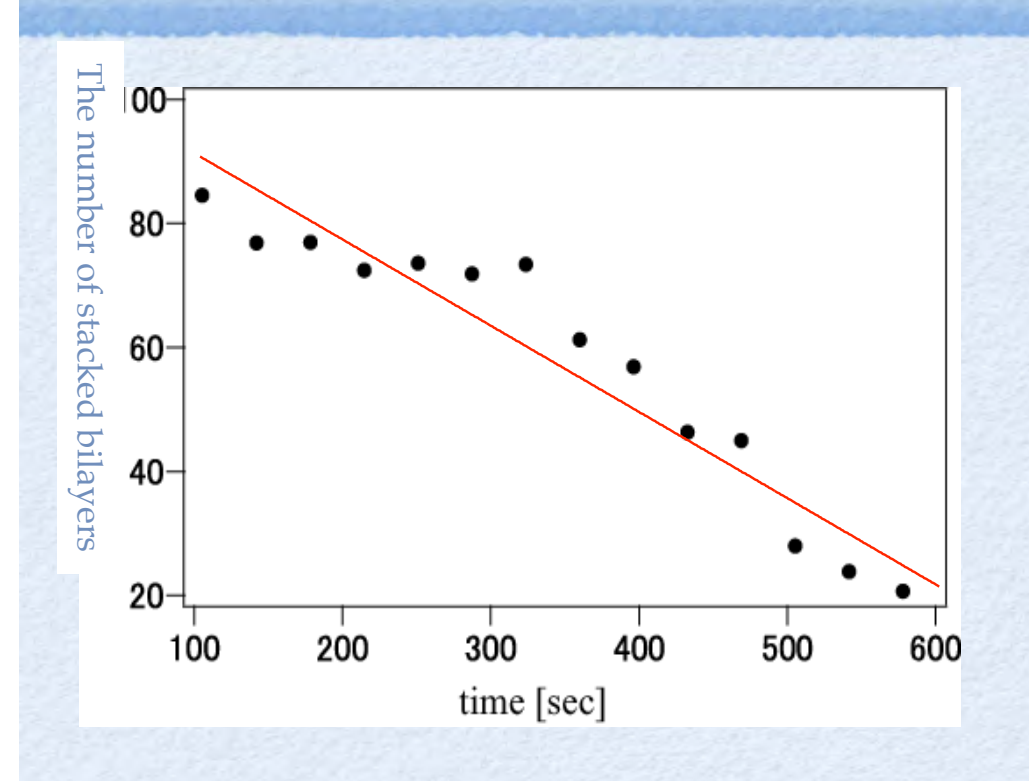
$$\frac{\partial f}{\partial t} = \frac{1}{\gamma m} \frac{\partial}{\partial d} \left(-Kf + k_B T \frac{\partial f}{\partial d} \right) K = -\frac{\partial F}{\partial d}$$

$$K = -\frac{\partial F}{\partial d}$$

The rate of unbinding through the energy barrier. (Kramers' rate)

$$r = \frac{1}{\sqrt{2\pi}} \frac{cc'm}{16\mu R} \exp\left(-\frac{\Delta F}{k_B T}\right)^{\frac{1}{2}}$$

Compared with the experimental result



The time-dependence of the number of stacked bilayers calculated with this assumption is consistent with the experimental result.

(A = 1.0433)



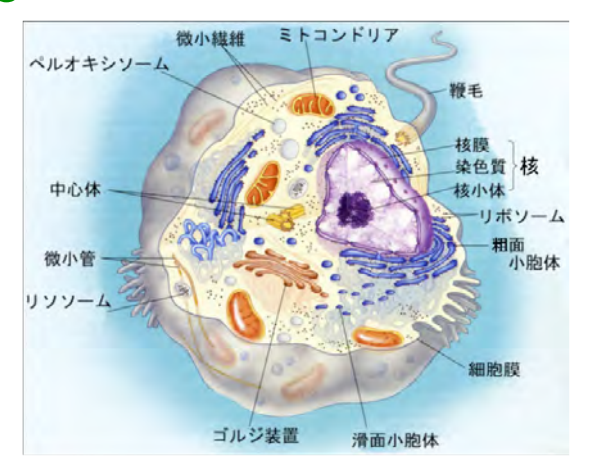
A few-percent increase in steric repulsion only for the outermost bilayer triggers the peeling-off of bilayers from the stack.

研究例-4

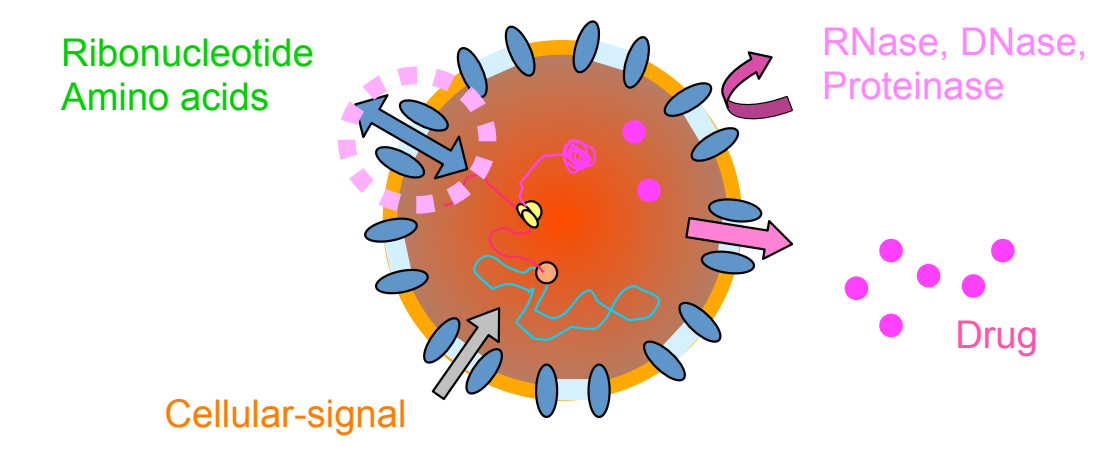
Spontaneous Blebbing of an Interface

How to characterize living systems?

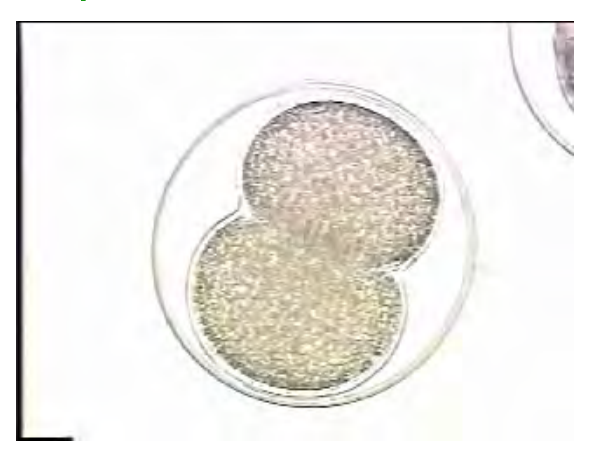
Self-organization



Exchange of materials/information



Self-duplication



Spontaneous motion / deformation





Spontaneous motion of cells

Amoeboid motion

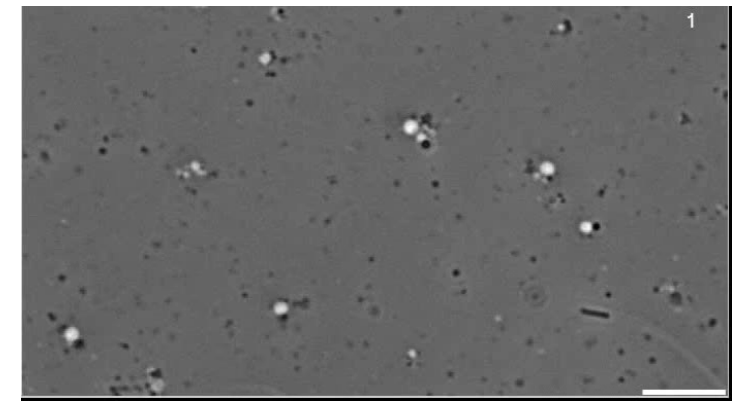
the extension of pseudopods is partially driven by generation of actomyosin gel (Amoeba, Keratocyte, Leukocyte, etc)



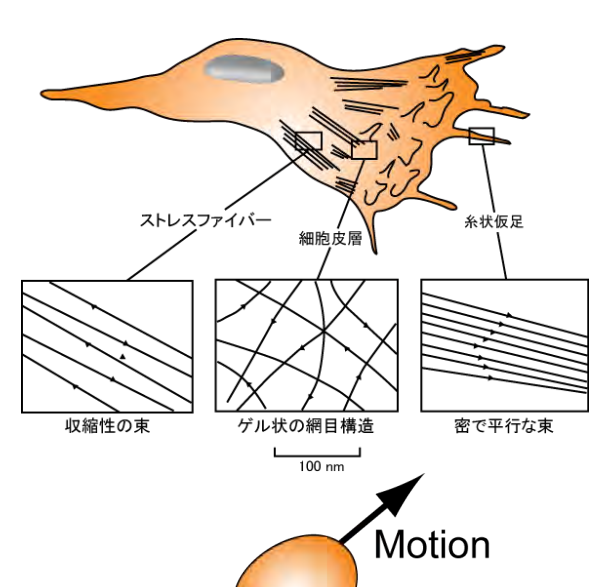
Listeria motion

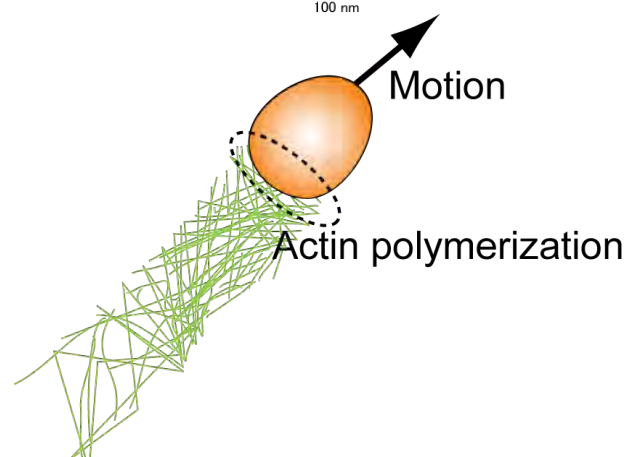
propels itself by generating a tail-like actin gel from G-actin in the cytoplasm of its host cell (actin rocket)

45 times speed









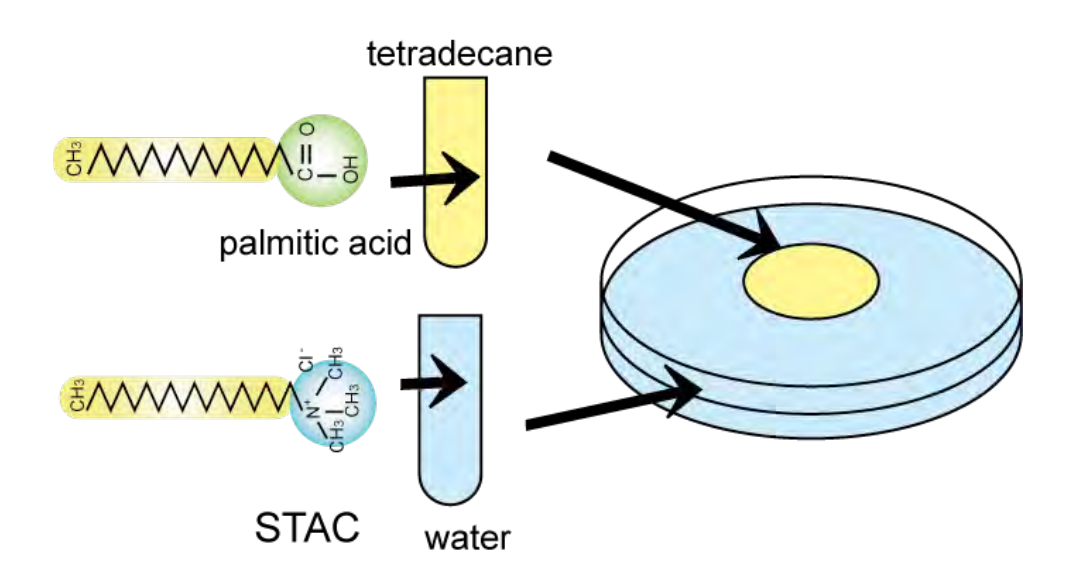
The generation of aggregates can be a simple and important factor of biological motility.



Model system to investigate spontaneous motion of interface

Tetradecane $(C_{14}H_{30})$ + Palmitic Acid (PA)

$$C_{\rm P} = 1 \sim 20 \, \text{mM}$$

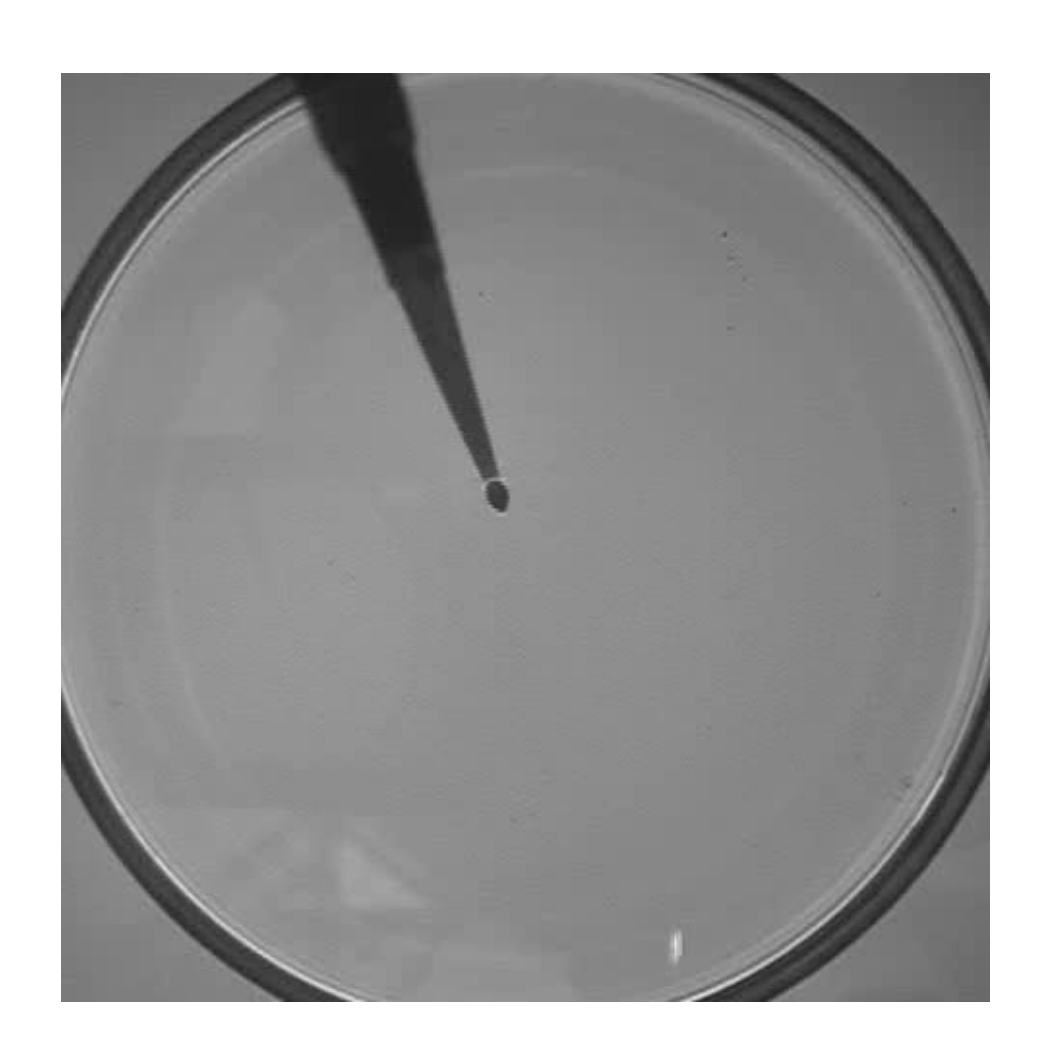


Water + SteayItrimethylammonium Chloride(STAC)

$$C_{\rm S}$$
=0.1~100 mM



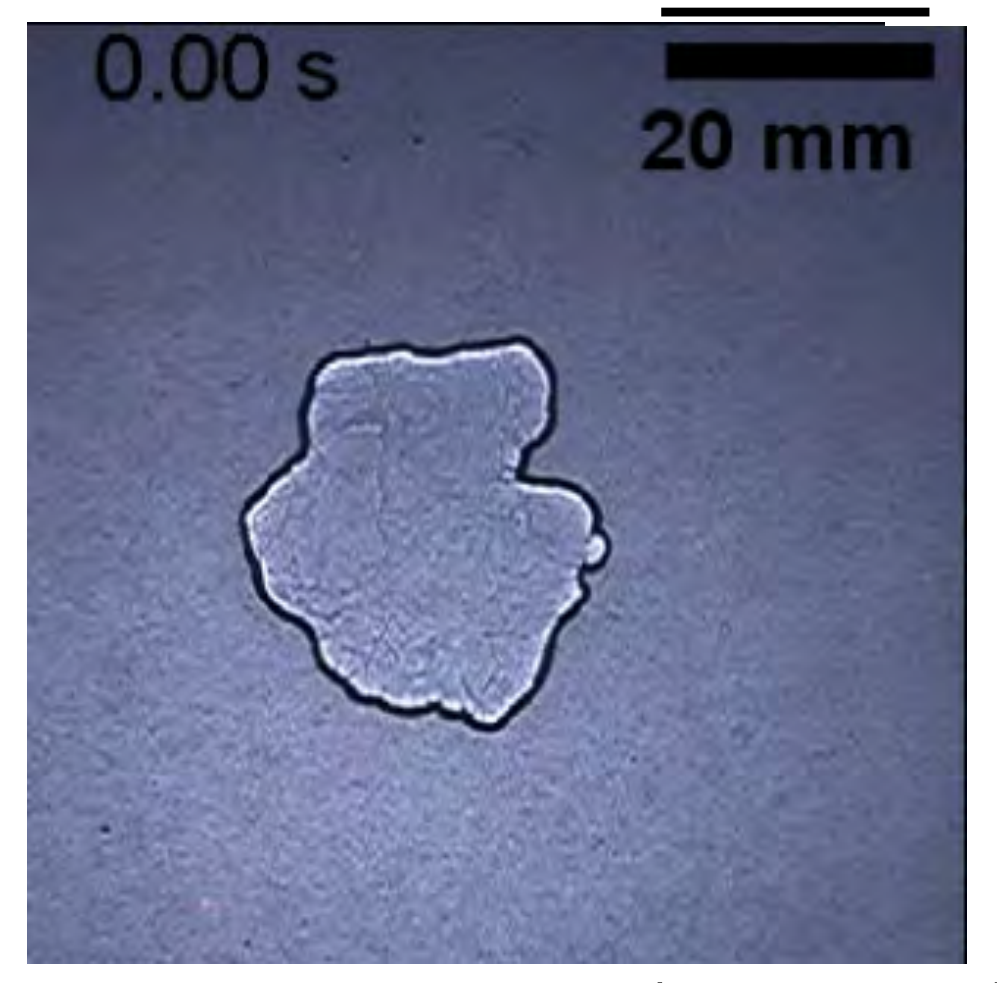
Typical example



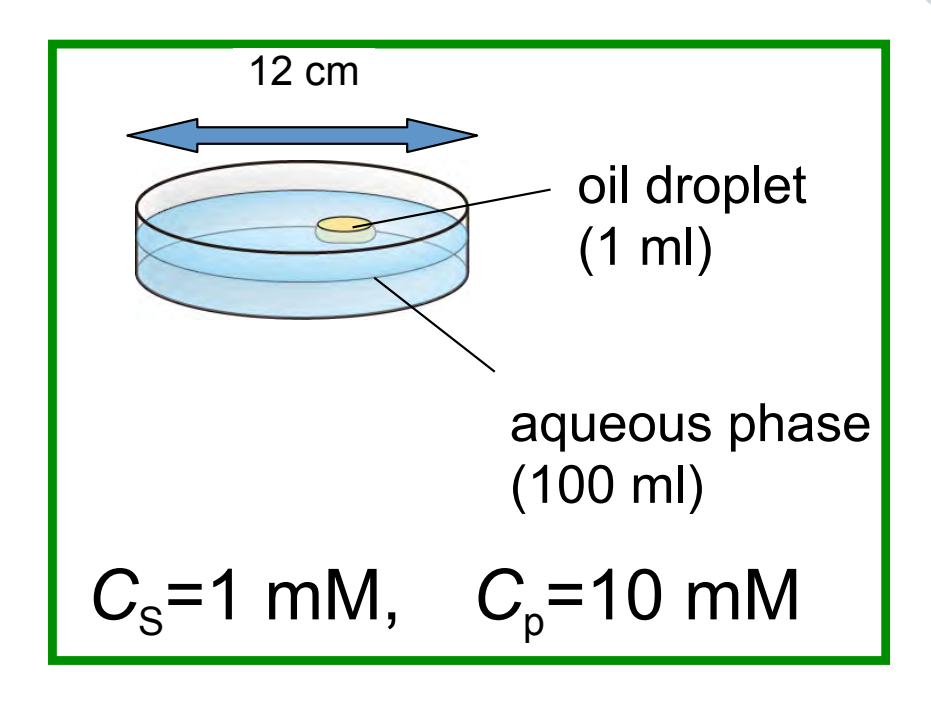


Blebbing of oil/water interface

20 mm



(speed x10)



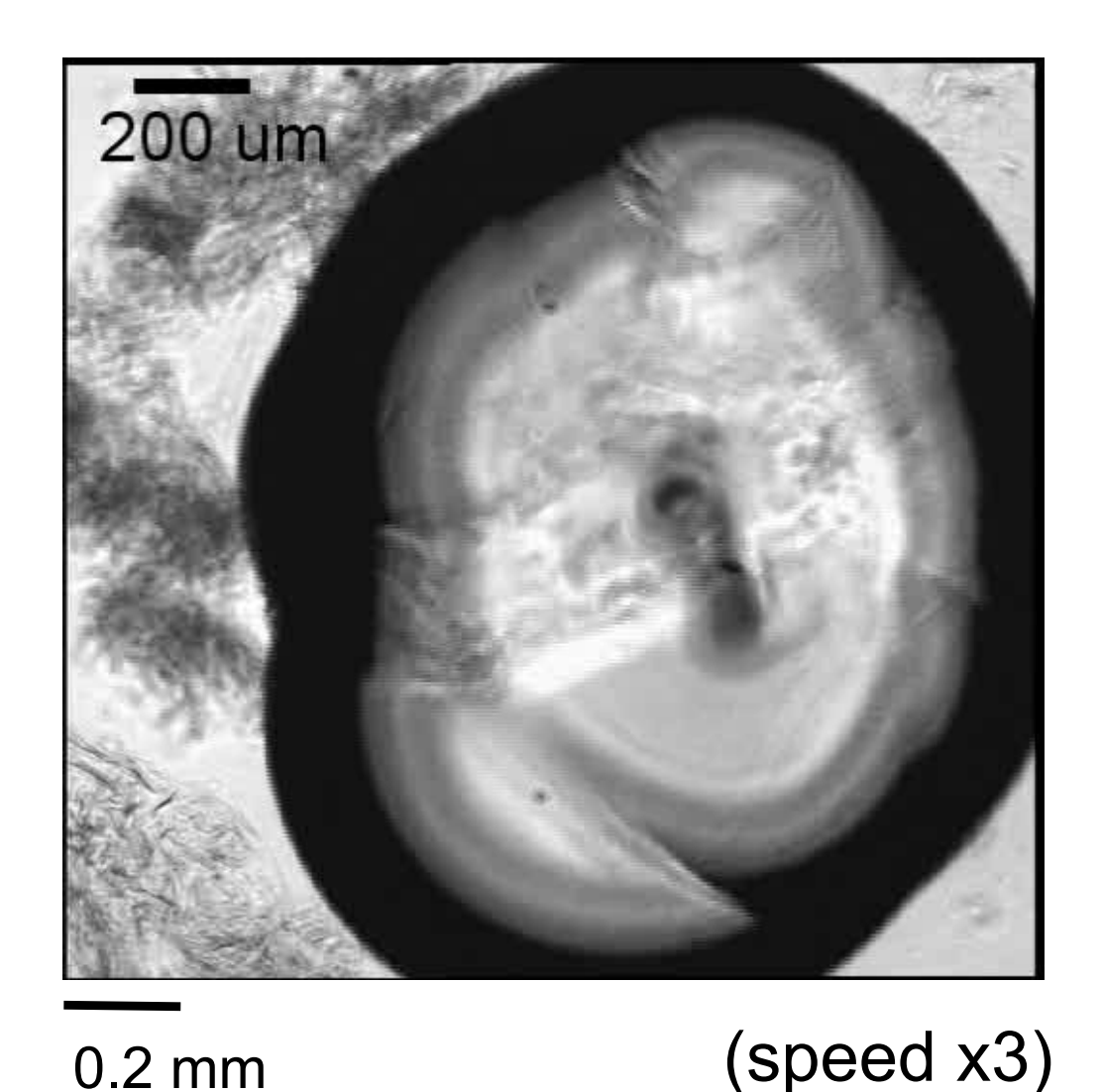
No convection flow was observed



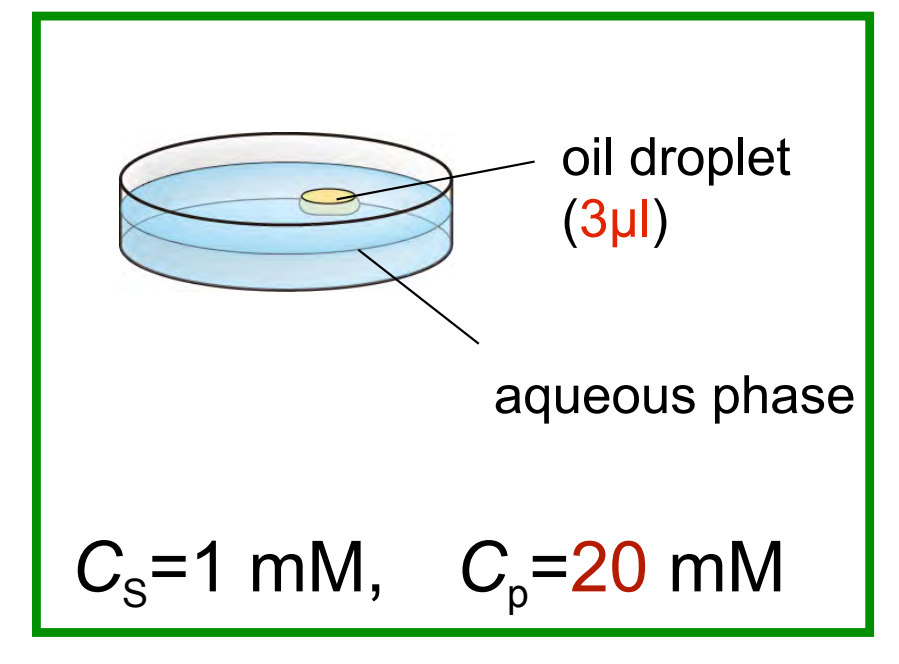
Marangoni instability

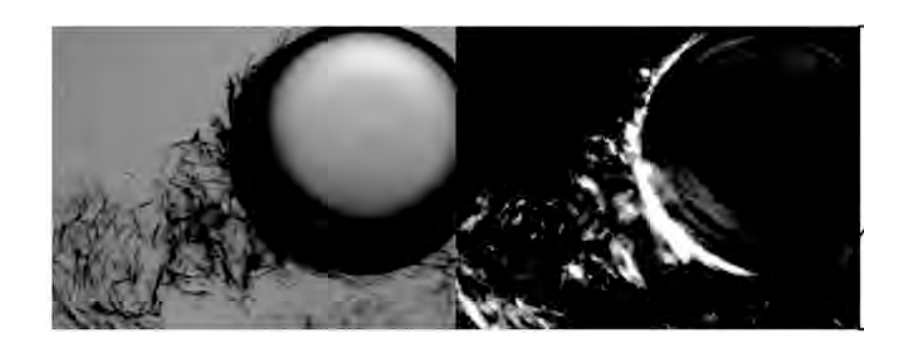


Generation of aggregates









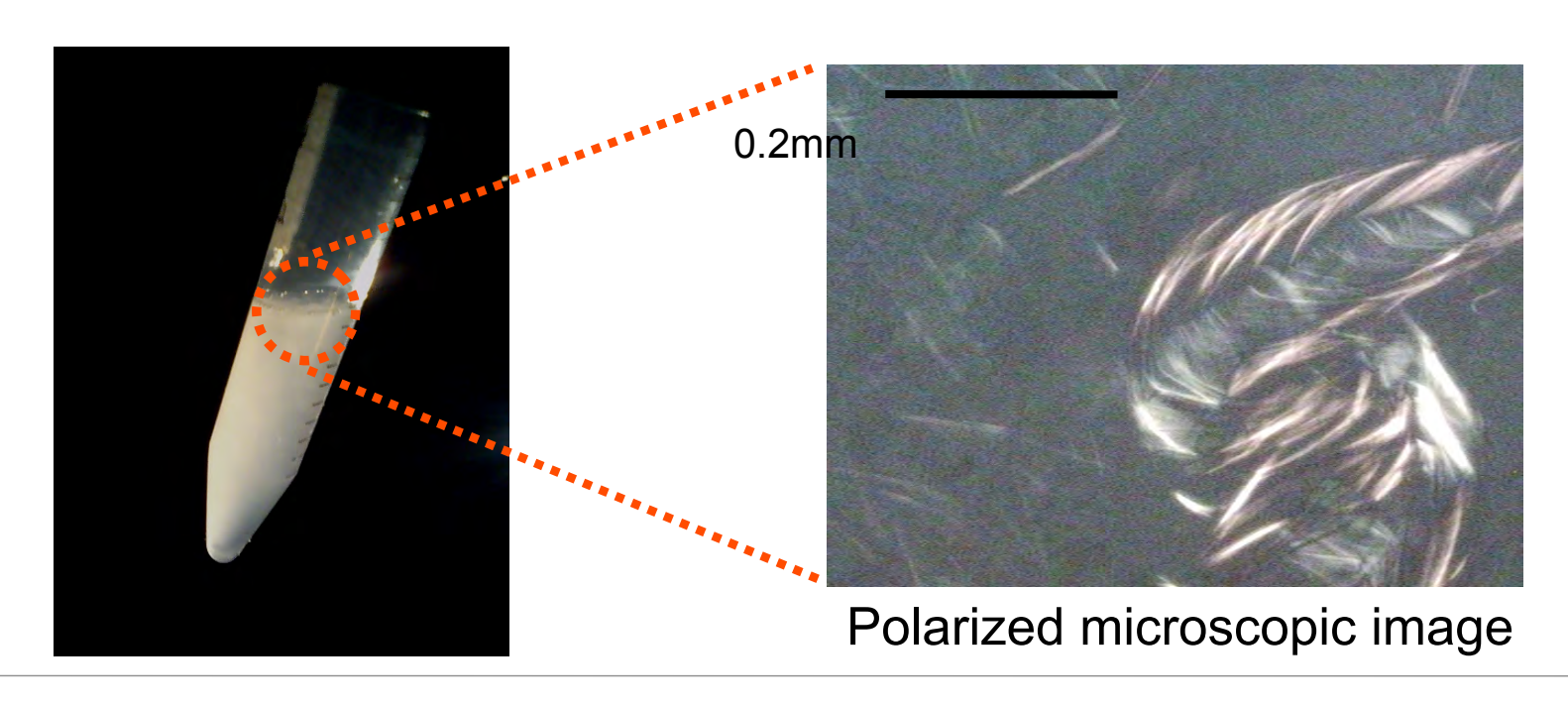


What is the aggregates?

Aqueous phase : STAC+PA

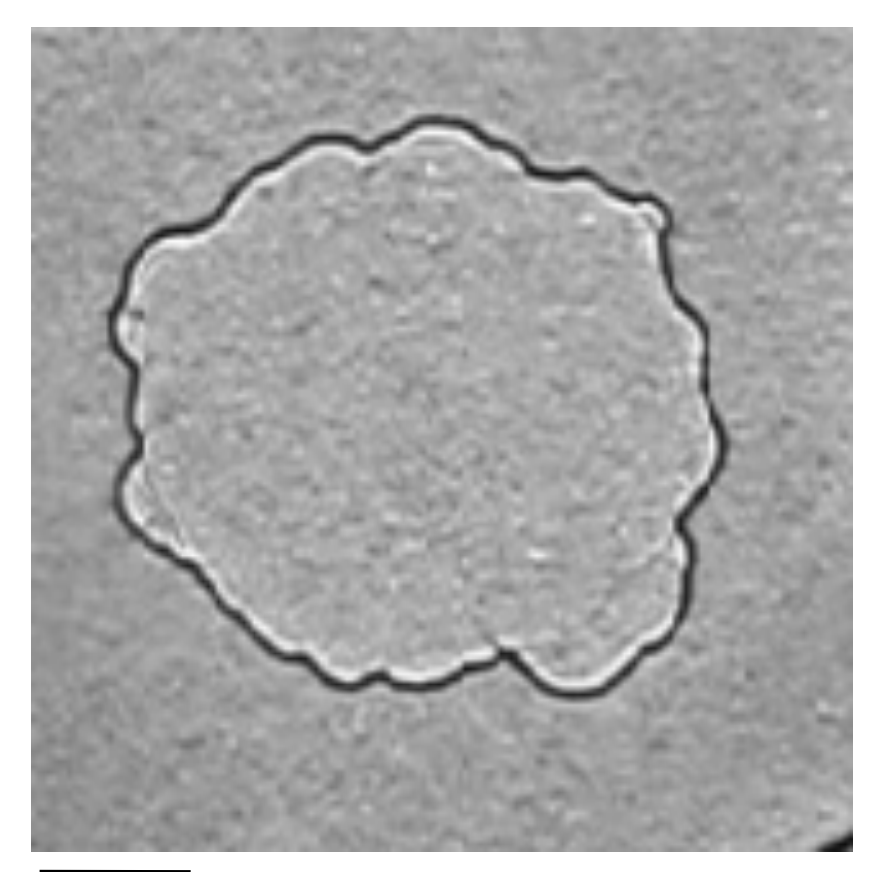
 $C_s=50 \text{ mM}, C_p=10 \text{ mM}$

There appears Coagel phase (L_c-phase) in aqueous phase.

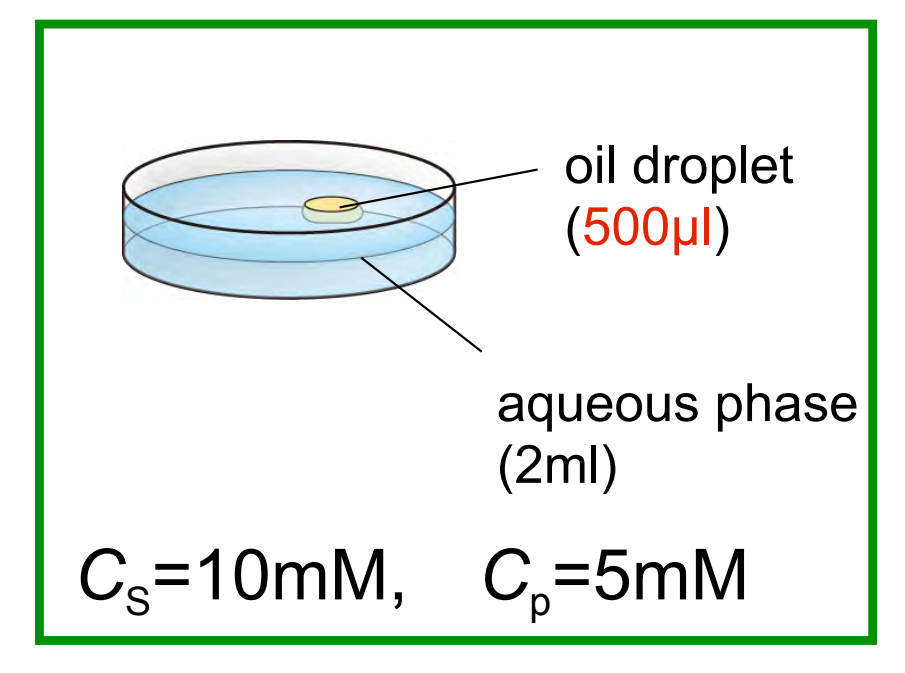




Characteristic features of blebbing



5 mm (speed x6)



Slow spherical protrusion ~10s Fast shrinkage ~1s No characteristic flow



Pressure-induced interfacial motion



Our first interpretation

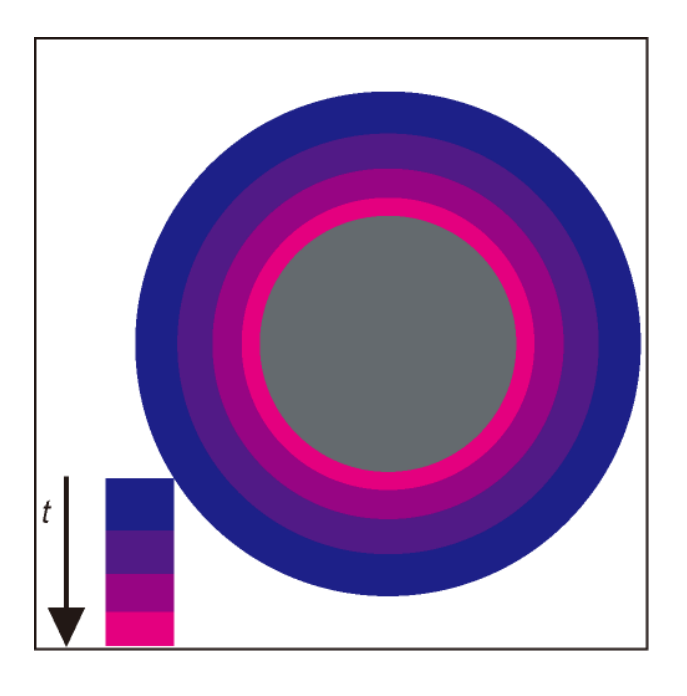
Pressure-induced interfacial motion

Stacked Rubber-Band Model

Assumption:

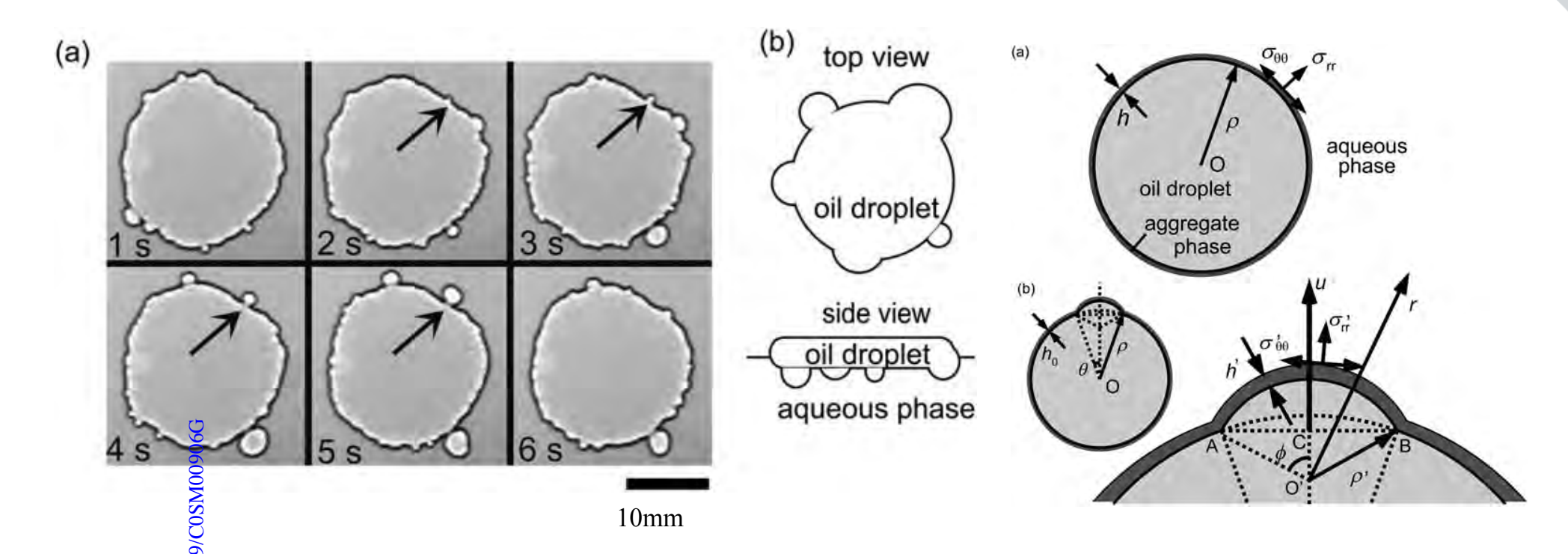
Aggregates are

- continuous (gel-like phase)
- deformable
- permeable





Theoretical consideration



The gel is generated only at the droplet interface, and the gel is pushed into the aqueous phase while it grows.

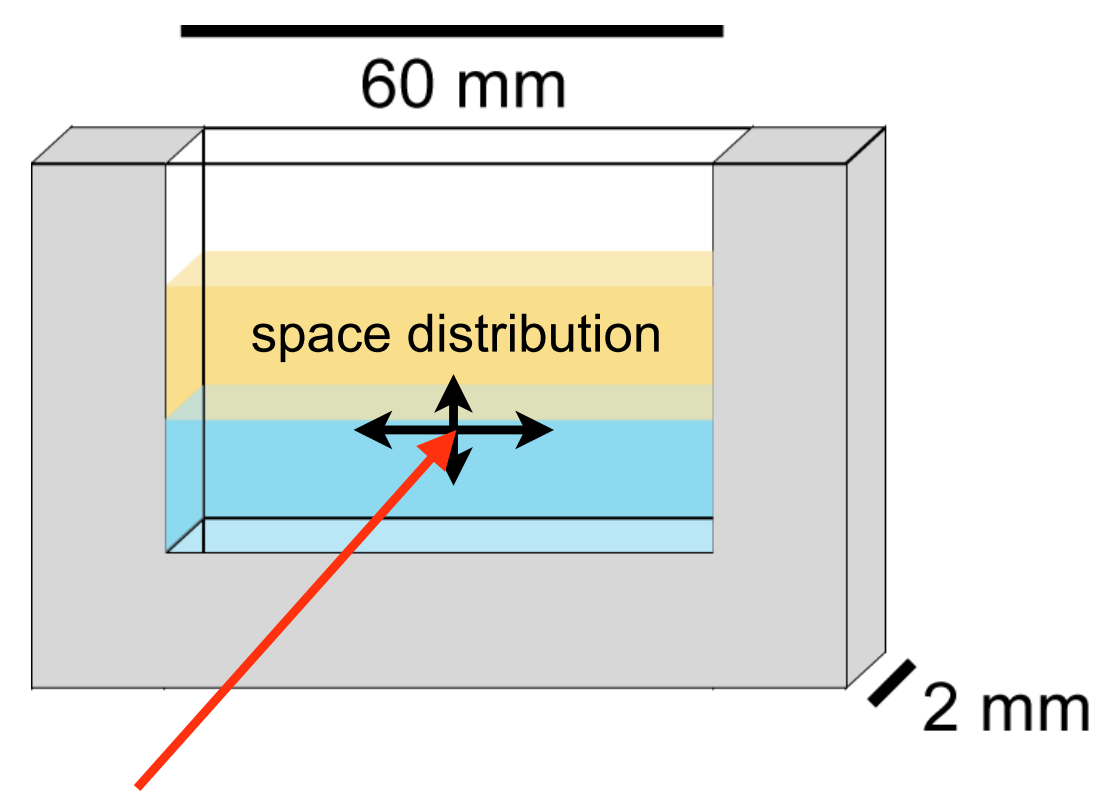


The radial stress increases the internal pressure of an oil droplet and the tangential stress promotes the breakage of the gel.



Structure of the aggregates

Micro-beam SAXS measurement at BL-4A, Photon Factory, KEK

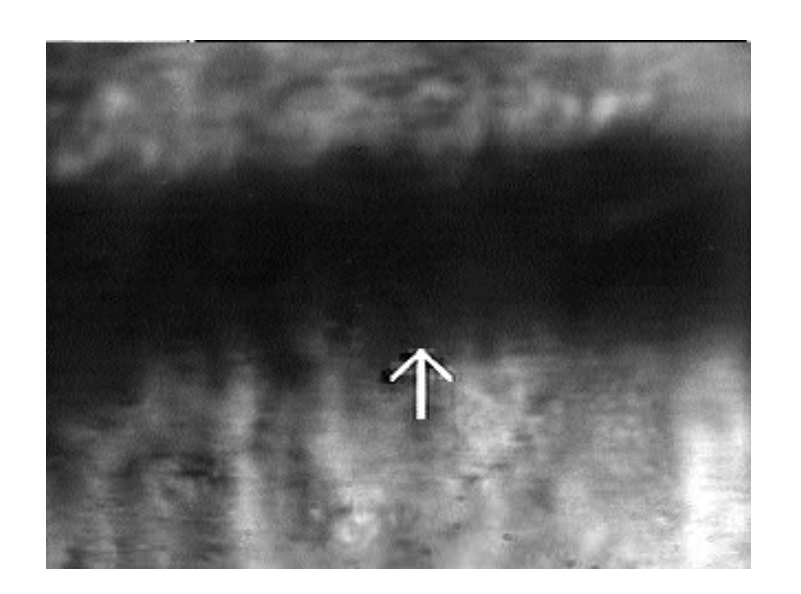


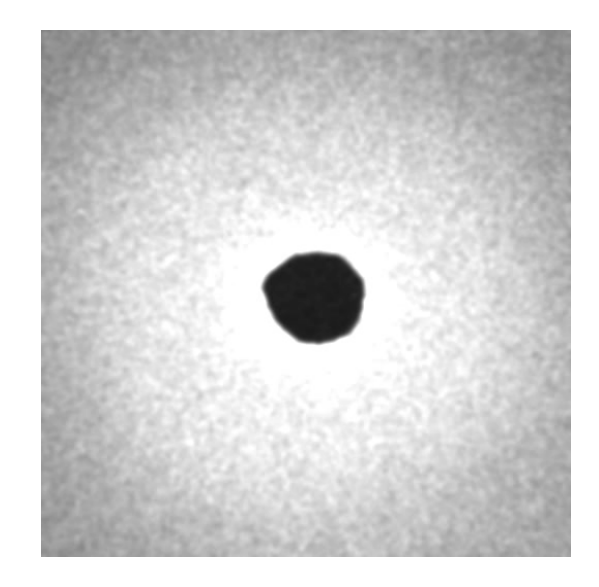
micro-beam X-ray: 4.5 μ m x 4.5 μ m, λ =1.1 $^{\text{A}}$

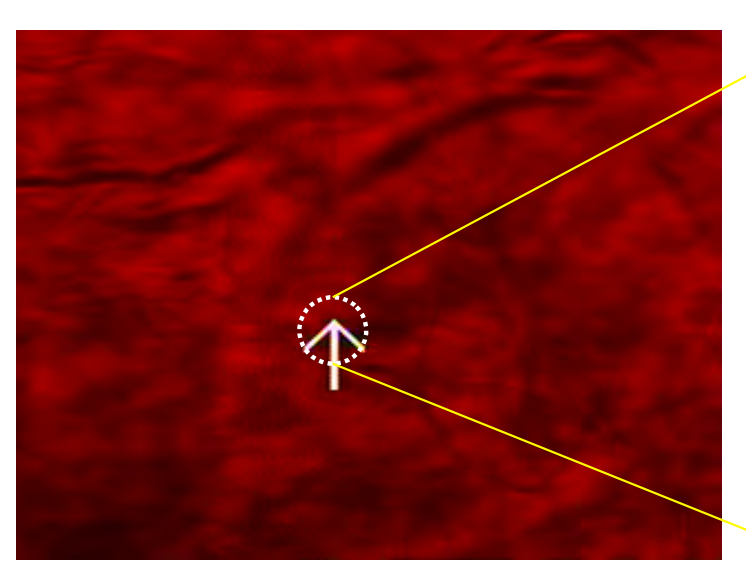
 $C_s=50$ mM, $C_p=20$ mM

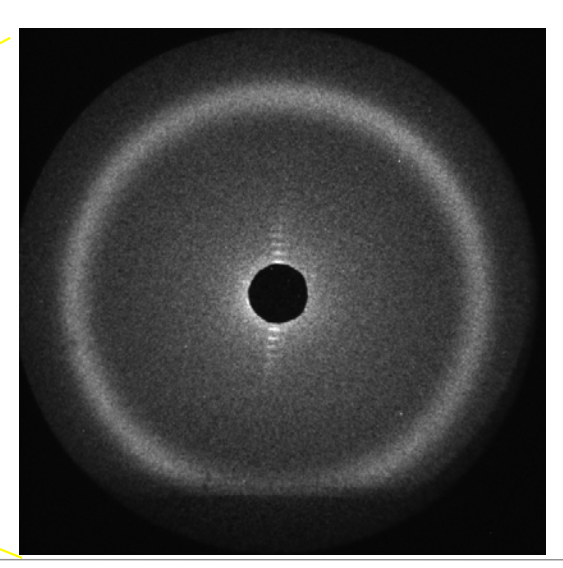


Real space vs Reciprocal space



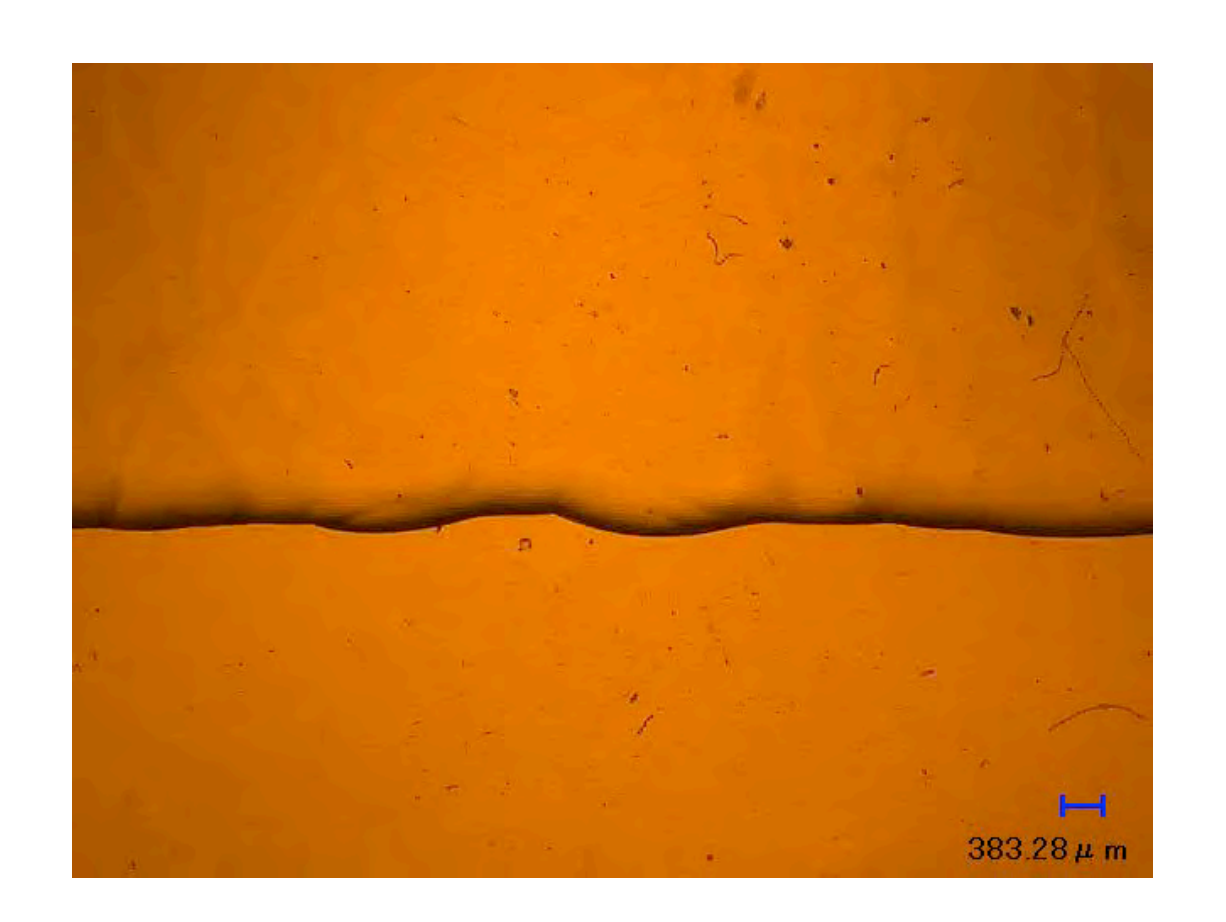


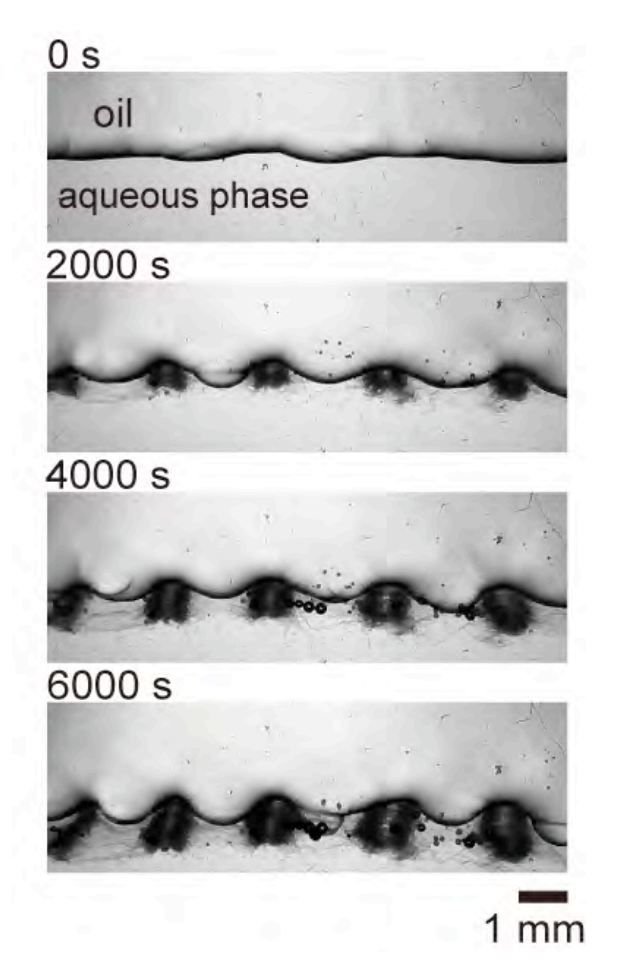






Blebbing & pillar formation

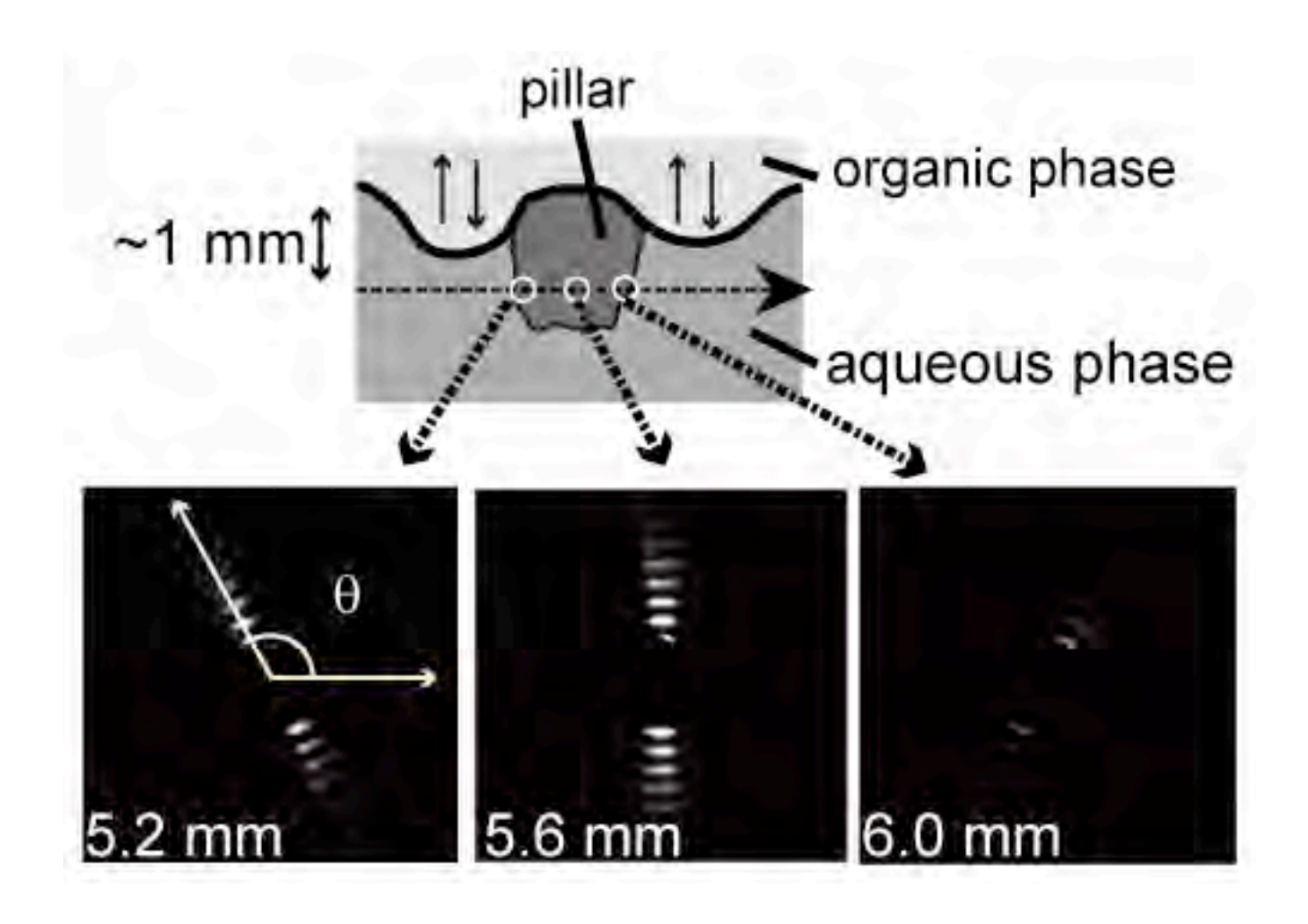




Periodic distribution of "blebbing regions" and "non-blebbing regions".

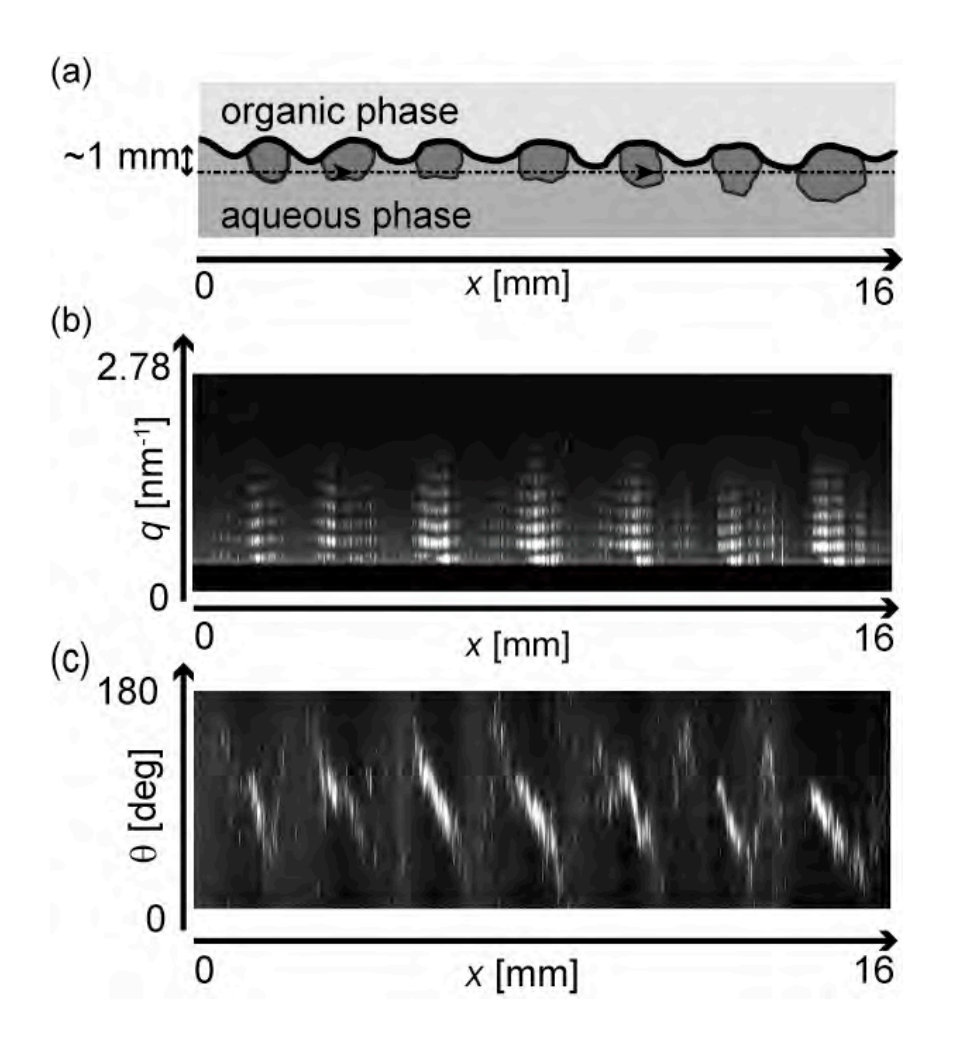


Detailed structure of a pillar





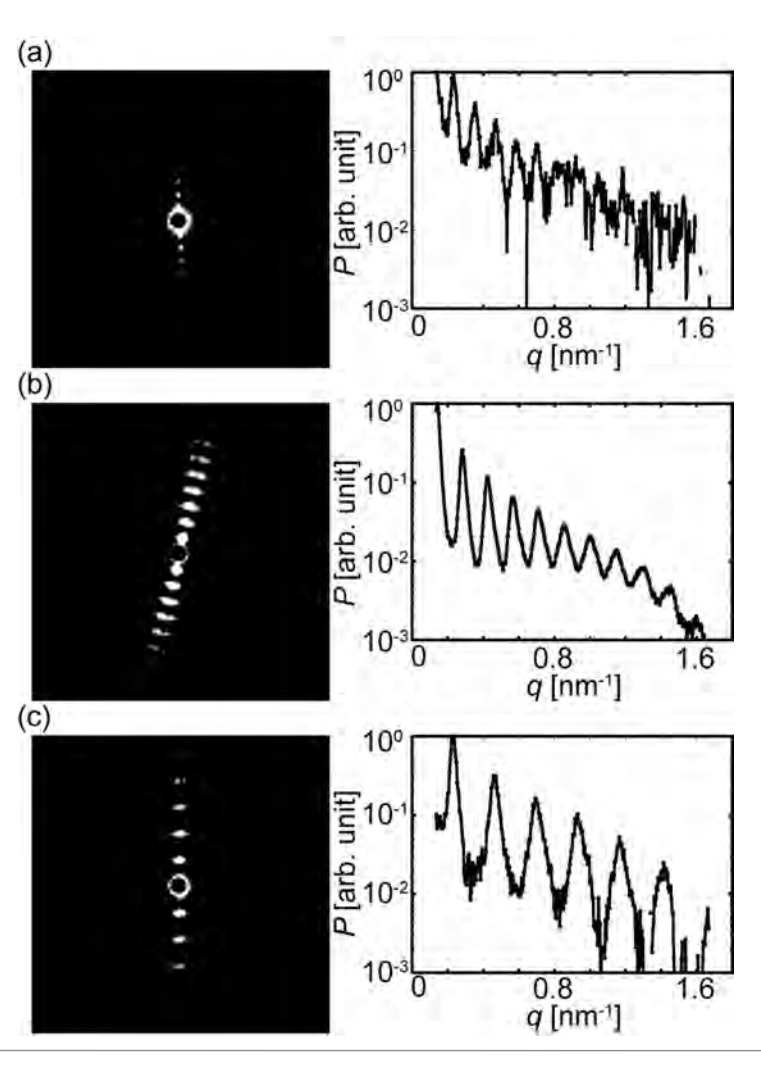
Structures of pillars





STAC concentration difference

Data were obtained 5400 s after the initial contact between organic and aqueous phases.



$$C_{\rm S} = 10 \; {\rm mM}$$

$$d = 52.8$$
nm

$$C_{\rm S} = 20 \, {\rm mM}$$

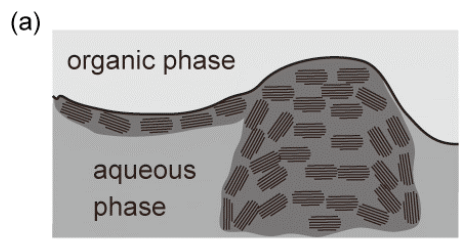
$$d = 43.6$$
nm

$$C_{\rm S}$$
 = 60 mM

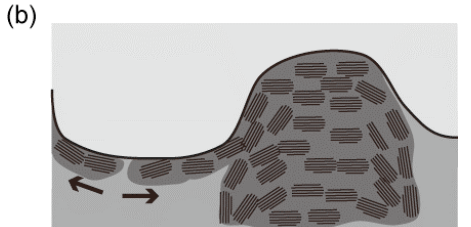
$$d = 26.6$$
nm



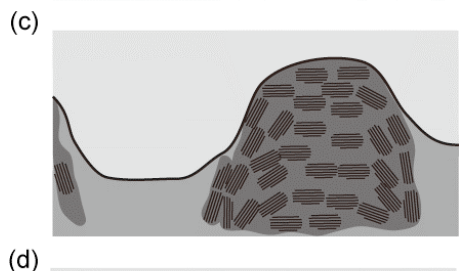
Pillar formation process



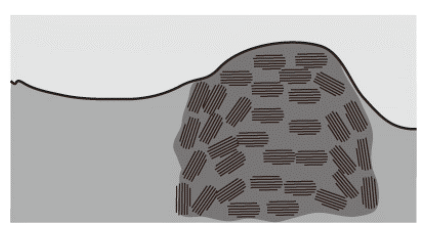
The aggregate layer is formed at the oil-water interface.



The aggregate layer is broken by the blebbing of the interface.



The layer is peeled off from the blebbing region and move to the non-blebbing region. The pillar grows downward by the continuous compression from the sides.

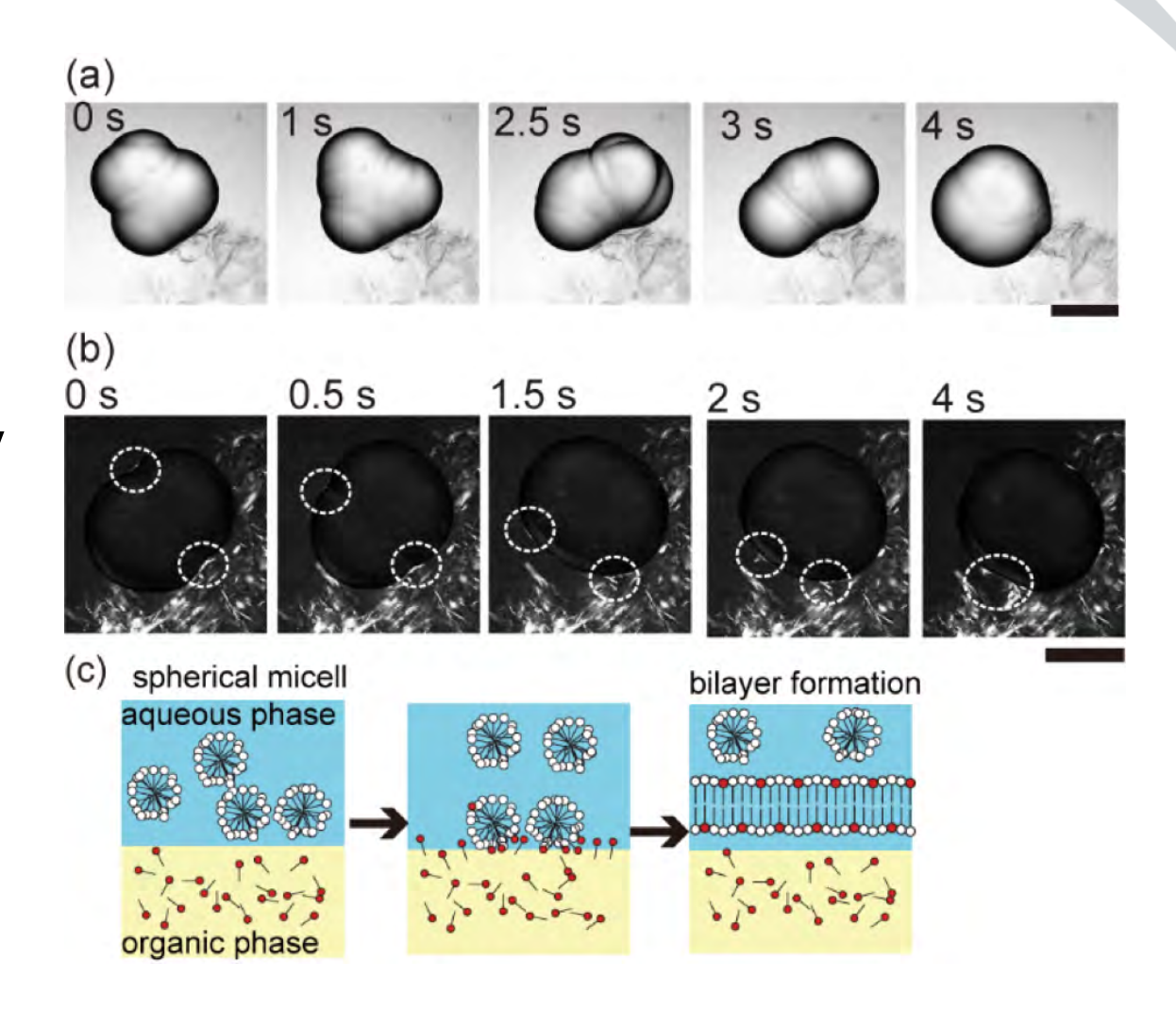


The blebbing region becomes flat due to the increase of interfacial tension.



Summary of SAXS studies

- A regular lamellar structure is formed at the moving interface.
- The construction and destruction of nanoscale structures is a key factor for spontaneous motions.

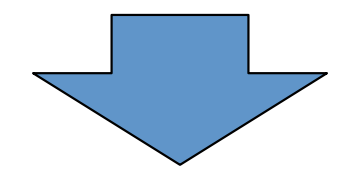




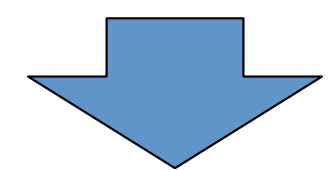
Problems to be solved

The blebbing motion is suppressed when turbid aggregates (instead of semi-transparent aggregates) are formed.

The requirement of positive curvature of the oil-water interface to have pressure increment in the organic phase.



Detailed structure and temporal transition of surfactant aggregate formed at and around an oil-water interface.



- Effect of surfactant concentration on the blebbing motion.
- In-situ & mm-beam SANS experiments.

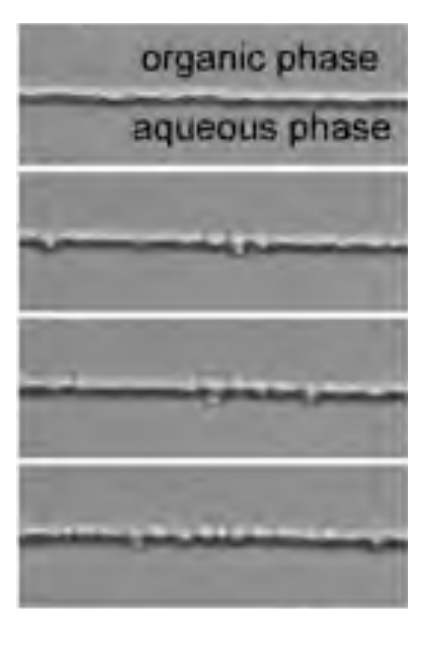


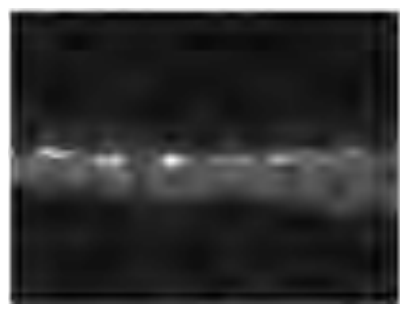
Lower surfactant concentration

 $C_{\rm S}$ =20 mM, $C_{\rm p}$ =20 mM



Blebs extend to aqueous phase for 2 s and retread back within 0.5 s. This motion continues for more than 1 hour. After an hour, semitransparent aggregate was observed on the oil-water interface.

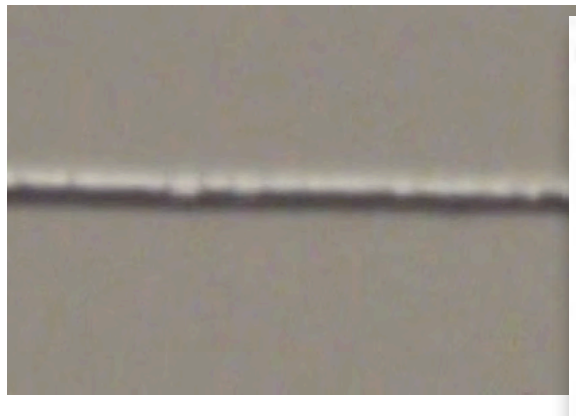




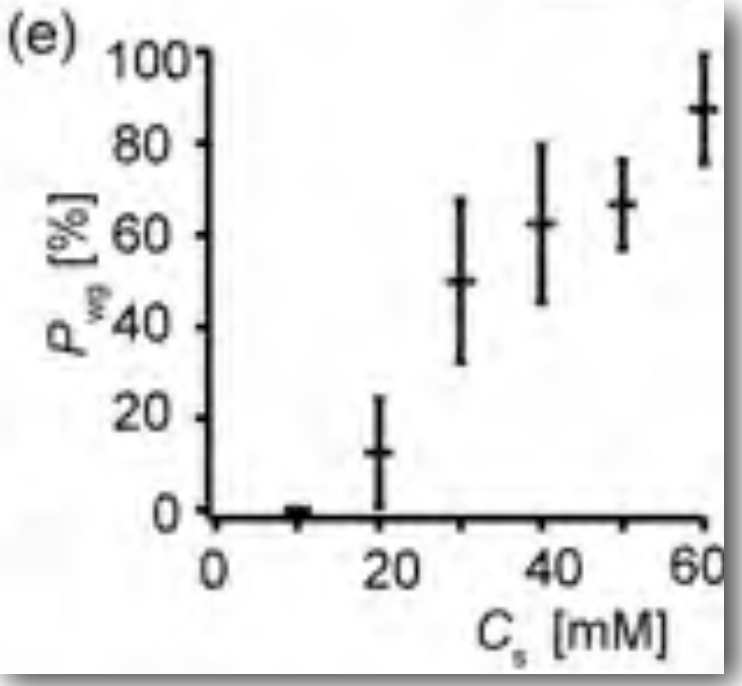


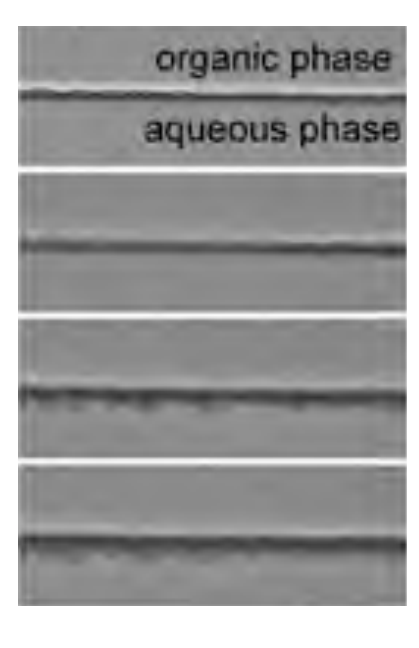
Higher surfactant concentration

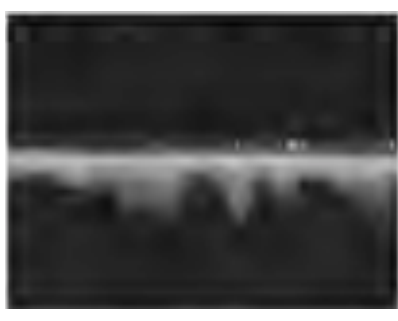
 $C_{\rm S}$ =50 mM, $C_{\rm p}$ =20 mM



The oil-water interface few minutes and stop aggregates appeared of the aggregates sprointerface.



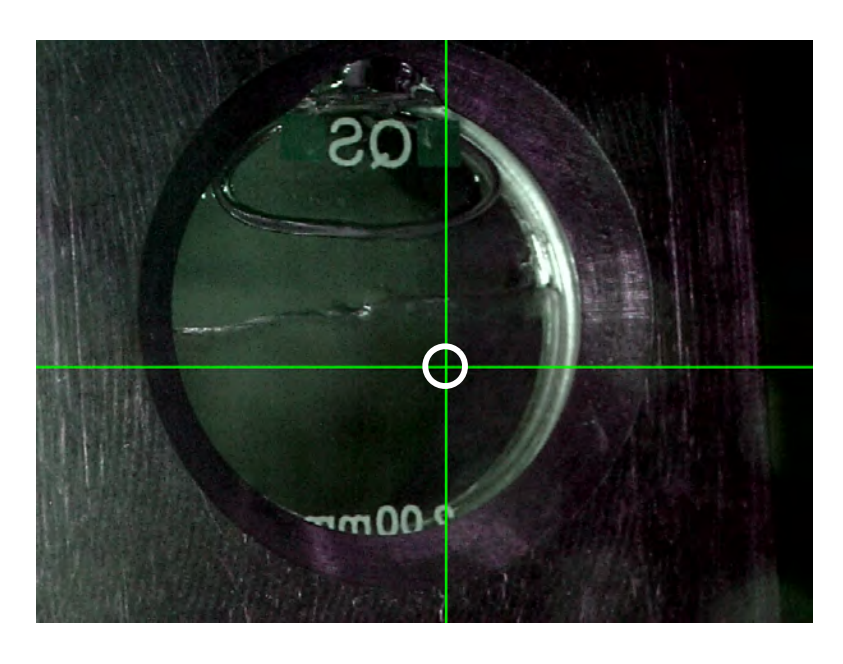


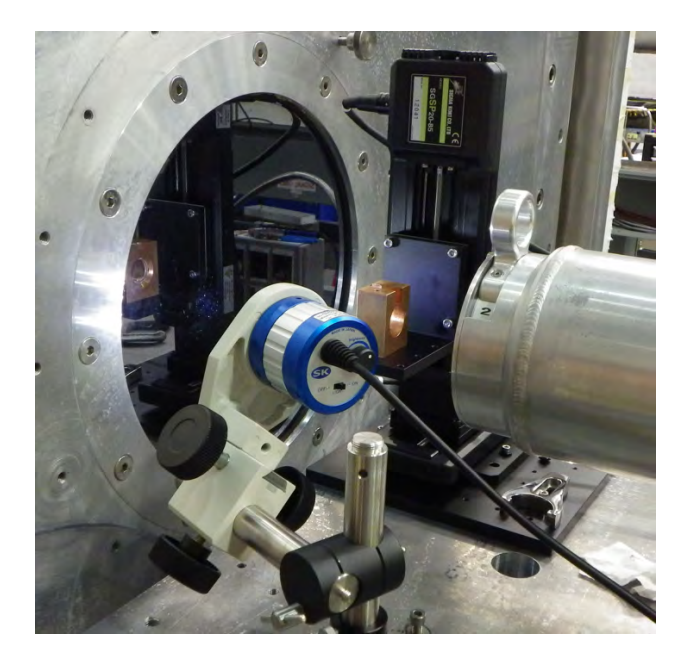




mm-beam SANS

CG-2, HFIR, ORNL (US), beam size = 2 mm ϕ , λ = 0.6 nm





Quasi-static meas. C_s =20 mM, C_p =20 mM; 12 hours elapsed, sample ($C_{14}D_{30}$, $C_{14}H_{30}$), position dependence

Dynamics meas. time dependence, sample($C_{14}H_{30}$)

 $C_{\rm S}$ =20 mM, $C_{\rm p}$ =20 mM(moving interface)

 C_s =50 mM, C_p =20 mM(static interface)

water: D_2O , oil: $C_{14}H_{30}$ or $C_{14}D_{30}$

 $C_{\rm S}$ =20 mM or 50 mM

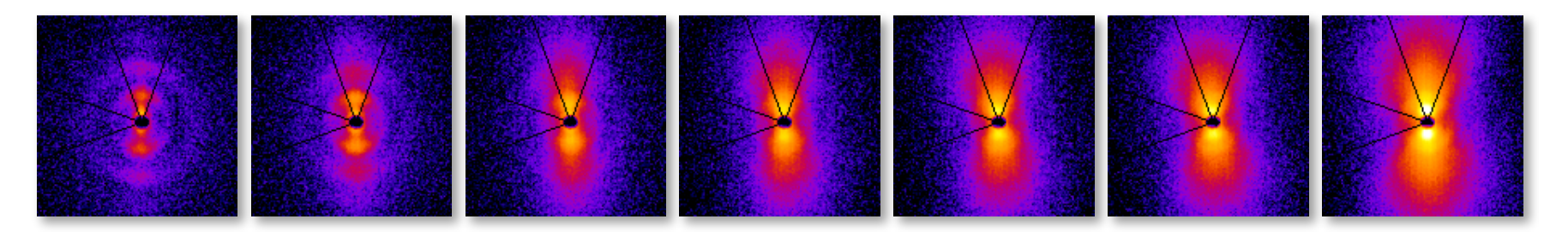
 $C_{p} = 20 \text{ mM}$



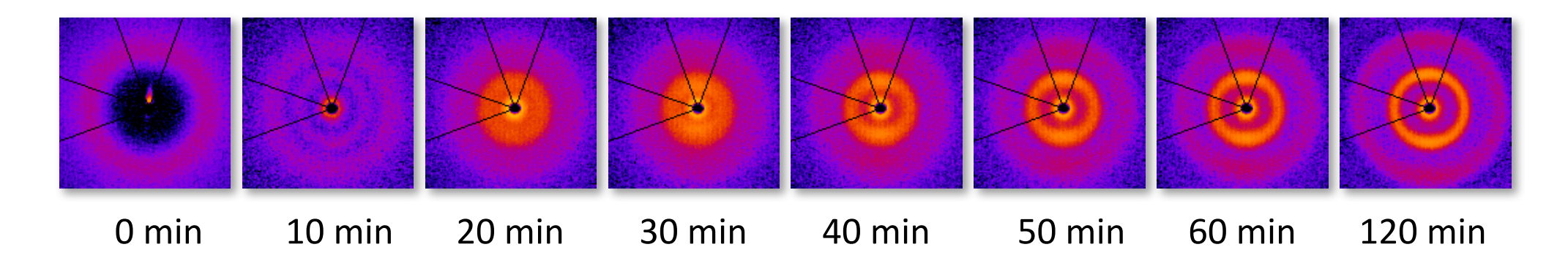
Time dependence

C_S= 20 mM: Blebbing interface (semi-transparent aggregates)





C_S= 50 mM: Static interface (turbid aggregates)

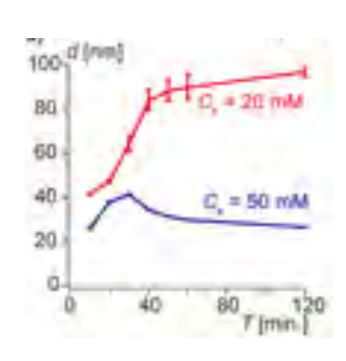


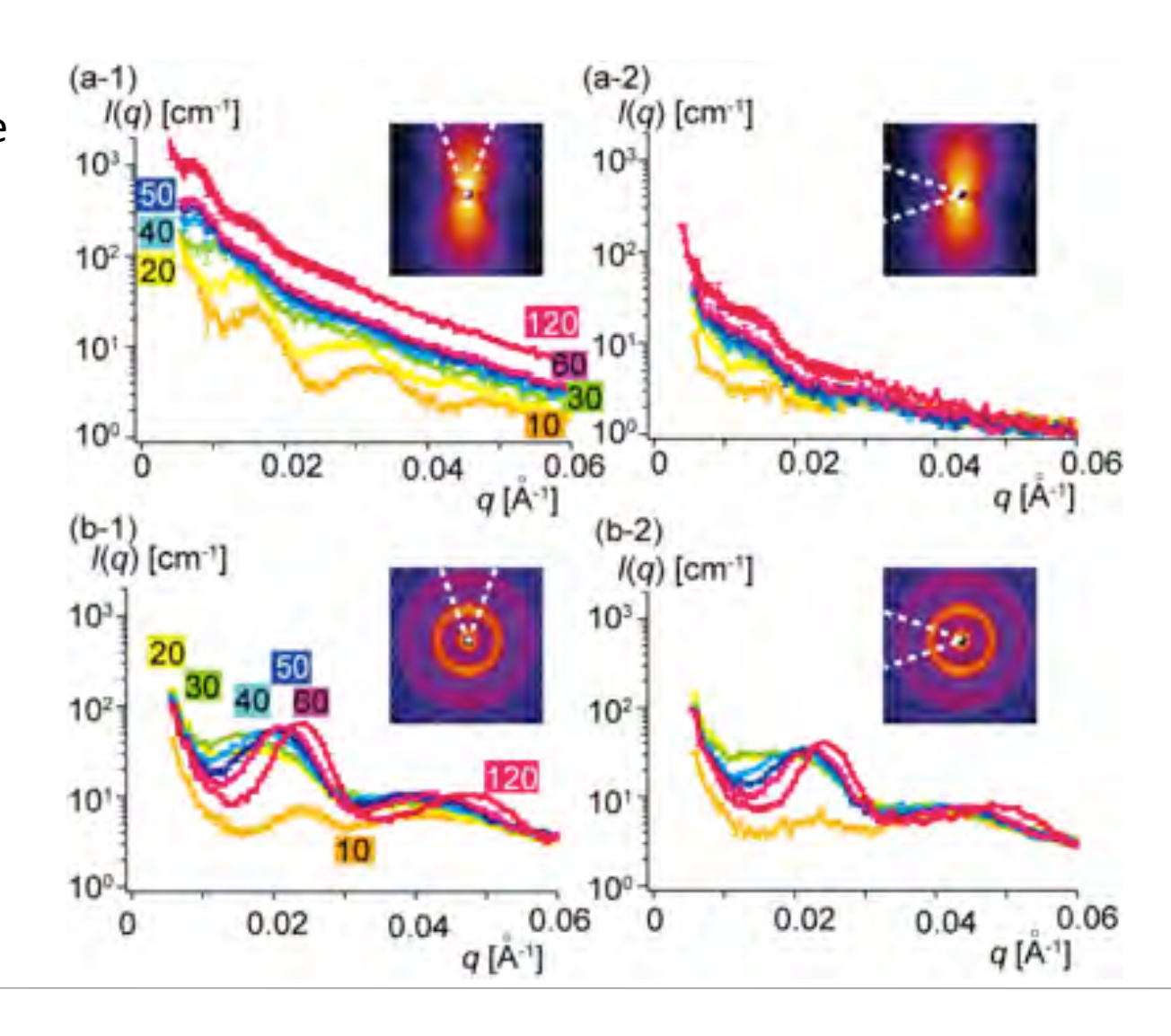


Vertical vs Horizontal

C_s= 20 mM: Blebbing interface (semi-transparent aggregates)

 C_s = 50 mM: Static interface (turbid aggregates)

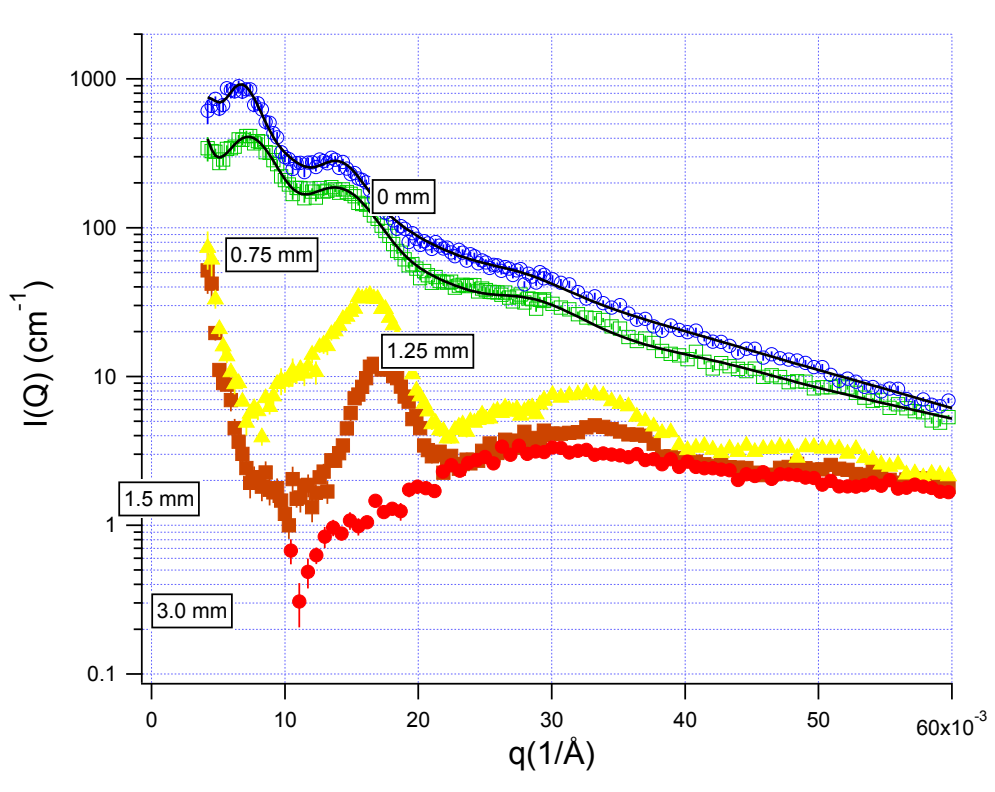


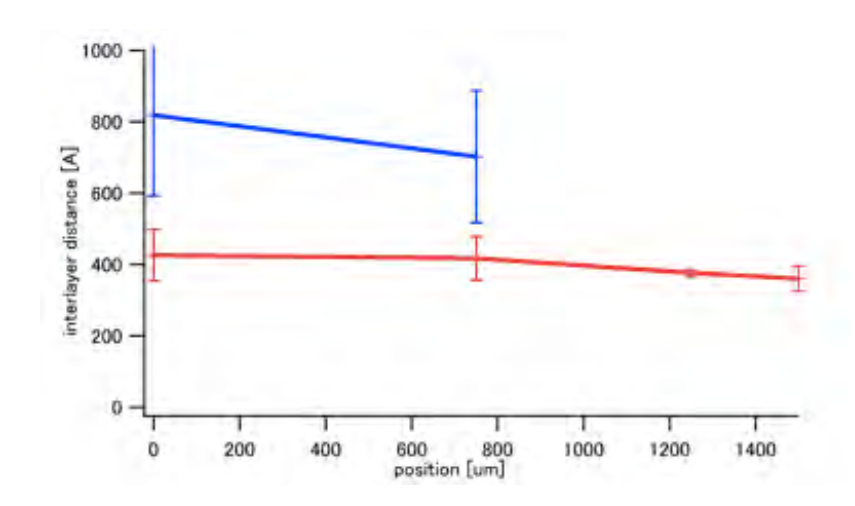




Position dependence of the semitransparent aggregates

The blebbing interface ($C_s = 20 \text{ mmol/L}$) 12 hours after preparation



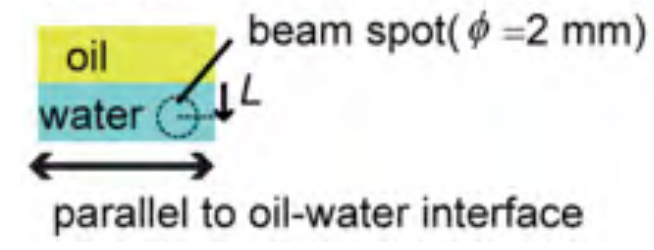


Fitting with paracrystalline model $d \sim 80$ nm, ~ 40 nm

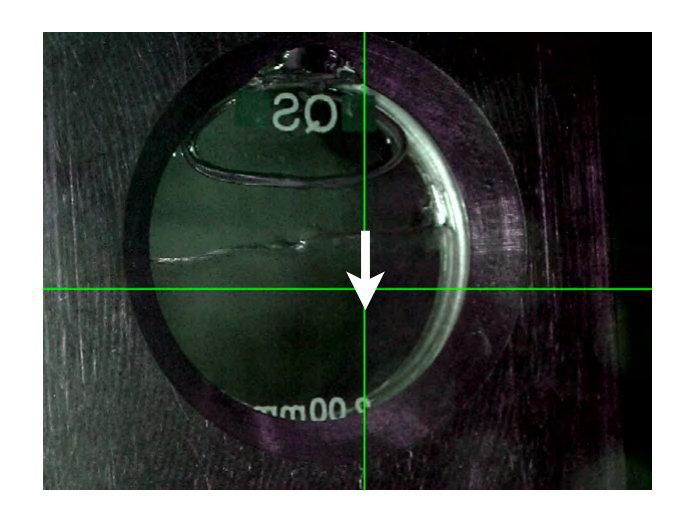


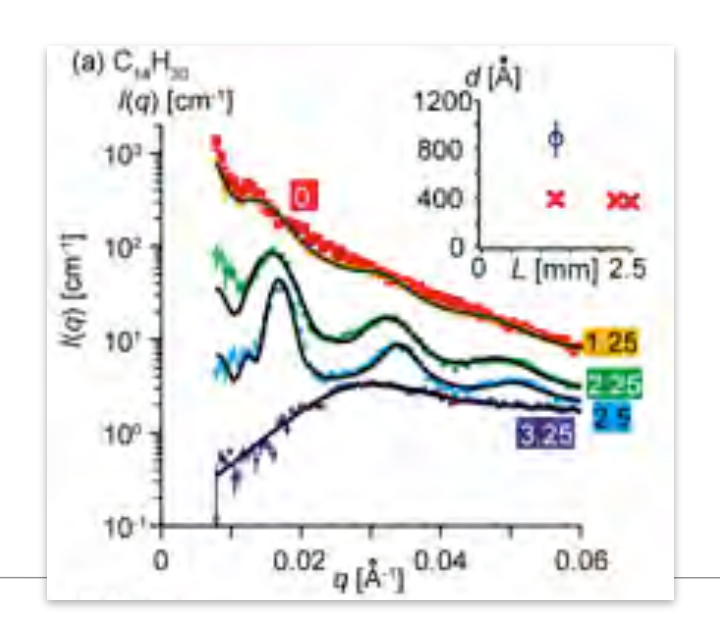
$C_{14}H_{30}/D_2O/STAC/PA$

 $C_{\rm S}$ =20 mM, $C_{\rm p}$ =20 mM; 12 hours elapsed



90-20 0-20 0-20 0 μm 1250 μm 2250 μm 2500 μm 3250 μm

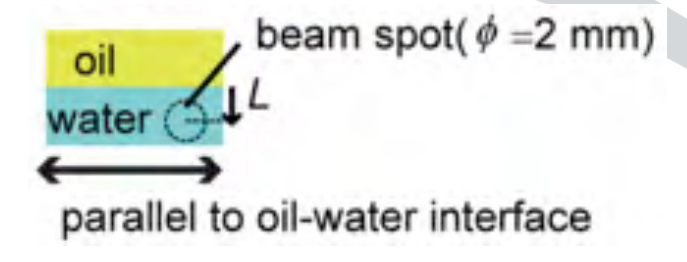






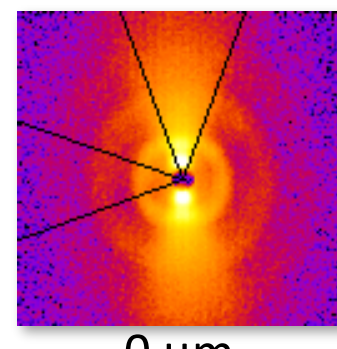
$C_{14}D_{30}/D_2O/STAC/PA$

 C_s =20 mM, C_p =20 mM; 12 hours elapsed

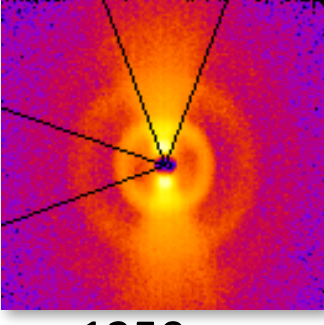


0-20

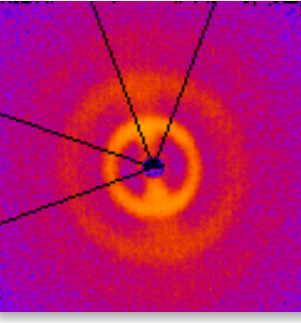
90-20



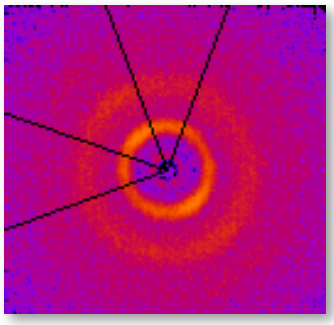




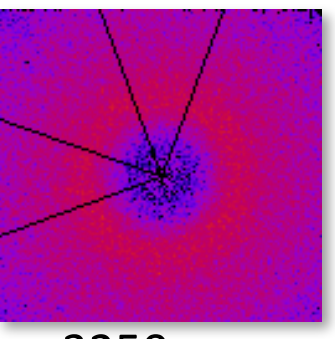
1250 μm



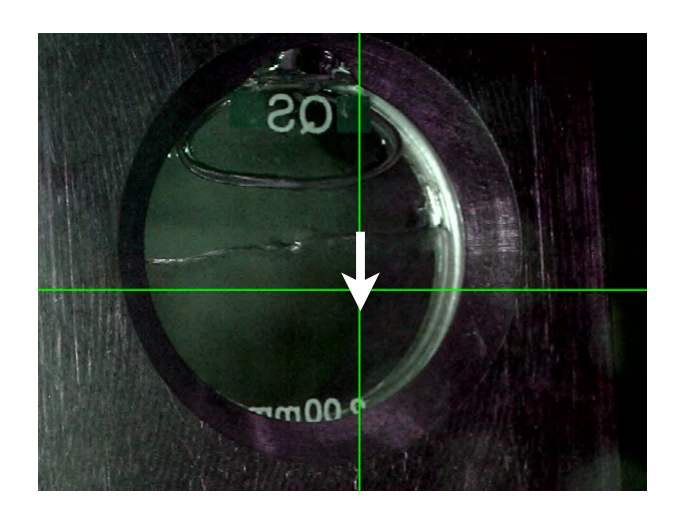
2250 μm

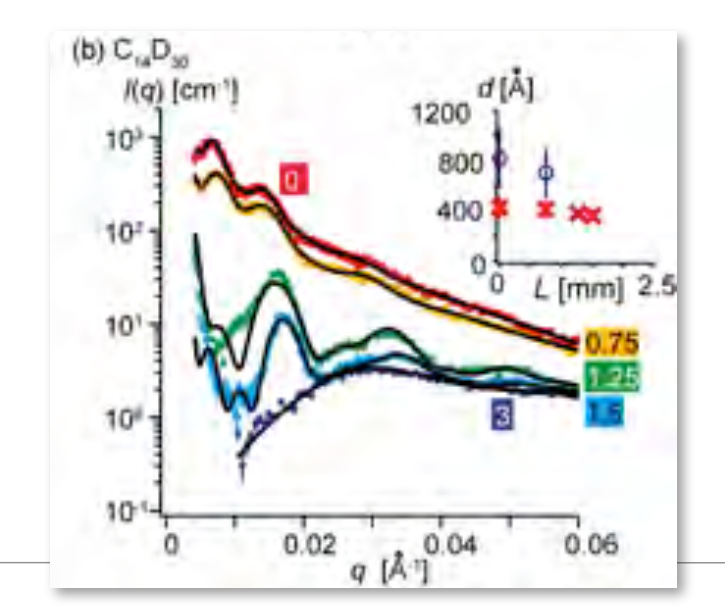


2500 μm



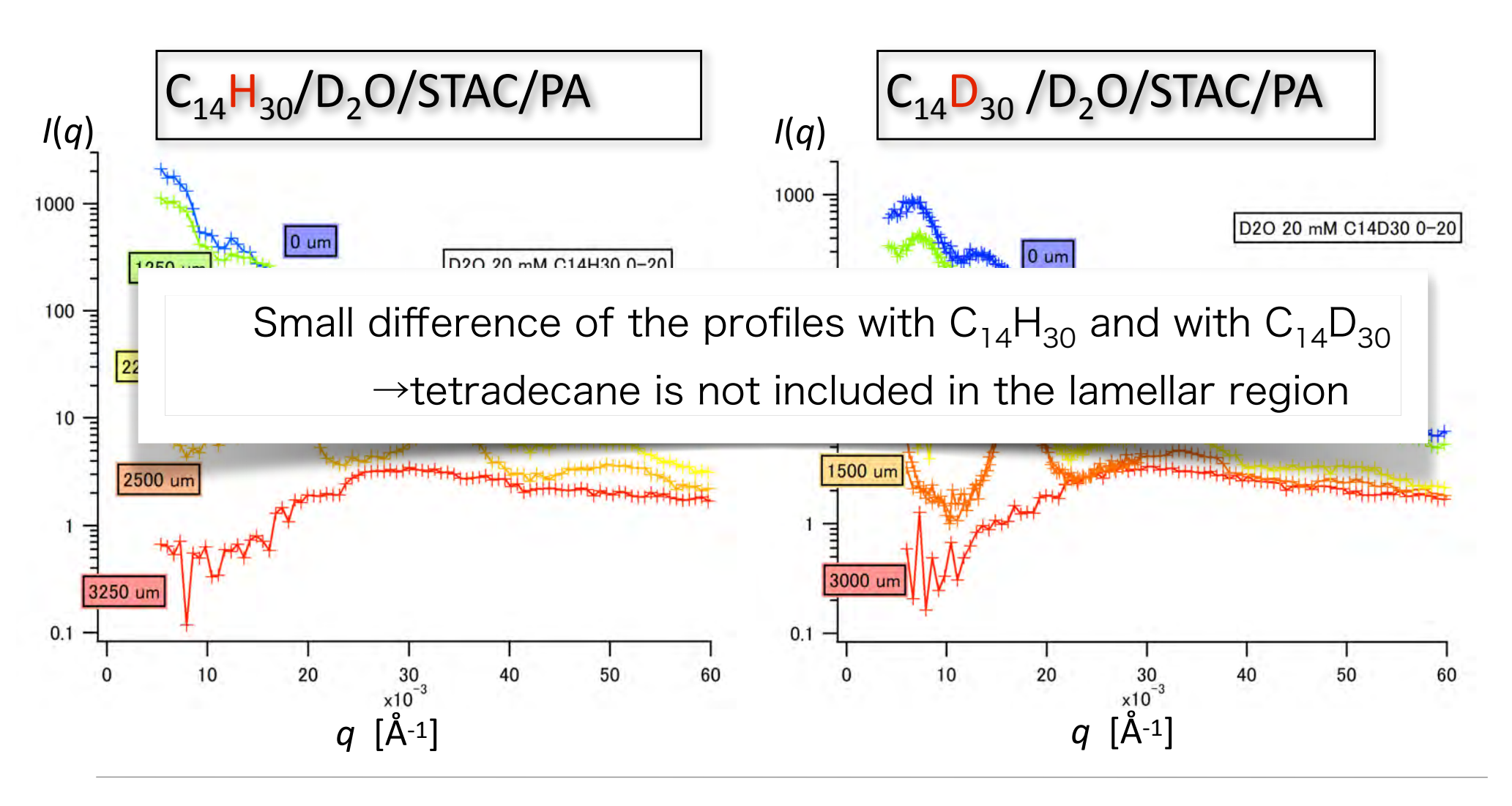
3250 μm







C₁₄H₃₀ VS C₁₄D₃₀





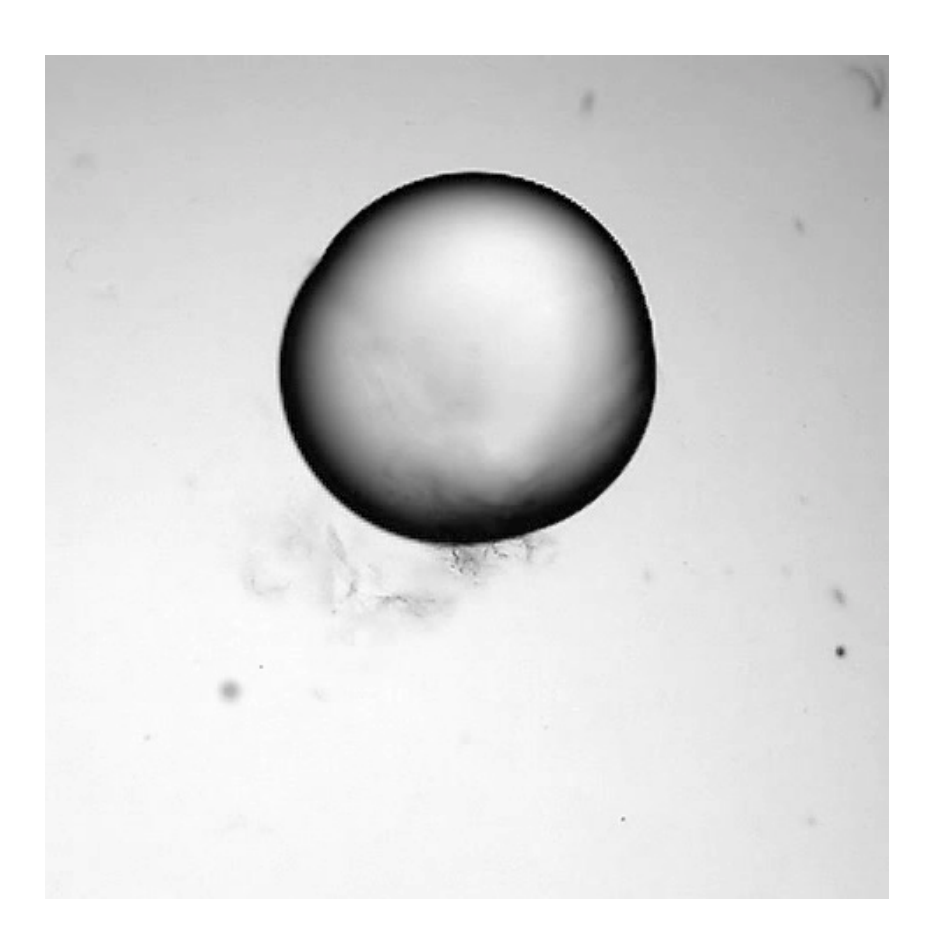
Experimental results indicate...

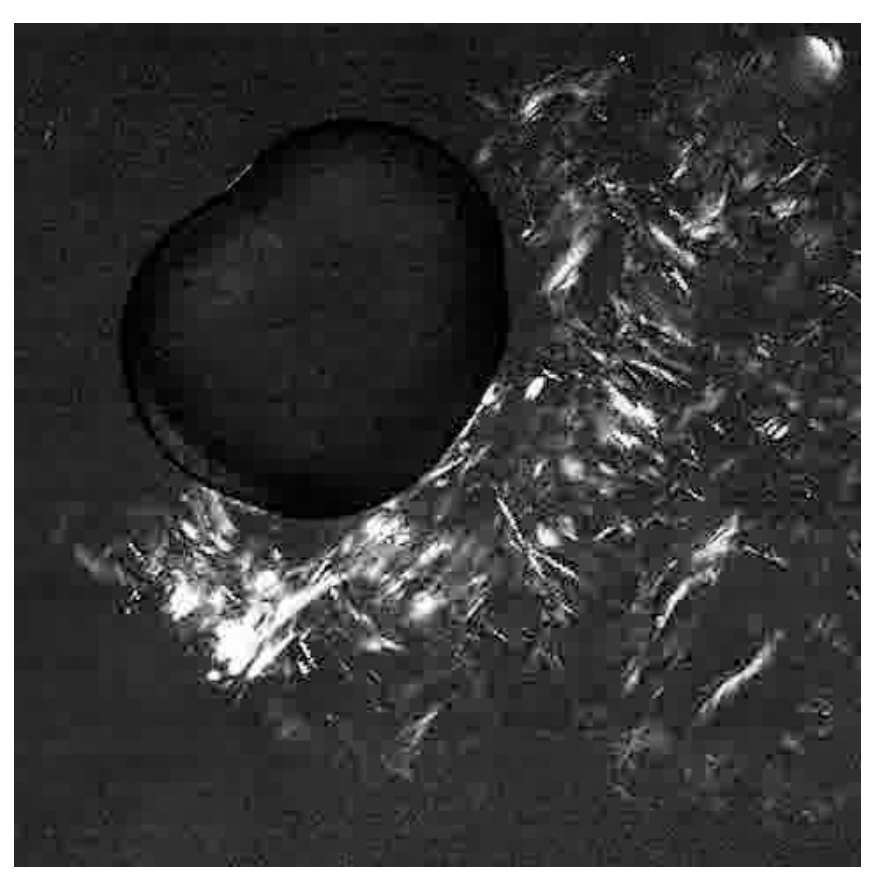
- Lower surfactant concentration: blebbing interface
 - 1) A lamellar structure parallel to the oil/water interface with large *d* (about 80nm) is formed at the interface.
 - 2) The lamellar structure immediately collapsed into an isotropic lamellar structure with approximately half d (\sim 40nm).
 - 3) The spontaneous blebbing of the interface continues for several hours, and the shorter lamellar aggregates stack between blebbing regions and pillars are formed.
- Migher surfactant concentration: static interface
 - 4) The blebbing motion continues only for minutes and the interface is covered with turbid gels.
 - 5) The small repeat distance lamellar structure with small d (\sim 25 40nm) is observed in the turbid gel region.

The formation of lamellar structure is not the sufficient factor for the blebbing motion. The drastic transition of lamellar structure from large *d* to small *d* is essential.



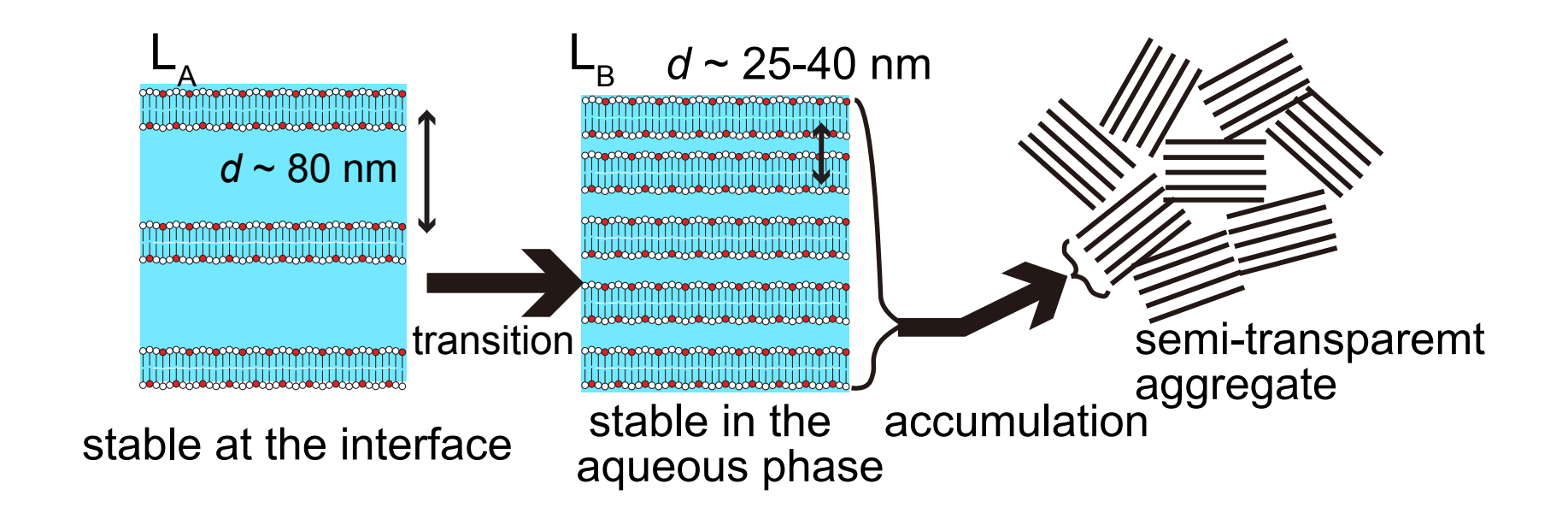
Aggregates near an interface







Lamellar-lamellar transition



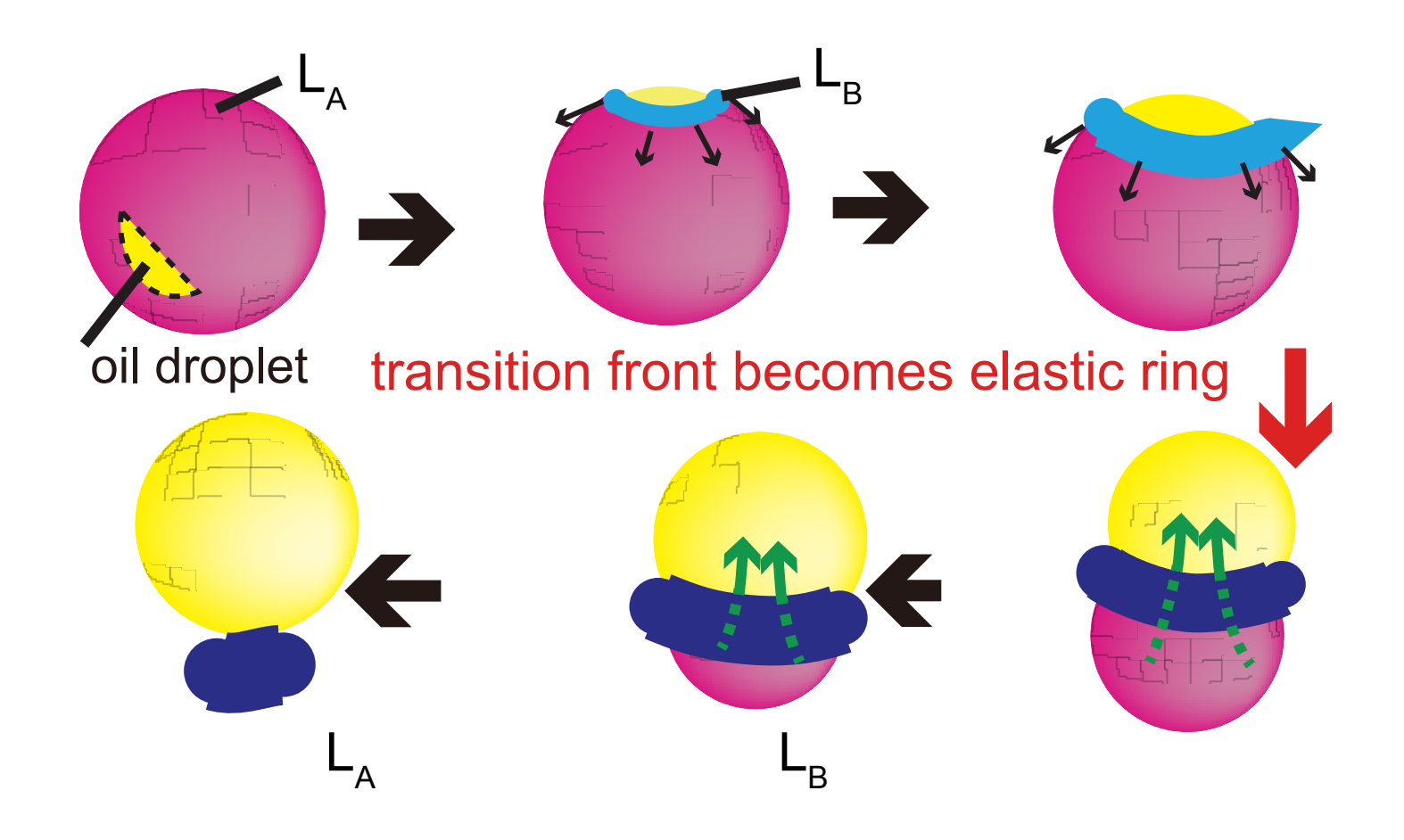
L_A: stable at small ϕ_{STAC}/ϕ_{PA}

L_B: stable at large ϕ_{STAC}/ϕ_{PA}

The transition occurs when STAC molecules are supplied form the aqueous phase.

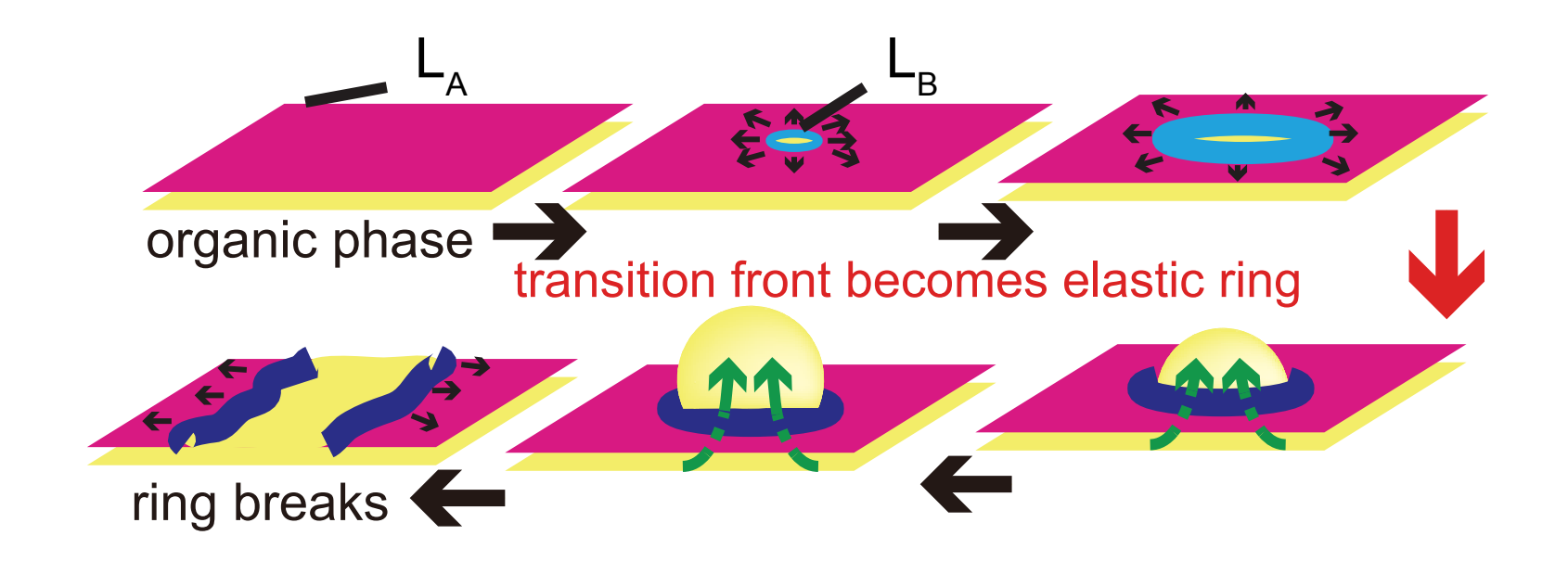


Droplet case





Flat interface case





Summary of SANS studies

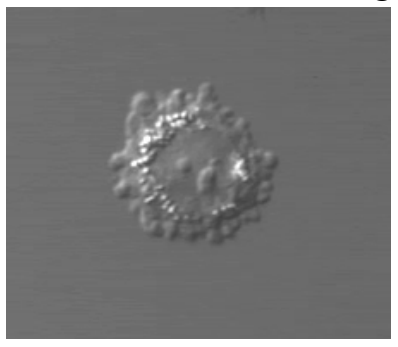
- At lower surfactant concentration: blebbing motion of the oil/water interface occurs and the semi-transparent aggregates are formed.
- At higher surfactant concentration: the turbid gel is formed around the interface and the blebbing motion stops immediately.
- ⊚The lamellar repeat distance *d* of aggregates at a blebbing interface is larger (~80nm) than that apart from the interface (~40nm), which is close to that of the turbid gel covering the static interface.
- The internal stress when the larger *d* lamellar structure shrinks into the smaller *d* could be the origin of the blebbing motion.



Summary

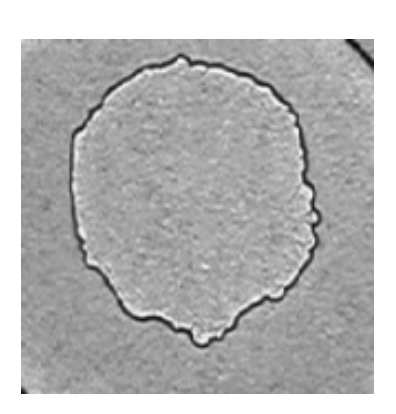
- We constructed a non-biological system mimicking amoeba-like blebbing motion.
- Theoretical model to explain the mechanism is introduced.
- The long-period lamellar structure is formed at the moving interface and transform to the short-period lamellar structure.
- The construction and destruction of nano-scale structures is a key factor for spontaneous motions.

Blebbing in cell
Melanoma cell fragment



10 μm

Blebbing droplet



5 mm



まとめ

• X線・中性子小角散乱

- Guinier近似やPorod近似など、基本的なモデルを用いた解析である程度のことは言える。
- 詳細な構造情報が必要であれば、形状因子と構造因子に分けて解析するのが基本。
- 形状因子をモデル化するのは比較的容易。単分散で希薄であれば、解ける場合が多い。またSANSとSAXSの併用や、コントラスト変化(相対形状因子法を含む)、ASAXS等を用いれば濃厚系でも解析可能性が上がる。
- 構造因子を決めるためには相互作用を仮定する必要がある。その仮定が正しいか どうかの判断が難しい上に、そもそも解けるモデルが多くはない。
- 多成分系の構造を解くためには、コントラスト変調法は必須。
- 構造に階層性があり、多成分系が多いソフトマターの秩序化研究には強力な武器 になる。また「生のまま」で測定できるのもメリット